Porosity design of a shaped zeolite for improved effective diffusivity

Rogéria Paula Martins Bingre Do Amaral

UNIVERSITÉ DE STRASBOURG

ÉCOLE DOCTORALE DES SCIENCES CHIMIQUES

Institut de Chimie et Procédés pour l'Energie, l'Environnement et la Santé, UMR 7515

THÈSE

présentée par :

Rogéria Paula MARTINS BINGRE DO AMARAL

soutenue le : **20 septembre 2019**

pour obtenir le grade de :
Docteur de l'université de Strasbourg

Discipline/ Spécialité : Chimie / Catalyse Hétérogène

Porosity Design of a Shaped Zeolite for Improved Effective Diffusivity

THÈSE dirigée par :

M. LOUIS Benoît	Directeur de Recherche CNRS, Université de Strasbourg

RAPPORTEURS :

Mme. MINTOVA Svetlana	Directeur de Recherche CNRS, Université de Caen
M. PINARD Ludovic	Maître de Conférences, Université de Poitiers

---

AUTRES MEMBRES DU JURY :

M. COASNE Benoît	Directeur de Recherche CNRS, Université de Grenoble Alpes
M. NGUYEN Patrick	New Market Manager/R&D Manager, C.R.E.E. Saint-Gobain Provence

“The good thing about science is that it’s true whether or not you believe in it.”

Neil deGrasse Tyson

Acknowledgements

During this Thesis, I had the opportunity to work in many different laboratories with different teams. Each one of them marked me in different ways and allowed the progression of the work herein presented. All this could not have been possible without the best supervisor a Ph.D. student could ever expect, Dr. Benoît Louis. To you, I must thank for everything: the warm welcome, the badminton plays, the discussions, the freedom, and all the travels opportunities. All this clearly exceeded your duties and my best expectations, and I wish our research paths will cross many times in the future.

An inseparable part of this group which so much I must thank for the opportunity is Dr. Patrick Nguyen. Working with you and Benoît meant lots of fun but never deviating from my responsibilities. Thank you for giving me the opportunity to meet the other side of research, and for putting all your confidence in me by giving me the freedom to do as I wish.

These three years may be divided in five sections, representing the five different places I had the luck to work in. The first part, LASYROCK, where the first one and half years of my Thesis was developed. I want to thank Patrick Pale for always being available for discussion even if my subject was very far from the remaining students. I would like to thank my colleagues and permanent staff for the discussions, the lunches at Fridays, the chalet, and all the help you always so kindly provided when I needed it: Valèrie, Marc, Chenng, Jean Marc, Aurélien, Romain, Fatih, and Robin. Thank you, Bruno Vincent, for the NMR analysis. Thank you very much, Olesia, for sharing the office with me during this time, for discovering the zeolite world with me, for the picnics, the dinners, and the whole month in Beijing. You are an amazing girl, and I wish the best for your future. Diane and Wang, my favourite master students, thank you for your help and for allowing me to practice my French. It was a pleasure to work with you.

The second half of this Thesis was spent in the Energy and Fuels for a Sustainable Environment Team at ICPEES. I would like to thank Anne-Cécile Roger for once again receiving me in her team. It is a great pleasure to finish my Thesis in your lab. Here, I would also like to thank my colleagues and the permanent staff for all the help, the beers after work, the barbecues, and the infinite discussions: Sébastien, Ksenia, Clémence, Claire, Francine, Lola, Arno, Pauline, Valentin, and Isabelle. I am especially grateful to Thierry Romero for all the SEM sessions. To you, Cristina, I am eternally grateful for all the discussions about zeolites, to sharing your experience with me, but most of all, for the friendship built during this time. While sitting with you, back against back, in the same office, I never felt loneliness. I could not have asked for better company in my second stay in Beijing, you made me see the same city with different eyes and create new memories.

I can consider as my second home the Centre de Recherche d'Études Européens in Cavaillon. There, I had the opportunity to meet very professional people, that always came to the workplace with a smile and always made me feel welcomed. I thank Béatrice, Lucas, and particularly, Nicole Rives. It was a huge pleasure to work with you, your experience is beyond vast, and I aspire to become a professional like you. Your good mood and kindness are admirable.

Two different countries, two different cultures, but both forever in my heart: China and Brazil. At the laboratory of Prof. Qiang Wang, to whom I am grateful for receiving me three times in his team, I got

to know hard work in such friendly environment. It is impossible for me to mention everyone to whom I am very thankful, but here are my especial acknowledgements to Liang and Qianwen for all the warm welcoming in my first time in Beijing, especially for the hot pot evening. Qianwen, I wish you the best of luck for your research, I know I let you in good hands. This is also for Nana, for her huge help, kindness and badminton plays. You are an amazing girl, and I wish you the best. Nido, words cannot explain how grateful I am for meeting you. You made me grow up in certain aspects, because besides our tremendous cultural differences, I've spent such good quality time with you at the lab and discovering Beijing.

To Prof. Marcelo M. Pereira for receiving me at his laboratory in Rio de Janeiro, for all the discussions, and for letting me sail your boat. What an experience! In simultaneously, my special thanks to Alessandra and Catarina for working side-by-side with me, with all your kindness and help. Everyone in that lab made me feel very welcomed and part of them: to Joana, Sérgio, Sérginho, Mateus, Bira, and Maria Aleixo my many thanks.

This Thesis however could not have been possible without the support of all the friends I did during these years. I would like to acknowledge all my colleagues from StrasAIR: Elsa, Youssef, Stephanos, Laetitia, Filipa, and Sayali for all the nice meetings, activities and conferences we organized together. We had lots of fun and this association became a very important part of myself! To Khyati, Cristina, Anton, Nour, Rafael, Sayali, Renata, Guido, and David for your friendship and support. And finally, to Filipa, my best friend, I don't know if our connection was due to the fact we are both Portuguese in a foreigner city, or, most probably, due to your wonderful personality, resilience, and kindness, but you are the one I must thank the most. You were there from day one, during all the struggles and joys, always keeping me sane. With you by my side, I always felt at home.

Last but never, ever, least, I thank my family. To my niece Sofia for always making me laugh with her crazy ideas. To my father for always inspiring me to go further and to my mother for always doing the impossible to make that happen. Your support is unconditional, and I know I will always have a safe place to come back to if everything goes wrong. It is for you all the sacrifice and hard work.

Table of contents

List of figures

List of tables

List of abbreviations

ABS – aluminium tri-sec-butoxide

CMC – carboxymethyl cellulose

COV – composés organiques volatils (in French)

CTAB – cetyltrimethylammonium bromide

DME – dimethyl ether

EISA – evaporation-induced self-assembly

FCC – fluid catalytic cracking

FT-IR – Fourier-transform infrared spectroscopy

HCA – hydro-carboxyl acids

HETP – height equivalent to a theoretical plate

HT – hydrotalcite

IGC – inverse gas chromatography

IZA – international zeolite association

LCO – light cyclic oil

LPG – liquefied petroleum gas

MC – methylcellulose

MEB – microscopie électronique à balayage (in French)

MIP – mercury intrusion porosimetrie

MTH – methanol-to-hydrocarbons

MTO – methanol-to-olefins

PEO – poly(ethylene oxide)

PFG-NMR – pulsed-field gradient NMR

PO – propylene oxide

SAR – Si/Al ratio

SEM – scanning electronic microscopy

TCD – thermal conductivity detector

TEOS – tetraethylorthosilicate

TMB – trimethylbenzene

TPAOH – tetrapropylammonium hydroxide

TPD – temperature-programmed desorption

VOC – volatile organic compounds

XRD – x-ray diffraction

Résumé en français

I. Introduction

Actuellement, la production de combustibles, textiles, plastiques, et bien d'autres matériaux est essentielle à la survie humaine. La plupart de ces dernières est obtenue à partir du pétrole, après raffinage, i.e., le craquage des molécules lourdes en molécules plus petites, notamment en hydrocarbures avec un point d'ébullition dans un intervalle de LPG (*liquefied petroleum gas* – gaz de pétrole liquéfié), C_3-C_4, naphta, 308 – 494 K, et LCO (*light cyclic oil* – huile cyclique légère), 308 – 616 K. Le procédé le plus utilisé à cet effet est le FCC (*fluid catalytic cracking* – craquage catalytique à lit fluidisé) dans les industries pétrochimiques et de raffinage[1] utilisant la zéolithe acide comme catalyseur.

Les zéolithes sont des aluminosilicates cristallisés de structure microporeuse qui peuvent être utilisées comme catalyseur acide en raison de leur forte acidité (de Lewis et de Brønsted). En fait, sa valorisation est surtout due à la capacité de se comporter comme un superacide et à la caractéristique de sélectivité de forme, mais aussi à sa stabilité thermique, son faible coût de production et sa capacité de régénération. Ce matériau a été découvert en 1756 par A.F. Crønstedt qui a donné le nom de 'zéolithes' du Grec « pierres qui bout » ou *'boiling stone'*. Deux siècles plus tard, R.M. Barrer a réussi les premières synthèses au laboratoire en forme de poudre, ouvrant une énorme possibilité d'applications dont la catalyse demeure la plus précieuse (55% du marché global).

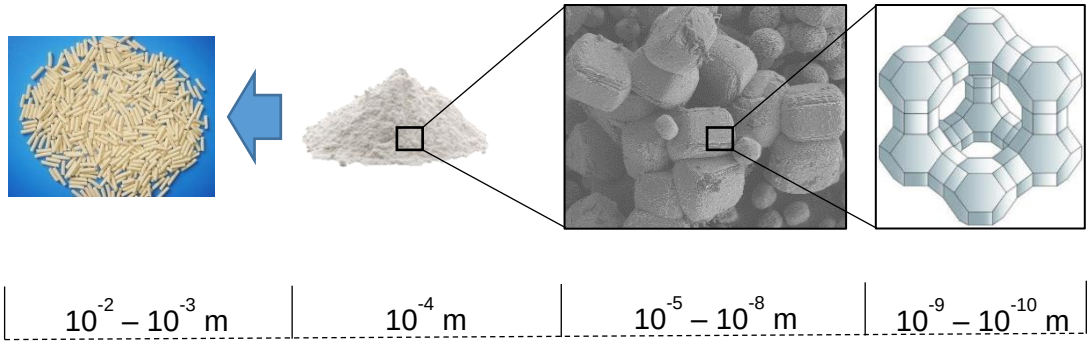

Figure I: Les différentes échelles d'observation de la zéolithe - des extrudés à sa structure cristalline

Dans les applications industrielles, à grande échelle, l'utilisation des poudres conduit à des problèmes de performance, car la poudre présente une résistance mécanique médiocre qui peut endommager ou dégrader le catalyseur, créant ainsi des particules fines et des débris à la sortie du réacteur. En plus, la perte de charge est aussi un paramètre extrêmement important à prendre en compte pour le bon fonctionnement de l'équipement. Comme conséquence, une mise en forme de la zéolithe est très souvent réalisée, par exemple sous forme de pastilles ou d'extrudés, habituellement en ajoutant un liant. Le liant choisi pour cette Thèse a été la boehmite qui se transforme en alumine par calcination. L'alumine possède une structure cristalline, une stabilité thermique élevée et une acidité de Lewis

[1] a) Harding, R. H.; Zhao, X.; Qian, K.; Rajagopalan, K.; Cheng, W. C. *Ind. Eng. Chem. Res.* **1996**, *35*, 2561–2569; b) Wang, G.; Gao, J. Sen; Xu, C. M. *Pet. Sci. Technol.* **2004**, *22*, 1581–1594.

modérée. Ensuite, la mélange des poudres peut être extrudé sous la forme souhaitée, séché pour évaporer l'eau utilisée dans l'homogénéisation du mélange, et calciné à haute température pour conférer les propriétés mécaniques et texturales appropriées.

Néanmoins, le transfert de masse au sein de la particule de la zéolithe peut être gêné par la présence du liant, comme cela a été décrit en détails dans le **Chapitre 2**. En associant cette caractéristique à la diffusion moléculaire lente connue dans les pores de la zéolithe[2], plusieurs stratégies visant à améliorer le transport moléculaire dans les catalyseurs zéolithiques réels ont été développées, telles que: (i) l'introduction de la porosité hiérarchisée dans la structure de la zéolithe; (ii) le dépôt de cristaux de zéolithe sur des monolithes; (iii) des stratégies sans liant. La première approche a été largement étudiée, avec des résultats montrant des améliorations de la conversion et de la durée de vie du catalyseur dans de nombreuses réactions acido-catalysées. [3] Toutefois, ce procédé peut mener à une perte partielle de la sélectivité de forme, de la cristallinité et le changement de l'acidité et, par conséquent, à une performance différente du matériau originel. En plus, il existe un manque de compréhension de l'influence réelle du liant sur les zéolithes présentant une porosité hiérarchisée, malgré les importantes contributions du groupe de Pérez-Ramirez.[4] Plusieurs approches pour préparer des macrostructures de zéolithes ont été reportées comme le 'coating' de zéolithes sur des structures céramiques / métalliques.[5] Par ailleurs, de nombreux chercheurs ont également réussi à éviter l'utilisation de liants pour résoudre les problèmes rencontrés au cours du processus de mise en forme. Ils se sont basés sur la compression de poudres de zéolithe, l'utilisation de matrice amovible, la transformation hydrothermale de gels d'aluminosilicate denses et l'utilisation de matériaux amorphes pré-formés.[6] Cependant, ces méthodologies restent à l'échelle du laboratoire en raison de l'utilisation de techniques et de matériaux coûteux ou peu pratiques, et ne permettent guère de prédire une utilisation industrielle dans un proche avenir.

Depuis la révolution industrielle du 19e siècle, la consommation de combustibles fossiles a atteint un tel niveau que la société moderne a pour principale préoccupation que notre planète Terre puisse faire face à nos demandes croissantes (Figure II). Les énergies renouvelables ont la capacité de satisfaire toutes nos demandes sans s'éteindre. Cependant, dans de nombreux cas, cette technologie n'a pas

[2] a) Chaikittisilp, W.; Suzuki, Y.; Mukti, R. R.; Suzuki, T.; Sugita, K.; Itabashi, K.; Shimojima, A.; Okubo, T. *Angew. Chemie - Int. Ed.* **2013**, *52*, 3355–3359; b) White, R. J.; Fischer, A.; Goebel, C.; Thomas, A. *J. Am. Chem. Soc.* **2014**, *136*, 2715–2718; c) Verboekend, D.; Pérez-Ramírez, J. *ChemSusChem* **2014**, *7*, 753–764; d) Nuttens, N.; Verboekend, D.; Deneyer, A.; Van Aelst, J.; Sels, B. F. *ChemSusChem* **2015**, *8*, 1197–1205; e) Zhang, H.; Hu, Z.; Huang, L.; Zhang, H.; Song, K.; Wang, L.; Shi, Z.; Ma, J.; Zhuang, Y.; Shen, W.; et al. *ACS Catal.* **2015**, *5*, 2548–2558.

[3] a) Louis, B.; Ocampo, F.; Yun, H. S.; Tessonnier, J. P.; Pereira, M. M. *Chem. Eng. J.* **2010**, *161*, 397–402; b) Milina, M.; Mitchell, S.; Michels, N. L.; Kenvin, J.; Pérez-Ramírez, J. *J. Catal.* **2013**, *308*, 398–407; c) Zhao, J.; Wang, G.; Qin, L.; Li, H.; Chen, Y.; Liu, B. *Catal. Commun.* **2016**, *73*, 98–102; d) Zhang, W.; Ming, W.; Hu, S.; Qin, B.; Ma, J.; Li, R. *Materials.* **2018**, *11*, 2–11.

[4] a) Mitchell, S.; Michels, N. L.; Kunze, K.; Pérez-Ramírez, J. *Nat. Chem.* **2012**, *4*, 825–831; b) Gueudré, L.; Milina, M.; Mitchell, S.; Pérez-Ramírez, J. *Adv. Funct. Mater.* **2014**, *24*, 209–219; c) Michels, N. L.; Mitchell, S.; Milina, M.; Kunze, K.; Krumeich, F.; Marone, F.; Erdmann, M.; Marti, N.; Pérez-Ramírez, J. *Adv. Funct. Mater.* **2012**, *22*, 2509–2518; d) Michels, N. L.; Mitchell, S.; Pérez-Ramírez, J. *ACS Catal.* **2014**, *4*, 2409–2417.

[5] a) Zamaro, J. M.; Ulla, M. A.; Miró, E. E. *Chem. Eng. J.* **2005**, *106*, 25–33; b) Buciuman, F. C.; Kraushaar-Czarnetzki, B. *Catal. Today* **2001**, *69*, 337–342; c) Ivanova, S.; Louis, B.; Madani, B.; Tessonnier, J. P.; Ledoux, M. J.; Pham-Huu, C. *J. Phys. Chem. C* **2007**, *111*, 4368–4374; d) Mitra, B.; Kunzru, D. *J. Am. Ceram. Soc.* **2008**, *91*, 64–70.

[6] a) You, Z.; Liu, G.; Wang, L.; Zhang, X. *Microporous Mesoporous Mater.* **2013**, *170*, 235–242; b) Mańko, M.; Vittenet, J.; Rodriguez, J.; Cot, D.; Mendret, J.; Brosillon, S.; Makowski, W.; Galarneau, A. *Microporous Mesoporous Mater.* **2013**, *176*, 145–154; c) Fakin, T.; Ristić, A.; Mavrodinova, V.; Zabukovec Logar, N. *Microporous Mesoporous Mater.* **2015**, *213*, 108–117.

encore atteint son stade de maturité, caractérisée par des coûts élevés pour sa mise en œuvre et sa maintenance, en particulier dans les pays en voie de développement. En conséquence, d'autres solutions plus rapides et déjà disponibles sont nécessaires pour gagner du temps jusqu'à ce que chaque pays soit converti à 100% en énergies renouvelables.

Le méthanol est une molécule simple qui a la polyvalence pour être utilisée comme combustible propre biodégradable ou comme matière première pour la production de nombreux composants de base pétrochimiques. Il peut être synthétisé à partir de gaz de synthèse obtenu à partir du reformage à la vapeur du gaz naturel ou de la gazéification du charbon. Il peut également être obtenu à partir de la biomasse, appelée ainsi biométhanol. [7]

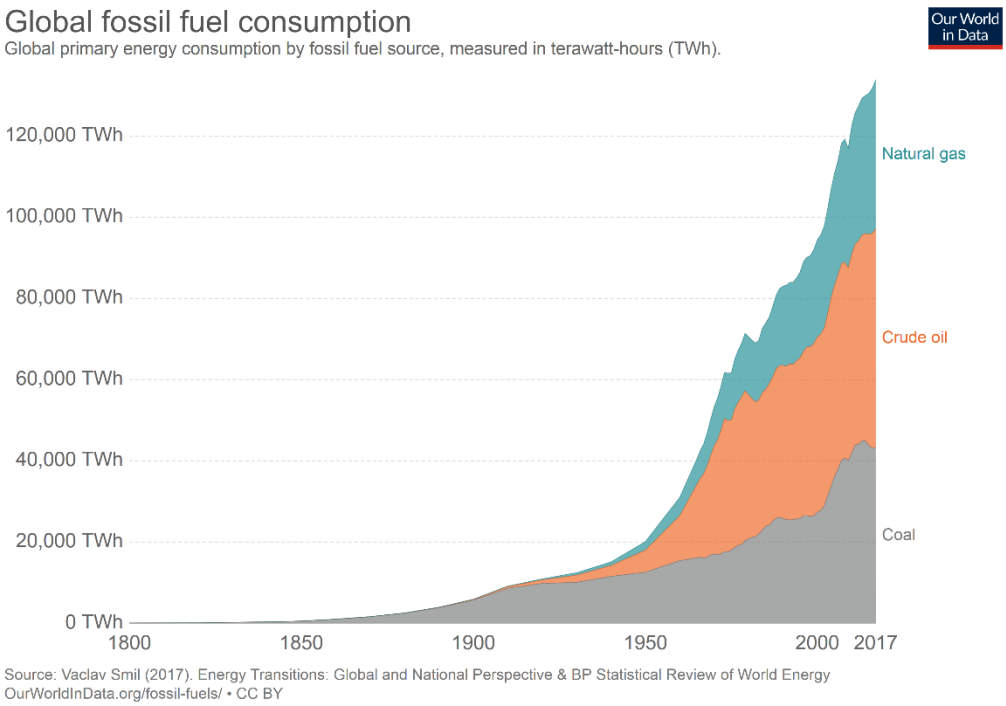

Figure II: Évolution de la consommation de combustibles fossiles dans le monde au cours des deux derniers siècles

Le **Chapitre 5** décrit un bon usage de cette molécule dans la conversion du méthanol en hydrocarbures (MTH).[8] Les principaux produits obtenus comprennent une large gamme de molécules, dont les principaux sont le méthane, l'éthylène, le propylène, les butylènes, l'isobutane et les hydrocarbures en C_{5+} contenant également des composés aromatiques constituant la fraction essence. Cette réaction représente également un intermédiaire – diméthyl éther (DME) – où deux molécules de méthanol se déshydratent pour former du DME, puis de nombreuses réactions supplémentaires pour produire des hydrocarbures. Comme on le voit clairement, la production d'éthylène et de propylène (utilisés dans les plastiques, les résines, les gels, etc.) et d'essence provenant d'une source autre que le pétrole promet déjà une moins grande dépendance vis-à-vis des combustibles fossiles.

[7] *Methanol Institute*. https://www.methanol.org/production/ (accessed May 22, 2019)
[8] Sapre, A. Conversion of Methanol to Olefins in a Tubular Reactor with Light Olefin Co-Feeding. U.S. Patent, 4 590 320, **1986**.

Deux autres réactions sont décrites dans le même chapitre: craquage du n-butylcyclohexane et craquage du n-hexane, ayant comme produits principaux le méthane, l'éthane, l'éthylène, le propane, le propylène, les butylènes, les hydrocarbures saturés et oléfines C_5, naphténiques et aromatiques. Ces deux réactions de craquage catalytique s'avèrent être un outil utile pour caractériser le catalyseur acide solide. En analysant la sélectivité des produits, on peut tirer certaines conclusions concernant l'influence de l'acidité et de la porosité sur la performance catalytique. En plus, pour représenter les processus d'adsorption en utilisant les zéolithes, l'adsorption du toluène a été effectuée. L'adsorption de composés organiques volatils (COV) revêt un intérêt primordial dans l'industrie, car elle est rejetée dans de nombreux types de gaz résiduaires. Cette famille de composés, le toluène étant le COV typique et nocif, constitue une menace pour l'atmosphère et la santé humaine en raison de sa haute toxicité.

Considérée comme la plus importante de cette Thèse, la diffusion des molécules dans la zéolithe est présentée dans le **Chapitre 6**. Cette étude révèle une importance capitale pour une meilleure compréhension des phénomènes de transfert de masse dans les zéolithes. Les premières études réalisées dans ce chapitre étaient la mesure de la masse du matériau sous flux continu d'une molécule sonde. La courbe de saturation permet de déterminer la diffusivité effective. Plus tard, la technique sophistiquée de RMN à gradient de champ pulsé a été développée et des résultats plus précis ont été obtenus, où les propriétés d'auto-diffusivité des molécules dans les cristaux de zéolithes ont été déterminées. La chromatographie gazeuse en phase inverse est également venue compléter ces études en étant réalisée à des températures plus élevées et dans des conditions de flux continu.

Finalement, un projet 'extra' est décrit dans le **Chapitre 7** qui traite de la valorisation des bio-déchets dans la synthèse de zéolithes ZSM-5. Un travail précédent de Louis et al. a montré la possibilité de diminuer le rapport Si/Al jusqu'à 8, le plus bas jamais obtenu avant ce travail, en utilisant de la bagasse de canne à sucre. Dans ce travail, nous avons vérifié que l'ajout de lignine modifiée permettait d'obtenir une zéolithe ZSM-5 ayant un rapport Si/Al < 4, qui a été confirmé par différentes techniques de caractérisation.

II. Préparation des zéolithes mises en forme à porosité hiérarchisée et caractérisation

Après une brève présentation de toutes les méthodes, procédures et techniques de caractérisation décrites au **Chapitre 3**, le **Chapitre 4** présente une nouvelle stratégie pour améliorer la diffusivité effective par introduction de la porosité dans le liant. Ceci a été fait par l'ajout des agents porogènes au mélange de zéolithe et boehmite, qui était humidifié par une solution d'acide nitrique 4% et extrudé dans une extrudeuse portable. Après calcination, les agents sont éliminés par combustion, laissant des vides dans la structure de l'alumine.

Les images de microscopie électronique à balayage (MEB) représentées dans la Figure III montrent la présence des macropores dans les échantillons Catal_10Propyl et Catal_P123, qui ont été préparés avec Propyltex et Pluronic P123, respectivement. Le premier présente des macropores d'environ 4 µm mesurés par porosimétrie d'intrusion de mercure, alors que Catal_P123 présente des mésopores d'environ 11 nm déterminés par N_2 adsorption-désorption et des macropores plus larges que 50 µm. Ces macropores ont été attribués à une faible efficacité d'extrusion de la pâte qui conduit à des

fissures n'ayant aucun liant avec la présence d'agent porogène. D'autres échantillons ont par ailleurs été préparés avec succès et étudiés en profondeur au cours de ce chapitre.

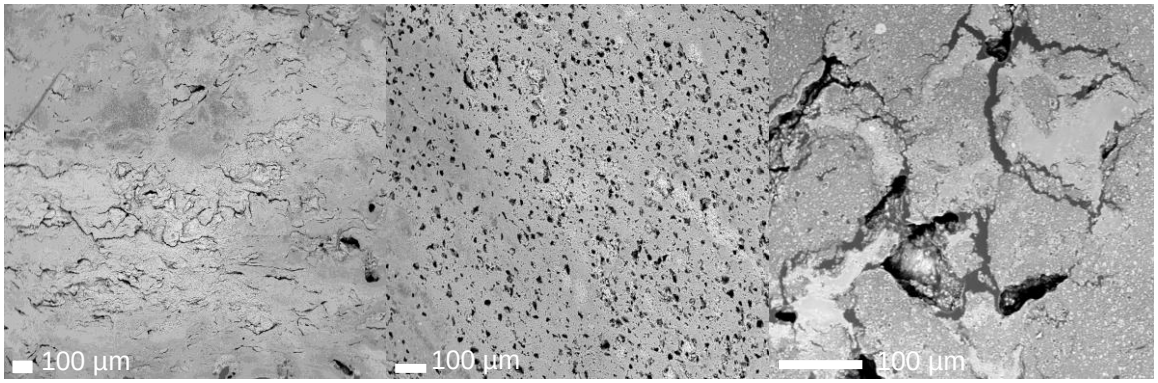

Figure III: Microscopie électronique à balayage (MEB) de Catal_ref (gauche), Catal_10Propyl (milieu) et Catal_P123 (droite)

Fait intéressant, l'augmentation de la quantité de Propyltex utilisée pendant l'extrusion augmente également le volume macroporeux et la densité des macropores (Catal_5Propyl et Catal_20Propyl). Grâce à cela, nous avons également pu étudier l'effet du volume des macropores lors de la diffusion.

En plus, la zéolithe commerciale, CBV3020E, a été traitée avec une solution de NaOH (appelée BAW) pour éliminer certaines espèces siliciques de la structure, laissant des mésopores pouvant améliorer la diffusion des molécules dans le catalyseur. Cette méthode est la plus utilisée actuellement en raison de son faible coût et de sa simplicité. Dans cette Thèse, ce type de traitement a été réalisé pour être comparé avec les échantillons étudiés. Les isothermes d'adsorption-désorption d'azote confirment BAW comme un matériau mésoporeux ayant des pores d'environ 12 nm. Cet échantillon a aussi été extrudé pour simuler la procédure industrielle (BAW_ext).

Différentes techniques de caractérisation ont été effectuées pour vérifier l'influence de cette méthode d'extrusion dans les caractéristiques des échantillons. Étonnamment, il a été vérifié que l'acidité et la stabilité mécanique (deux caractéristiques très importantes dans une réaction à l'échelle industrielle) étaient maintenues et, par conséquence, seule la porosité additionnelle pouvait influencer la performance des catalyseurs.

III. Les réactions catalytiques

Les échantillons ont été testés dans trois différentes réactions catalytiques pour vérifier l'impact de la porosité additionnelle et elles sont décrites dans le **Chapitre 5**. La conversion du méthanol en hydrocarbures n'a pas une limitation de diffusion du réactif mais éventuellement celle de ses produits, spécialement les précurseurs du coke, peuvent être influencés de manière significative par la présence des méso- et/ou des macropores. Les différents types d'échantillons préparés ont été testés dans cette réaction et la conversion du méthanol et du DME en fonction du temps de réaction est présentée dans la Figure IV.

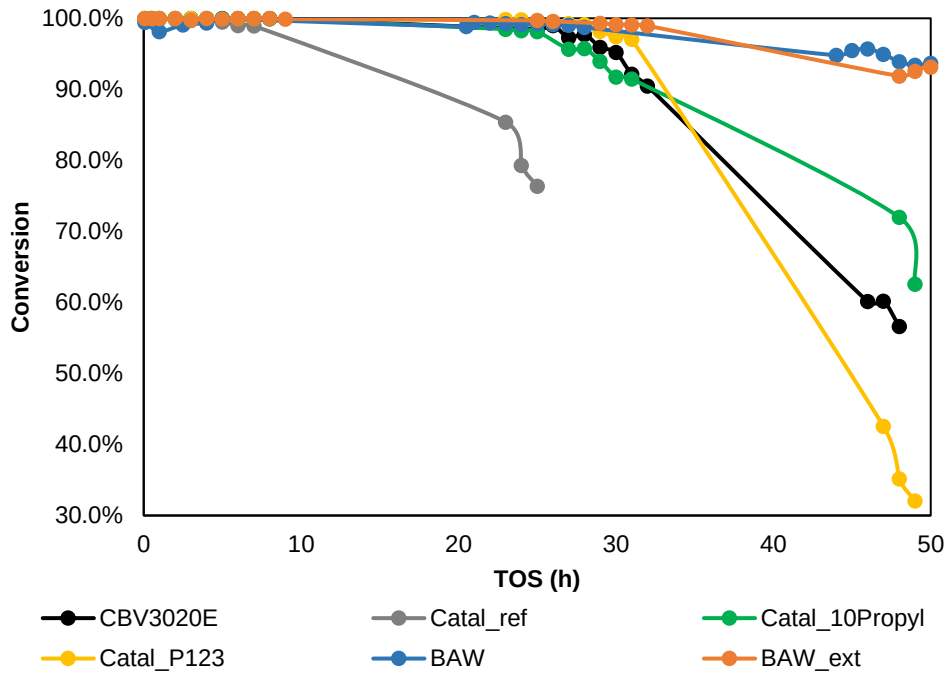

Figure IV: Conversion du méthanol et DME en hydrocarbures en fonction du temps d'opération (time-on-stream TOS)

Comme prévu, la conversion du méthanol diminue fortement quand la zéolithe est extrudée (en comparant CBV3020E à Catal_ref). Ceci peut être expliqué par une diminution de la diffusivité effective causée par un blocage des pores de la zéolithe par le liant. En fait, les échantillons Catal_10Propyl et Catal_P123 démontrent une durée de vie proche de la zéolithe commerciale, ce qui représente une amélioration notoire (3 fois supérieure) par rapport à l'extrudé de référence.

En ce qui concerne les échantillons avec différentes quantités de Propyltex, on peut observer une augmentation de la durée de vie du catalyseur. Il semblerait que l'augmentation du volume macroporeux induit une forte influence dans la performance catalytique pour cette réaction. Ceci peut être attribué à la capacité des précurseurs du coke à quitter facilement la structure et, probablement, de s'adsorber dans les macropores proches de la maille élémentaire de la zéolithe.

Par ailleurs, BAW a montré également une augmentation de la durée de vie, néanmoins, aucune perte de cette dernière n'a été vérifiée après l'extrusion (BAW_ext). Il semble que l'introduction de mésopores dans la zéolithe augmente la diffusion des molécules, comme décrit dans la littérature.

D'autre part, la sélectivité des produits est plus sensible au changement de l'acidité, toutefois un changement significatif de l'acidité des échantillons n'a pas pu être vérifié dans le chapitre ultérieur. Du coup, les sélectivités ont été maintenues, sauf après le traitement basique de la zéolithe commerciale. En effet, une augmentation de la formation de composés possédant 5 carbones ou plus, de l'éthylène, et une diminution de la sélectivité en propylène a été observée. Néanmoins, après l'extrusion, les sélectivités demeurent similaires à celles des zéolithes extrudées.

Les réactions modèles sont très utiles pour vérifier l'impact des caractéristiques des catalyseurs, comme par exemple, le cracking du n-hexane et le cracking du n-butylcyclohexane. Le premier est seulement dominé par les sites acides, ce qui permet d'être très sensible au changement de l'acidité du matériau. Le second, une fois que la molécule réactive présente un diamètre plus large que les pores de

la zéolithe, est fortement limité par la diffusion. Dans ce cas, cette réaction peut donner des informations concernant la porosité du matériau et son inter-connectivité.

Tableau I: Vitesse initiale et sélectivités de la réaction du cracking du n-hexane

Échantillon	Taux [mmol/(g.min)] (conversion)	$\frac{\text{Propane}}{\text{Propylène}}$	Sélectivité (%)		Sites actives Brønsted (µmol/g)[b]
			Ethène	Propylène	
Boeh_ext	31 (1.4%)[a]	0.90	5	12	-
Catal_ref	522 (6.7%)	0.94	8	27	223
Catal_10Propyl	529 (6.7%)	0.90	8	26	287
Catal_P123	452 (5.7%)	0.89	9	26	218

a) expérience réalisée avec 35 mg d'échantillon; b) obtenu par intégration du pic d'haute température de l'analyse d'adsorption de NH_3.

La Table I montre des vitesses initiales de craquage du n-hexane des échantillons et le ratio entre le propane et le propylène. Ces deux restent inchangés pour tous les échantillons. Comme vu précédemment, les techniques de caractérisation n'ont suggéré aucun changement de l'acidité et celui-là peut maintenant être confirmé par la similarité des performances des échantillons dans cette réaction de catalyse acide.

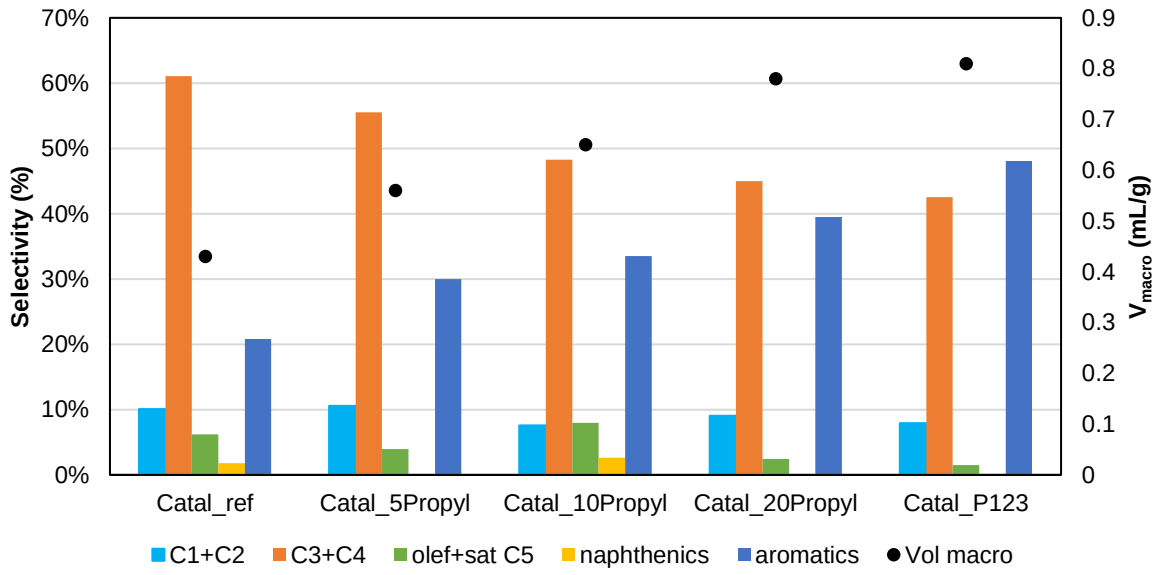

Figure V: Sélectivités des produits du cracking du n-butylcyclohexane des échantillons. Le volume macroporeux est représenté par les points noirs.

Par contre, la Figure V montre clairement une augmentation de la sélectivité en produits plus lourds au détriment des oléfines légères dans le craquage du n-butylcyclohexane. Cette tendance suit l'augmentation du volume macroporeux déterminé par intrusion au mercure décrit dans la Section II. Il

semble que la présence des macropores facilite l'arrivée du réactif à la structure zéolithique, permettant de rester plus longtemps au sein de la microporosité et de reconvertir les oléfines en aromatiques.

IV. L'étude de la diffusivité effective

Une partie très importante de cette Thèse consistait en l'étude de la diffusion dans les catalyseurs industriels. L'impact de la présence des méso- et/ou macropores dans la diffusion a été déterminé par trois techniques différentes et complémentaires. Les résultats ont été détaillés dans le **Chapitre 6**.

La méthode gravimétrique, une technique pionnière de l'étude de la diffusion dans la zéolithe, a été réalisée par mesure d'adsorption de toluène. En suivant la masse du catalyseur pendant le processus en fonction du temps (Figure VI), on peut déterminer la diffusivité effective par la partie linéaire des courbes d'adsorption. Par contre, les résultats ne peuvent être comparés entre les poudres et les extrudés car l'équation mathématique prend en compte le diamètre de la particule. En tout cas, une amélioration de la diffusivité effective des échantillons Catal_10Propyl et Catal_P123 en comparaison avec Catal_ref est vérifiée, prouvant un effet positif de la présence des méso- et macropores dans la diffusion des molécules au sein de l'extrudé.

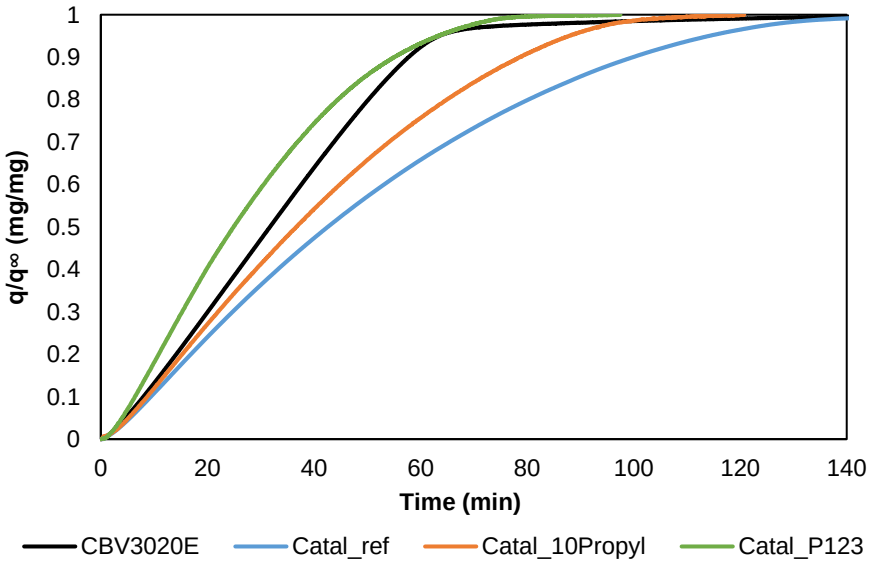

Figure VI: Courbes d'adsorption du toluène dans les différents échantillons

Les échantillons ont été également analysés par la RMN à gradient de champ pulsée (PFG-NMR), une technique plus sophistiquée qui détermine l'auto-diffusivité d'une molécule sonde au sein du matériau. Fait intéressant, deux mécanismes de diffusion du toluène ont été détectés, pouvant être attribués à la structure de la zéolithe et à la structure de l'alumine. En plus, les échantillons présentant des macropores présentent une valeur de diffusivité effective 1000 fois plus élevée que Catal_ref, montrant une amélioration de la diffusion comme observée par la méthode gravimétrique.

Cette technique apporte une observation microscopique tandis que la méthode gravimétrique traite d'une observation macroscopique. En conséquence, on ne peut pas espérer pouvoir comparer les

valeurs absolues obtenues par les deux techniques pour les mêmes échantillons. Cela est visible dans le Tableau II qui reporte les différentes valeurs de diffusivité effective obtenues par les trois techniques.

Pour terminer, la chromatographie gazeuse en phase inverse (IGC) a été réalisée avec du benzène à haute température. A nouveau, une tendance similaire entre les deux autres techniques est observée, avec Catal_10Propyl et Catal_P123 montrant une diffusivité effective plus élevée que Catal_ref.

Tableau II: Valeurs de la diffusivité effective des échantillons obtenus par les trois différentes techniques

Échantillons	**D_{eff} (m^2/s)**		
	Méthode Gravimétrique	**PFG-NMR**	**IGC**
CBV3020E	1.5×10^{-13}	16×10^{-9}	-
Catal_ref	4.8×10^{-11}	1.2 et 7.9×10^{-9}	1.0×10^{-4}
Catal_10Propyl	6.6×10^{-11}	3.0 et 1700×10^{-9}	1.8×10^{-4}
Catal_P123	9.8×10^{-11}	0.9 et 4.0 et 19×10^{-9}	1.5×10^{-4}

V. Conclusion

Cette Thèse a montré une nouvelle stratégie pour augmenter la diffusivité effective par introduction de macropores et/ou mésopores. La caractérisation en profondeur a permis d'identifier les types et tailles des pores créés par l'ajout d'agents porogènes.

Les échantillons ont montré une amélioration significative de la performance dans la conversion du méthanol en hydrocarbures, en particulier sur la durée de vie du catalyseur. Ceci a été expliqué par une augmentation de la diffusivité effective qui a été déterminée à l'aide de trois différentes techniques.

Ce travail devrait permettre de développer de nouvelles stratégies pour la compréhension de l'influence du liant dans la performance de la zéolithe et le rôle de la diffusion au sein de catalyseurs industriels, tels que des extrudés. Ainsi, les réactions catalytiques étudiées en laboratoire devraient pouvoir être extrapolées aux catalyseurs industriels dans des réacteurs réels.

Chapter 1 – Introduction

Abstract

In this chapter, the concept of zeolite is firstly defined along with some generalities and details regarding their structure, main features and properties, and their mainly industrial applications.

Then, the next part is focused on the zeolite applications concerning the ZSM-5 zeolite type, namely toluene adsorption for the removal of volatile organic compounds and the methanol-to-hydrocarbons reaction.

Finally, a brief introduction to diffusion concepts and corresponding measurement techniques are presented.

1.1 What are zeolites?

1.1.1. The natural “boiling” stone

The term zeolite was defined in 1756 by the Swedish mineralogist Axel Fredrik Crønstedt[9] after heating the mineral stilbite with a blowpipe flame, while observing the release of large amounts of steam previously adsorbed in the material[10]. In fact, the term “zeolite” comes from the Greek ζέω (*zéo*), meaning “to boil” and λίθος (*líthos*), meaning “stone”, literally the boiling stone. The raw zeolite is naturally formed in Earth’s crust due to rapid crystallization under particular hydrothermal and geological conditions. Normally, the deposition of volcanic ashes is necessary at high-pH saline groundwater during several million years. However, natural zeolites are rarely pure, often being contaminated by other minerals, metals, quartz, or other zeolite structures. For this reason, their industrial application is excluded, being mostly used in geological museums, jewellery, or as construction materials. Figure 1 presents Thomsonite zeolite crystals to illustrate the natural occurrence of those amazing materials.

Figure 1: Thomsonite - one of the rarest natural zeolite[11]

Fortunately, zeolites can also be synthesized. In 1948, Richard M. Barrer reported the first definitive synthesis of zeolite mineral mordenite and a later-identified KFI framework[12]. His work inspired Robert M. Milton from the Linde Division of Union Carbide Corporation to study zeolite synthesis, discovering few commercially important types, such as LTA and FAU (X and Y). After that, the number of classified zeolites has grown, counting with more than 230 different structures. Although millions of theoretical structures have been predicted to be stable, only a few of them have been synthesised yet. The International Zeolite Association (IZA) database keeps record of the existent structures but also approves newly discovered ones, where a trivial three-letter code is attributed based on a characteristic X-ray powder diffraction pattern and chemical composition. For example, the code LTA corresponds to Linde zeolite A, FAU to molecular sieves with a faujasite topology (e.g., zeolites X, Y) and MFI to ZSM-5 and silicalite topologies.

[9] Cronstedt, A. F. *Akad.Handl.Stockholm* **1756**, *18*, 120–130.
[10] Colella, C.; Gualtieri, A. F. *Microporous Mesoporous Mater.* **2007**, *105*, 213–221.
[11] *The mineral and Gemstone kingdom*. http://www.minerals.net/mineral/thomsonite.aspx (accessed Jun 10, 2018)
[12] a) Barrer, R. M. *J. Chem. Soc.* **1948**, 127–132; b) Barrer, R. M.; Riley, D. W. *J. Chem. Soc.* **1948**, 133–143; c) Barrer, R. M. *J. Chem. Soc.* **1948**, 2158–2163.

1.1.2. Nomenclature and topologies

Zeolites are crystalline microporous materials with a framework constructed by the association of TO_4 tetrahedra, most commonly $[SiO_4]^{4-}$ or $[AlO_4]^{5-}$ linked by shared oxygen atoms (Figure 2). Other elements such as B, P, Ge, Ga, Ti or Fe may also be incorporated, and the presence of water and cations (alkalis, alkaline-earths) allows the compensation of the negative charges generated by the presence of aluminium ions, giving birth to the general formula:

$$\mathbf{M_x(AlO_2)_x(SiO_2)_y.zH_2O}$$

with **M** being the cation compensating the negatively charged framework (as H^+ or Na^+), **y/x** the Si/Al ratio (SAR), and **z** the number of molecules of water. Based on the Löewenstein's rule[13] Al-O-Al linkages are not allowed and, therefore, y/x ≥ 1.

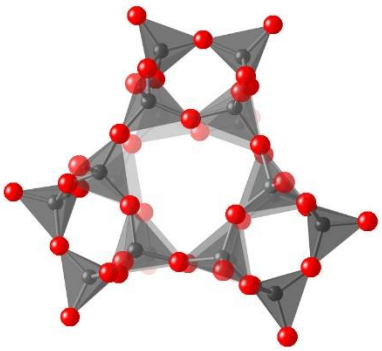

Figure 2: TO4 tetrahedra self-assemblies to create a 3D structure

This particular geometry is what makes the zeolites so important in the industry, since it originates cavities, referred to as cages, of molecular dimension. Typically, these zeolite pores have diameters up to 2 nm[14] and so-called micropores, and due to their openings of regular size, they can let small molecules pass straight through but trap larger ones acting like molecular sieves, leading to other common name for zeolites. Normally these pores are filled with water and other cations, but they can be exchanged with other positively charged ions.

1.2 Zeolite properties and applications

Since the 1950s, the industry has been extensively employing synthetic zeolites in a wide range of processes. Their high surface area (>300 m^2/g) and high thermal stability allow these materials promising performances and great potential to new processes or improvement of existing ones. Up to now, one can describe three main applications of zeolites: ion-exchange, adsorption and heterogeneous

[13] Loewenstein, W. *Am. Mineral.* **1954**, *39*, 92–96.
[14] Ertl, G.; Knözinger, H; Schüth, F.; Weitkamp, J. Physical Properties - Microporosity. In *Handbook of Heterogeneous Catalysis Vol 1*, Wiley VCH, **2009**, 729.

catalysis. For each feature, different zeolites properties enter in action, showing the great versatility of this subject.[15]

1.2.1 Ion-exchange

As seen previously, there are cations present in the void channels and cages of the zeolitic structure to compensate the negative charge of the framework induced by the aluminium tetrahedra. As their interactions result from ionic bonds, these cations have the capacity to easily exchange with others. Ideally, the exchange capacity of a zeolite is as much higher as the quantity of aluminium atoms present in the structure, which in more depth, can be translated to low Si/Al ratios. It is then easy to understand the possibilities that this characteristic can provide. The bigger application in this area consists in water softening: the alkali metals such as sodium or potassium are replaced by “hard” ions of calcium and magnesium from the water (Figure 3). Plus, LTA zeolite has effectively replaced the phosphates, such as sodium tripolyphosphates, in detergent builders, that are responsible for eutrophication of water bodies.

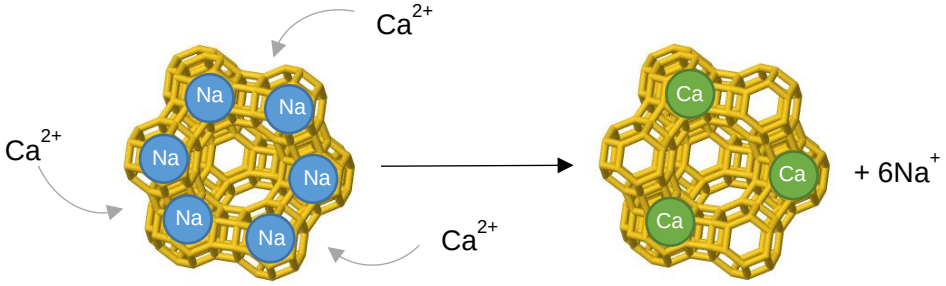

Figure 3: Scheme of water softening, where there is an exchange of the cations of sodium by calcium

In a more dramatic case, zeolite has also proved itself to be a powerful material to solve many humankind problems, for example, the removal of radioactive isotopes, particularly $^{137}Cs^{+}$, released during the nuclear accidents in Chernobyl and Fukushima that contaminated water and soils.[16] It is important also to mention that this ability has made great progress in the organic chemistry field, where the zeolite is doped with metal ions that actively participate in the reactions.[17]

1.2.2 Adsorption – Separation

Besides being able to exchange, the cations of zeolites can link with other molecules by dipolar interactions. In this way, when a molecule enters the pores and cages of the framework, it can be adsorbed and depending on the strength of this adsorption that comes associated with the nature of the cation, the molecule may or may not be easily removed.

[15] Corma, A. *Chem. Rev.* **1995**, *95*, 559–614.
[16] a) Bosch, P.; Caputo, D.; Liguori, B.; Colella, C. *J. Nucl. Mater.* **2004**, *324*, 183–188. b) Kobayashi, T.; Ohshiro, M.; Nakamoto, K.; Uchida, S. *Ind. Eng. Chem. Res.* **2016**, *55*, 6996–7002.
[17] a) De Vos, D. E.; Dams, M.; Sels, B. F.; Jacobs, P. A. *Chem. Rev.* **2002**, *102*, 3615–3640; b) Olmos, A.; Louis, B.; Pale, P. *Chem. - A Eur. J.* **2012**, *18*, 4894–4901; c) Olmos, A.; Rigolet, S.; Louis, B.; Pale, P. *J. Phys. Chem. C* **2012**, *116*, 13661–13670; d) Chassaing, S.; Bénéteau, V.; Pale, P. *Catal. Sci. Technol.* **2016**, *6*, 923–957.

Moreover, as described before, different structures of zeolites possess different dimensions of pores and cages. This is a big deal in adsorption – separation processes. In fact, many molecules have sizes bigger than the micropores and channels of the zeolitic framework, and so recalling the common name *molecular sieves*, which means that some can pass straight through the zeolite channels while the diffusion of others will be either hindered or even blocked. Associating this feature with the interactions between the cations, there are several processes of adsorption and/or separation where zeolites are implemented, as for example:

- Air drying: for hydrophilic zeolites, the water from a gas stream is easily adsorbed, while hydrophobic zeolites have the tendency to repulse the water molecules. This hydro-affinity can be tuned, i.e., lower Si/Al ratio leads to hydrophilic zeolites whilst a lower content of aluminium cations increases the hydrophobicity.[18]
- Removal of CO_2: innovative strategies have been developed to remove this greenhouse - effect gas from a stream before being released to the atmosphere. The molecule of CO_2 has higher affinity towards alkali ions such as, lithium, calcium, sodium, being adsorbed on the active sites of the cages and channels of the framework.[19]

1.2.3 Heterogeneous Catalysis

Although only one third of zeolite consumption is applied in heterogeneous catalysis, this area remains the most valuable (around 55% of the global market).[20] Their strong acidity can be compared with commonly applied mineral acids, when the cation compensating the negative charge of the framework is a proton. In this case, zeolites act as a Brønsted acid which associated with high temperatures can behave as a *superacid*, able to catalyse numerous reactions, involving sometimes non-classical carbocationic intermediates (carbonium-type).

Moreover, the capacity of adsorption – desorption seen above is crucial for many reactions where the interaction between reactants is necessary, i.e., both molecules will adsorb near each other in the framework of the zeolite and transform into a more stable product. Also, in case of isomerisation and propagation reactions, the size of the pores or cages where the molecule is present greatly influences the final shape of the product. For example, in the case of xylene isomerisation, it has been showed that the small pores of ZSM-5 form preferentially *para*-xylene over *meta*- (favoured thermodyamically) and *ortho*-xylene since the first has better diffusivity through the zeolite channels.

The main applications are centred in petrochemical industry, being the Fluid Catalytic Cracking (FCC) process that accounts the most, but also oil refining, fine chemistry and synfuel production. In these processes, after a determined time, the zeolite deactivates due to the deposition of coke in the structure that blocks the access of the molecules to the acid sites, thus diminishing the catalyst lifetime. Fortunately,

[18] a) Ülkü, S.; BalkÖse, D.; Baltacloglu, H.; Yildlrim, A. *Dry. Technol.* **1992**, *10*, 475–490; b) Atuonwu, J. C.; Straten, G. Van; Deventer, H. C. Van. *J. Chem. Eng. Trans.* **2011**, *25*, 111–116.
[19] a) Frantz, T. S.; Ruiz, W. A.; Da Rosa, C. A.; Mortola, V. B. *Microporous Mesoporous Mater.* **2016**, *222*, 209–217; b) Resasco, J.; Chen, L. D.; Clark, E.; Tsai, C.; Hahn, C.; Jaramillo, T. F.; Chan, K.; Bell, A. T. *J. Am. Chem. Soc.* **2017**, *139*, 11277–11287.
[20] Rhodes, C. Zeolites and World Markets http://ergobalance.blogspot.com/2006/05/zeolites-and-world-markets.html (accessed Jun 11, 2018).

the zeolite can often be regenerated during several cycles by combustion of the coke, recovering nearly its original performance, bringing great economic advantages.

1.3 Acid catalysis

As seen in the previous section, catalysis remains the main application of zeolites. A very important group of this domain is acid catalysis that often begins with the addition of a proton (Brønsted acid). These acids can be hydrofluoric acid, phosphoric acid, toluenesulfonic acid, polystyrene acid, heteropoly acid, and the most important for this Thesis, zeolites. The latter, when exchanged to its proton form, exhibits the ability to exchange protons by acting as a Brønsted acid site and it is widely used in hydrocarbon reactions, such as, Friedel-Crafts alkylation and acylation, aromatization, isomerization, cracking, …

It has been frequently assumed that the activation mechanism for these reactions over acid zeolites occurs by the addition of a proton or hydride abstraction, which implicates the formation of a carbocation in either transition state or intermediate, named 'classical' carbenium or 'non-classical' carbonium.[21] Alkylcarbenium ions contain a tri-coordinated positively charged C-atom, the three substituents being alkyl groups or H-atoms, while alkylcarbonium ions contain a penta-coordinated positively charged C-atom, having the same type of substituents. These species account with different formation mechanisms, briefly described in Figure 4 to Figure 9.

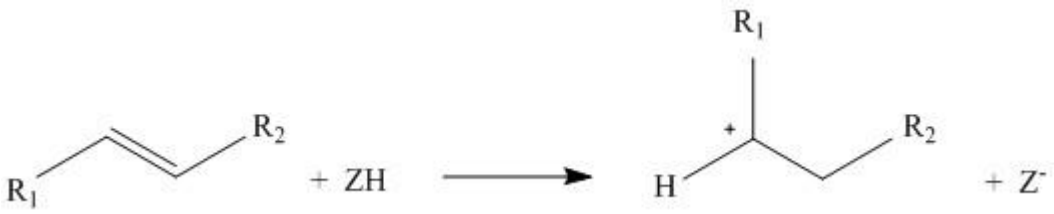

Figure 4: Protonation of an alkene - formation of an alkylcarbenium ion

A proton from the catalyst is added to an alkene molecule forming a tri-coordinated C-atom that is positively charged and compensated by the negative charge of the zeolite framework. This type of activation involves bimolecular reaction, which means that the zeolite pores have to be large enough.[22]

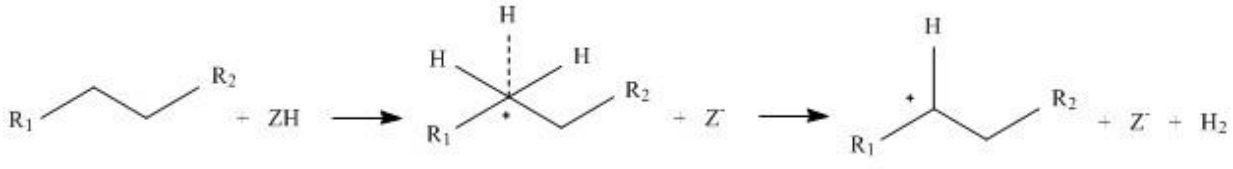

Figure 5: Protonation of an alkane - formation of an alkylcarbonium ion

[21] a) Olah, G.A. et al., *Superacids*, Wiley – Interscience: New York, **1995**; b) Olah, G.A. et al., *Hydrocarbon Chemistry*, Wiley & Sons: New York, **1987**; c) Jacobs, P.A., *Carboniogenic Activity of Zeolites*; Elsevier: New York, **1977**.
[22] Kotrel, S.; Knözinger, H.; Gates, B. C. *Microporous Mesoporous Mater.* **2000**, *35–36*, 11–20.

The protonation of an alkane occurs by the transfer of a proton from the active site to a saturated molecule. As the alkylcarbonium formed is unstable, it can be transformed into a smaller alkylcarbenium ion by protolytic cracking that consists in the removal of an electroneutral molecule (an alkane or molecular hydrogen).[23] This type of activation involves monomolecular reaction, which is favoured by zeolites containing medium pores that allow this reaction but hinders the bimolecular reaction (hydrogen transfer) due to steric limitations.

Figure 6: Hydride abstraction - formation of an alkylcarbenium ion

The formation of an alkylcarbenium in a saturated molecule consists in the abstraction of a hydride from the electroneutral molecule. This mechanism involves acidic centres of the Lewis type (Z) that bind to the hydride.[24]

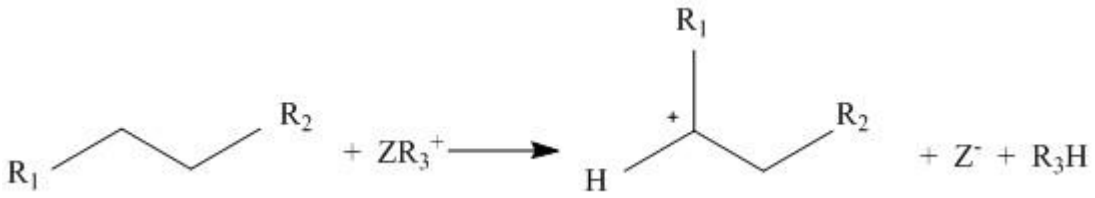

Figure 7: Hydride transfer - alternative formation of an alkylcarbenium ion

Afterwards, if a carbenium ion R^+ is adsorbed on the surface within the zeolite pore, a hydrogen transfer from a saturated molecule can occur, and the latter will be desorbed from the zeolite, being favoured by medium pores. In this way, alkylcarbenium ions act as chain carriers.[24]

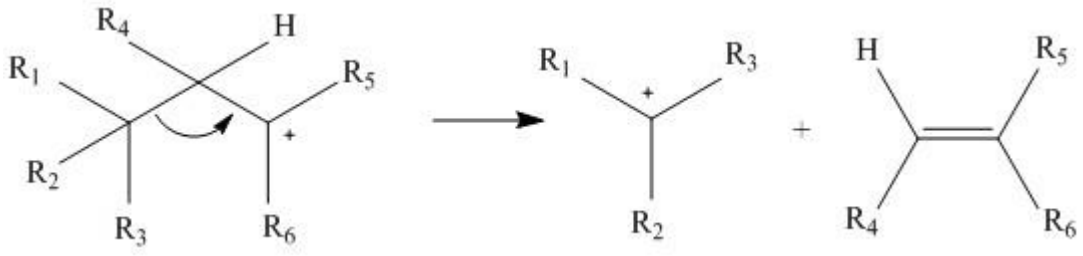

Figure 8: β-scission - formation of a smaller alkylcarbenium and an olefin

[23] Haag, W.O. and Dessau, R.H., in Proceed. 8th International Congress on Catalysis, Dechema, Frankfurt am Main, **1984**, vol II, p. 305
[24] Marcilly, C. In *Acido-Basic Catalysis: Application to Refining and Petrochemistry vol 1*, IFP: Publications, **2005**.

A large alkylcarbenium can promote a β-scission, i.e., breaking C-C or C-H bond located in the β position with respect to the carbocation. This reaction leads to the formation of a smaller alkylcarbenium ion and an olefin.[24]

Figure 9: Oligomerization - formation of larger alkylcarbenium ions

Finally, the active sites can be covered by molecules blocked insidde the pores and thus behaving like tertiary alkylcarbenium ions. In this case, C-C bonds are favoured, generating the alkylation of these tertiary alkylcarbenium ions with alkenes giving rise to larger alkylcarbenium ions.[25] This exothermic reaction is responsible for the coke formation.[24]

1.4 The methanol-to-hydrocarbons reaction

Since the industrial revolution in 19th century, the consumption of fossil fuels has reached such levels that the main concern of modern society is if our planet Earth is able to cope with our increasing demands. Many scientists believe that in the next century, at the current production rate, the reserves of fossil fuels will run out. This is very concerning! Without even considering the consequences of the release of millions of tons of carbon dioxide into the atmosphere by burning all fossil fuels, it is clear that the next generations will face great challenges in terms of energy production and management. Nowadays, everything runs under electricity: the computer where this manuscript is being written, the light, the heating and all the equipment that allowed the obtaining data presented in this Thesis, even the bus busily running in the city.

But let's not panic yet. Due to the hard work of brilliant scientists and engineers, a reliable solution comes closer to us than we hopefully think. These saviours given by the name of renewable energies, have the capacity to fulfil all our needs without extinguishing. Ours *frenemies* fossil fuels have, literally, their days counted. However, in many cases, this technology still remains at an immature state, characterized by high costs for both implementation and maintenance, particularly in developing countries.[26] As a consequence, other faster and already available alternatives are needed to buy us more time until every country is 100% converted to renewable energies. Methanol can be our solution. Indeed, this simple molecule has the versatility to be used as clean-burning, biodegradable fuel or as a feedstock for the production of numerous key petrochemical building blocks, such as foams, resins, plastics, paints,

[25] a) Andy, P.; Gnep, N.; Guisnet, M.; Benazzi, E.; Travers, C. *J. Catal.* **1998**, *173*, 322–332; b) Blomsma, E.; Martens, J. A.; Jacobs, P. A. *J. Catal*. **1995**, *155*, 141–147; c) Blomsma, E.; Martens, J. A.; Jacobs, P. A. *J. Catal.* **1996**, *159*, 323–331.

[26] a) Mustapa, S. I.; Leong Yow Peng; Hashim, A. H. Issues and Challenges of Renewable Energy Development: A Malaysian Experience. *Proc. Int. Conf. Energy Sustain. Dev. Issues Strateg. (ESD 2010)* **2010**, No. July 2010, 1–6; b) Horbach, J.; Chen, Q.; Rennings, K.; Vögele, S. *Environ. Innov. Soc. Transitions* **2014**, *10*, 42–58.

polyesters, and a variety of health and pharmaceutical products (Figure 10). It can be synthesized from syngas which is obtained from steam reforming of natural gas or coal gasification. It can also be obtained from biomass, being so-called bio-methanol. But more interestingly, the carbon neutral cycle allows the production of methanol without the use of any fossil fuel. This can be achieved by converting CO_2 and hydrogen, the first being captured from the atmosphere or from factories and plants, while hydrogen may be obtained from the excess of energy from renewable sources.[27]

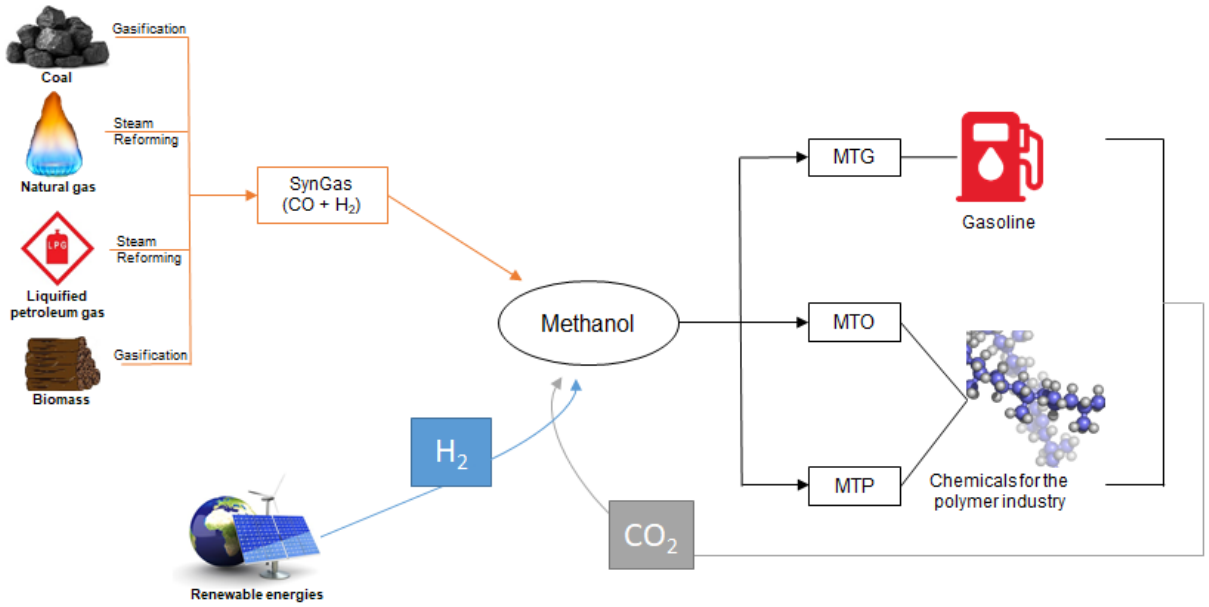

Figure 10: Production route and economy of methanol until its conversion into raw chemicals

This Thesis outlines one great use of this molecule in the methanol-to-hydrocarbons (MTH) reaction, with olefins and gasoline as main products. As clearly seen, the production of ethylene and propylene (monomers of polymers used in plastics, resins, gels, etc) and gasoline from a source other than oil, already promises a lower dependence on fossil fuels, thus a step further towards the fossil-fuels-free-society journey.

The MTH reaction was discovered by Mobil Oil company in the 70's while attempting to prepare methyl-tert-butylether (MTBE) from the conversion of methanol and isobutene over acidic ZSM-5 zeolite. From there on, its success led to the commercialization of the process with an increasing interest from the academics. The main products obtained comprise a large range of molecules, being the most important methane, ethylene, propylene, butylenes, isobutane, and C_{5+} hydrocarbons containing also aromatics that constitute the gasoline fraction. This reaction also accounts with dimethyl ether (DME) intermediate – two molecules of methanol dehydrate to form DME, followed by further reaction to produce hydrocarbons. The early stages of MTH process consist in a direct mechanism where methanol is firstly adsorbed onto a Brønsted acid site of the zeolite. After a long-lasting debate, it is now admitted that it undergoes carbonylation through dehydrogenation of methanol / formaldehyde to form direct C-C bond-containing surface acetate species. The production of hydrocarbons is now accepted as a result of an

[27] Olah, G. A. *Angew. Chemie - Int. Ed.* **2005**, *44*, 2636–2639.

auto-catalytic process through olefins chain growth and cracking, called hydrocarbon-pool mechanism, being initiated by the formation of methyl acetate coming from the surface acetate species, later proved by Weckhuysen et al. by spectroscopic evidence.[28] This term was first mentioned by Mole et al.[29] that showed the hydrocarbon species present on the catalyst were essential to guarantee methanol conversion into olefins, and thus acting as co-catalysts during the reaction. Shape selectivity plays a key role here, as the final products to leave the zeolite structure strongly depend on their capacity to diffuse through the pores and channels. From there on, several authors have provided new insights on the MTH mechanism being described in Haw's review[30] and drawn by Lesthaeghe et al.[31]

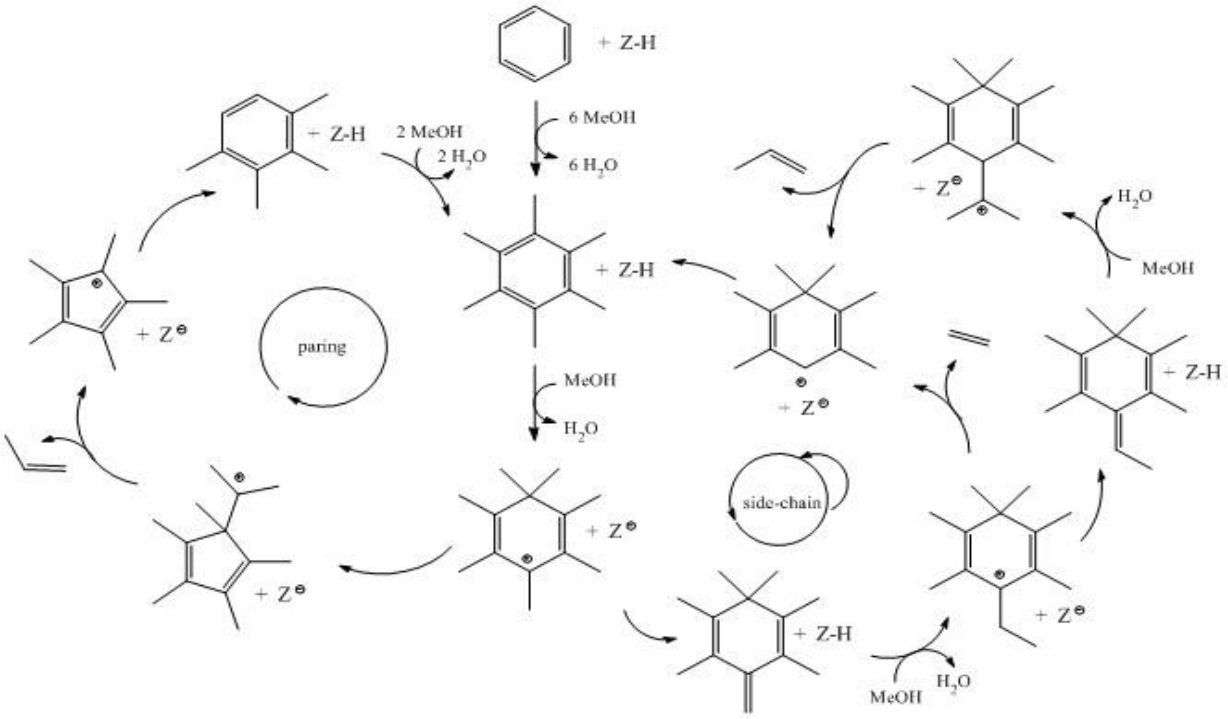

Figure 11: The aromatics-based hydrocarbon pool re-drawn from Lesthaeghe et al. The zeolite is represented by Z-H or Z^- in its protonated or deprotonated form, respectively.

The main components of the hydrocarbon pool have been assessed, i.e., polymethylated phenyl rings, which are quite similar to ordinary coke (Figure 11). These compounds, trapped within the zeolite pores, serve as co-catalysts where methanol is added, and olefins are eliminated in a (closed) catalytic cycle. This is why different zeolite structures provide different products range in the same way that the same type of zeolite with different acidity (changes in the Si/Al ratio) or different pore size (additional

[28] a) Chowdhury, A. D.; Houben, K.; Whiting, G. T.; Mokhtar, M.; Asiri, A. M.; Al-Thabaiti, S. A.; Basahel, S. N.; Baldus, M.; Weckhuysen, B. M. *Angew. Chemie - Int. Ed.* **2016**, *55*, 15840–15845; b) Liu, Y.; Müller, S.; Berger, D.; Jelic, J.; Reuter, K.; Tonigold, M.; Sanchez-Sanchez, M.; Lercher, J. A. *Angew. Chemie - Int. Ed.* **2016**, *55*, 5723–5726; c) Chowdhury, A. D.; Paioni, A. L.; Houben, K.; Whiting, G. T.; Baldus, M.; Weckhuysen, B. M. *Angew. Chemie - Int. Ed.* **2018**, *57*, 8095–8099.
[29] Mole, T.; Bett, G.; Seddon, D. *J. Catal.* **1983**, *84*, 435–445.
[30] Haw, J. F.; Song, W.; Marcus, D. M.; Nicholas, J. B. *Acc. Chem. Res.* **2003**, *36*, 317–326.
[31] a) Lesthaeghe, D.; Horré, A.; Waroquier, M.; Marin, G. B.; Van Speybroeck, V. *Chem. - A Eur. J.* **2009**, *15*, 10803–10808; b) Lesthaeghe, D.; VanderMynsbrugge, J.; Vandichel, M.; Waroquier, M.; VanSpeybroeck, V. *ChemCatChem* **2011**, *3*, 208–212.

mesoporosity, for instance) results in different products selectivity.[32] Many scientists have dedicated their research to better understand the characteristics that are able to influence the catalytic activity of zeolites, that may be summarized into:

- Acidity – strong active sites are directly related to the aluminium present in the framework. Indeed, a structure with higher Si/Al ratio (less aluminium) exhibits fewer active sites able to further react, forming bigger molecules leading to coke formation[33];
- Diffusion – either by crystal size, pore size or pore interconnectivity. As seen, the stabilization of the intermediates of the hydrocarbon pool is strongly influenced by the shape selectivity of the zeolite. Higher diffusion capacity may lead to lower deactivation rate as bigger molecules are eluted from the cages[34] or enhance certain product selectivity by proper design of the crystal[35].

With the financial crisis in 2007 marking the great technological development of China[36], the demand for light olefins increased along with an increase in oil prices. These two factors are the main drivers of the search for alternative methods for ethylene and propylene production. Methanol-to-hydrocarbons remains a promising alternative process for light olefins production due to its higher selectivity towards propylene when selecting the right zeolite type. Methanol can be produced from alternative feedstocks by steam reforming of natural gas, gasification of coal or biomass, with the addition of low CO_2 emissions.

1.5 Diffusion

1.5.1 Concept

One of the fundamental phenomena in nature is the particle movement caused by the particles' thermal energy. This process is called diffusion and it occurs in any type of matter, with different scales and lengths.

In zeolite structures and catalytic bodies, the active sites are mainly located within the cavities and pores of micro- and nanometre size, which means that the molecules have to diffuse through them to reach and accumulate close to the active site. If this mass transport (physical process) is slower than the chemical reaction, the catalytic system is less efficient than expected and the full potential of the catalyst particle is not explored. This phenomenon is called diffusional limitation, and the prevention of its occurrence is of paramount interest to scientists when designing the catalytic system.

Depending on the types of pores where the mass transport occurs, the mechanism of diffusion is different (Figure 12). In the micropores region ($0.5 \leq x \leq 2$ nm), there is mainly interaction between the

[32] Hwang, A.; Le, T. T.; Shi, Z.; Dai, H.; Rimer, J. D.; Bhan, A. *J. Catal.* **2019**, *369*, 122–132.
[33] Asadi, M.; Thalkhoncheh, A. M. Propylene via Methanol over Aluminosilicate Catalyst. Canadian Patent, 2642395, **2010**.
[34] a) Mitchell, S.; Michels, N. L.; Kunze, K.; Pérez-Ramírez, J. *Nat. Chem.* **2012**, *4*, 825–831; b) Choi, M.; Na, K.; Kim, J.; Sakamoto, Y.; Terasaki, O.; Ryoo, R. *Nature* **2009**, *461*, 246–249; c) Wu, L.; Degirmenci, V.; Magusin, P. C. M. M.; Szyja, B. M.; Hensen, E. J. M. *Chem. Commun.* **2012**, *48*, 9492–9494.
[35] Losch, P.; Pinar, A. B.; Willinger, M. G.; Soukup, K.; Chavan, S.; Vincent, B.; Pale, P.; Louis, B. *J. Catal.* **2017**, *345*, 11–23.
[36] William H. Overholt (**2010**) China in the Global Financial Crisis: Rising Influence, Rising Challenges, The Washington Quarterly, 33:1, 21-34, DOI: 10.1080/01636600903418652

molecule and the pore walls, being dominated by intracrystalline diffusion. In mesopores ($2 \leq x \leq 50$ nm), the diffusion path is larger than the micropores which allows the molecules to be transported more freely but still with occasional interruptions by sorption on the walls (Knudsen diffusion). In macropores (≥ 50 nm), the diffusion is characterized by the free motion of molecules in the gas phase, with no interactions with the zeolite pores walls.

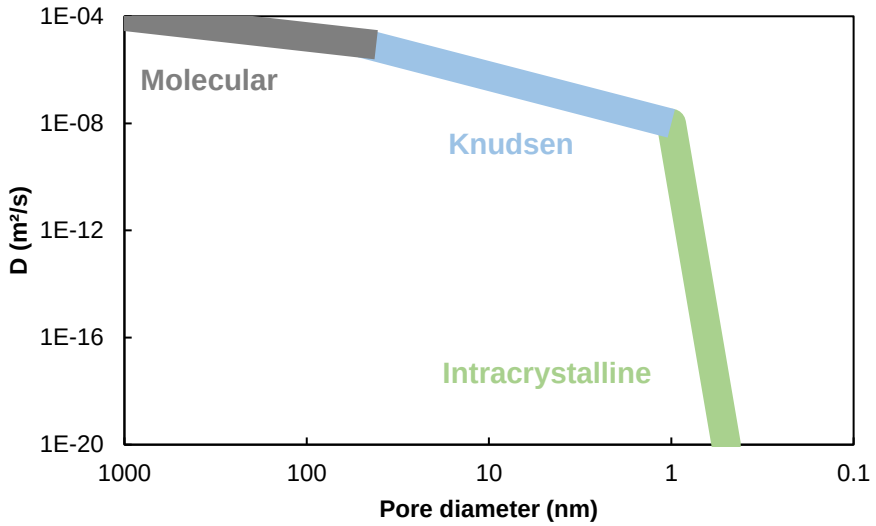

Figure 12: Different diffusion regimes in the zeolite pores. Adapted from Hartmann et al.[37]

In a heterogeneous catalytic reaction, it occurs first the mass transfer of the reactant from the bulk fluid to the external surface of the catalyst particle. Then, the reactants should diffuse from the external surface into and through the pores and channels of the pellet to reach the catalytic surface of the pores, where the reaction occurs (Figure 13).

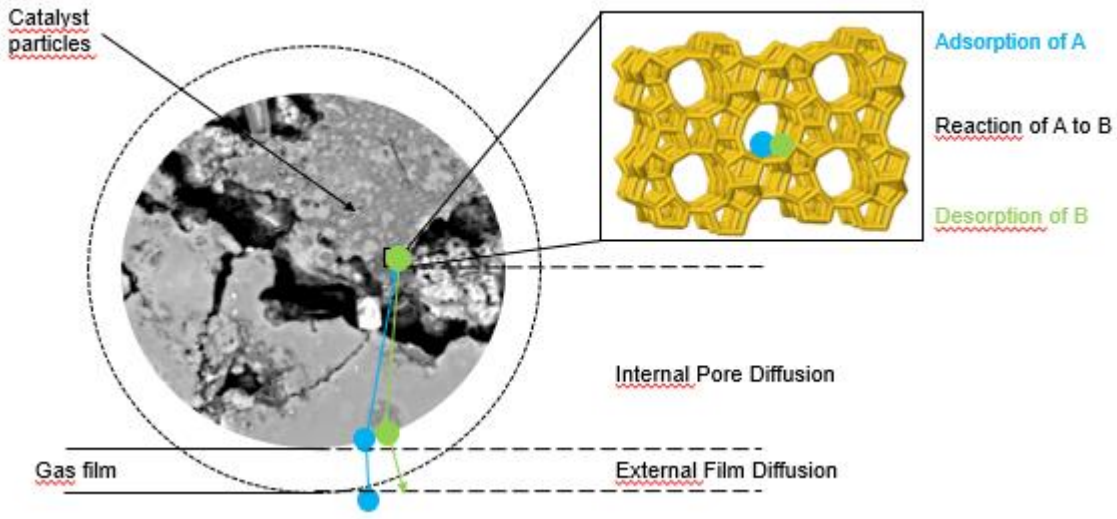

Figure 13: Mass transfer and reaction steps for a catalyst particle

[37] Hartmann, M.; Machoke, A. G.; Schwieger, W. *Chem. Soc. Rev.* **2016**, *45*, 3313-3330.

However, the pores in the pellet are not straight and cylindrical but rather a network of tortuous paths interconnecting the different pores present in the catalyst particle with varying cross-sectional areas. As it is difficult and non-practical to describe diffusion within each and every one of the paths individually, it is necessary to define an effective diffusivity coefficient to describe the average diffusion at any position of the pellet with radius R. This is related with the effectiveness factor (ranging from 0 to 1) that relates the importance of diffusion in the reaction rates, and described by Eq. 1.

$$\eta = \frac{reaction\ rate\ on\ catalyst\ particle}{reaction\ rate\ without\ limitations} = \frac{r}{r^*} = \frac{3}{\varphi}\left(\frac{1}{tanh\varphi} - \frac{1}{\varphi}\right) \quad (1)$$

being φ the Thiele modulus, that can be described for a first-order reaction on a spherical catalyst particle by:

$$\varphi = \frac{d_p}{2}\sqrt{\frac{k_i \rho S}{D_{eff}}} \quad (2)$$

with d_p as the diameter of the catalyst particle; k_i the constant for the intrinsic rate; ρ the density of the catalyst particle; S the specific surface area of the catalyst particle; and D_{eff} as the effective diffusion of the reactant on the pores.

When the particle diameter becomes very small, φ decreases and the effectiveness factor η approaches 1 indicating that the reaction is limited by itself only. However, when the Thiele modulus φ is large (~30), the effectiveness factor becomes small (η << 1), and the reaction is diffusion-limited within the catalyst particle (Figure 14).

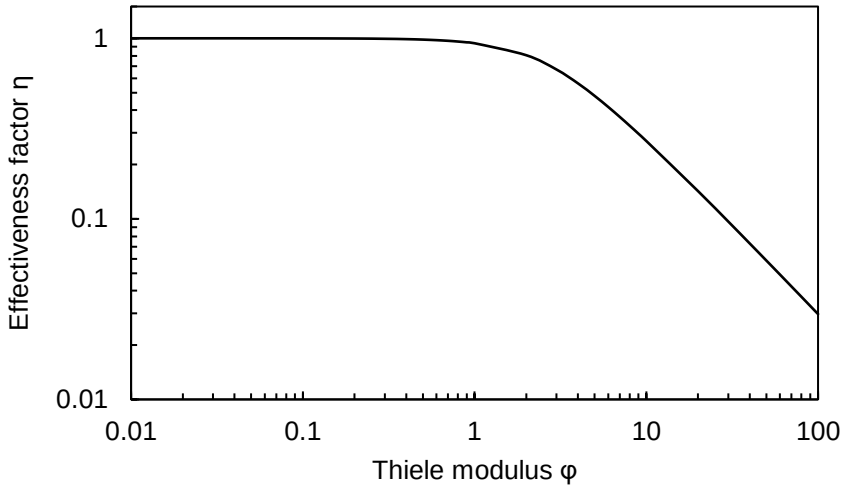

Figure 14: Effectiveness factor plot for first-order reaction on spherical catalyst particles

To increase the overall reaction rate, several strategies can be implemented, such as:

1. Decrease the catalyst particle (case of fluidized particles or trilobes vs extrudates);
2. Decrease the density of the particle (it can be achieved by increasing the porous volume);
3. Increase the effective diffusivity (by increasing porosity and macroporosity).

1.5.2 Measurement techniques

The effective diffusivity in porous materials has been assessed by different techniques throughout the decades. The methods of diffusion characterization may be divided into two classes: equilibrium and non-equilibrium techniques.[38] The first category occurs when a distinction between different probe molecules is possible as it is the case for pulsed-field gradient (PFG)-NMR. This technique involves the measurement of the molecular displacement, by detection of the phase shift caused by a motion of nuclear spin, in this case ^{1}H, in the presence of an external magnetic field within short time interval. On the other side, the non-equilibrium techniques are characterized by transient or boundary conditions that ensure a stationary state as, for instance, the case of uptake measurements of a given probe molecule adsorbed in a material. However, this technique fails to give a proper understanding of the transport mechanisms within such situations giving rise to further development of the PFG-NMR technique among others.[39] Moreover, uptake rate measurements occur in static conditions and suffer from mass transfer resistance at the external surface area of the zeolite crystals.[38c)] Later on, the inverse gas chromatography (IGC) technique was developed, based on the determination of the diffusion coefficient by concentration gradients and the flow of the carrier gas, mimicking realistic operating conditions such as the fluid catalytic cracking process, or reactions under plug-flow regime. [38a),40] However, the latter macroscopic technique does neither have the capability to distinguish between different types of diffusion mechanisms, nor to consider the total pores present but only the transport-available pores.

1.5.2.1 Gravimetric method

The coefficient of diffusion (the diffusivity) is defined as the factor of proportionality between the flow density and the concentration gradient of the particles species (Fick's first law).

The first studies of molecular diffusion in zeolite were performed by following the rate of adsorption or desorption, after subjecting the sample to a pressure step in the surrounding atmosphere. This technique, nominated gravimetric method, turned out to be controlled not only by intracrystalline diffusion but also sorbate access to the samples, sorbate permeation through the bed of crystallites, mass transport resistances at the external surface of the crystallites and dissipation of the heat of adsorption. This may imply that uptake measurements are controlled by processes different from intracrystalline diffusion, and to deduce it from this technique, it is mandatory to demonstrate that these aspects are negligible or to accurately consider them. If one has to deal with the first case, the intracrystalline diffusion controls the process and there is no significant change in the adsorbate phase concentration. The transient diffusion can then be expressed by Eq. 3, for a spherical particle of radius r.

$$\frac{\partial q}{\partial t} = D_{eff}\left(\frac{\partial^2 q}{\partial r^2} + \frac{2}{r}\frac{\partial q}{\partial r}\right) \tag{3}$$

[38] a) Kärger, J. *Adsorption* **2003**, *9*, 29–35; b) Kärger, J.; Valiullin, R. *Chem. Soc. Rev.* **2013**, *42*, 4172–4197; c) Kärger, J.; Ruthven, D. M. *New J. Chem.* **2016**, *40*, 4027–4048.
[39] a) Galarneau, A.; Guenneau, F.; Gedeon, A.; Mereib, D.; Rodriguez, J.; Fajula, F.; Coasne, B. *J. Phys. Chem. C* **2016**, *120*, 1562–1569; b) Dvoyashkina, N.; Freude, D.; Stepanov, A. G.; Böhlmann, W.; Krishna, R.; Kärger, J.; Haase, J. *Microporous Mesoporous Mater.* **2018**, *257*, 128–134.
[40] Wallenstein, D.; Fougret, C.; Brandt, S.; Hartmann, U. *Ind. Eng. Chem. Res.* **2016**, *55*, 5526–5535.

The initial and boundary conditions for a gravimetric uptake experiment are

$t < 0$, $C = C_0$, $q = q_0$ (independent of r and t)

$t \geq 0$, $C = C_\infty$, $q(r_c, t)$

$t \to \infty$, $C = C_\infty$, $q(r, t)$

$\left.\frac{\partial q}{\partial r}\right|_{r=0} = 0$ for any r

The solution, in terms of the uptake of sorbate by the solid, is given as follows (Eq. 4):

$$\frac{q - q_0}{q_\infty - q_0} = 1 - \frac{6}{\pi^2}\sum_{n=1}^{\infty}\frac{1}{n^2}exp\left(-\frac{n^2\pi^2 D_{eff}t}{r^2}\right) \quad (4)$$

The linear part of the uptake curves can then be expressed by Eq. 5:

$$\frac{q - q_0}{q_\infty - q_0} = \frac{6}{\sqrt{\pi}}\left(\frac{D_{eff}}{r^2}\right)^{1/2}\sqrt{t} \quad (5)$$

1.5.2.2 Inverse Gas Chromatography

The inverse gas chromatography at infinite dilution (IGC) measures the effective diffusivity of a probe molecule in a material based on gas chromatography but where the mobile phase and the stationary phase are inverted. Here, the stationary phase is replaced by the zeolite to be analysed, while the mobile phase consists in a carrier gas (helium) and probe molecules chosen specifically for the study.

The measurements are made by injecting individually and in very small quantities (infinite dilution conditions) each probe molecule together with methane. The latter serves therefore as reference to determine the dead-time of the column (t_{CH4}). By subtracting this value by the retention time of the molecule, one gets access to the time that the molecule was in contact with the stationary phase (t_R). By doing several injections at different gas probe flows and by determining the height equivalent to a theoretical plate [$HETP$ (cm)] under each condition, the results can be represented as a function of the linear velocity of the carrier gas [μ (cm/s)]. This representation corresponds to a curve of van Deemter[41] and can be described by Eq. 6:

$$HETP = A + B/\mu + C\mu \quad (6)$$

This equation contains terms corresponding to different types of diffusion: A = Eddy diffusion; B = longitudinal diffusion; and C = mass-transfer resistance in the stationary phase.

While using high values of carrier gas velocities, the term B/μ becomes negligible and the equation is simplified to:

$$HETP = A + C\mu \quad (7)$$

Where μ can be calculated taking into account the diameter of the column (d_{col}), the flow of the carrier gas (F), the room temperature and the temperature of the column (T_0 and T_{col}, repectively), and the compressibility factor of James-Martin (j), proposed by J. V. Hinshaw[42] in Eq. 8:

[41] van Deemter, J. J.; Klinkenberg, A.; Zuiderweg, F. J. *Chem. Eng. Sci.* **1956**, *5*, 271–289.
[42] Hinshaw, J. V. Measuring Column Flow and Velocity. In *LC.GC Europe*; **2003**.

$$\mu = \frac{4jF}{\pi d_{col}^2}\left(\frac{T_{col}}{T_0}\right) \tag{8}$$

The compressibility factor is obtained by the pressure at the entrance and exit of the column (P_i and P_0,respectively).

$$j = 1.5\frac{\left({}^{P_i}/_{P_0}\right)^2 - 1}{\left({}^{P_i}/_{P_0}\right)^3 - 1} \tag{9}$$

$HETP$ is calculated by the length of the column (L), the variance of the peak (σ) and the corresponding retention time (t_r), taking into account the asymmetry of the chromatograms (Eq. 10):[43]

$$HETP = L\frac{\sigma^2}{t_r^2} \tag{10}$$

Finally, with all the data in hand, the diffusion coefficient (D) can be easily obtained by the relation given by Eq. 11:

$$D = \frac{16}{\pi}\frac{d_m^2}{C}\frac{k}{1+k} \tag{11}$$

where d_m corresponds to the average size of the particles and $k = {}^{(t_R - t_{CH4})}/_{t_{CH4}}$.

1.5.2.3 Pulsed-Field Gradient NMR

Pulsed Field Gradient – Nuclear Magnetic Resonance (PFG-NMR) technique is a suitable tool to study static properties of matter and dynamic properties like self-diffusion, flow and relaxation, being extensively studied during the past decades.[44]

The precession of a proton in a magnetic field is described by the Larmor equation (Eq. 12):

$$\omega_0 = \gamma B_0 \tag{12}$$

γ – gyromagnetic ratio; B_0 – strength of the external static magnetic field

If an additional magnetic field is applied, B_z , the effective frequency becomes:

$$\omega_{eff} = \omega_0 + \gamma B_z \tag{13}$$

if the gradient is constant: $g = \frac{\partial B_z}{\partial z}$, then

$$\omega_{eff} = \omega_0 + \gamma g z \tag{14}$$

The measurement of diffusion implies a pulse magnetic field gradient. This gradient causes the spin in different positions in the samples to process differently. If the spin maintains its position throughout the experiment, it will refocus completely into a spin echo by the pulse sequence. If it changes position, the refocusing will be incomplete, resulting in a decrease in the intensity of the spin echo.

At the first pulse gradient, the phase shift is given by Eq. 15:

$$\emptyset_1 = \emptyset_0 + \int \gamma g z \, dt = \emptyset_0 + \gamma g z_1 \delta \tag{15}$$

[43] Conder, J. R. *Encyclopedia of Separation Science*; Academic Press: Detroit, **2000**.
[44] a) Hahn, E. L. *Phys. Rev.* **1950**, *80*, 580–594; b) Stejskal, E. O.; Tanner, J. E. *J. Chem. Phys.* **1965**, *42*, 288–292; c) Slichter, C. P. *Principles of Magnetic Resonance*; Springer-Verlag: Berlin, **1996**; d) Levitt, M. H. *Spin Dynamics*; John Wiley and Sons, **2002**.

z_1- position of the spin

After the second pulse:

$$\emptyset_2 = \emptyset_0 + \gamma g \delta (z_1 - z_2) \quad (16)$$

A typical measurement of a self-diffusion consists in acquiring a set of spectra employing to different values of the field gradient strength, g, or the length of the gradient pulse, δ, while the other parameters are kept constant. The decay of the echo intensity will be given by Eq. 17:

$$\Psi = {}^{I}/_{I_0} = exp\left[-\gamma^2 \delta^2 g^2 D_{eff}\left(\Delta - \frac{\tau}{2} - \frac{\delta}{3}\right)\right] \quad (17)$$

Δ- observation time (time interval between the gradient pulses); τ- time interval between the last radio-frequency pulse and the spin echo (echo time).

The effective diffusivity is obtained from the slope of the echo attenuation curves $ln\Psi = f(g^2)$, and the spectra are treated by DOSY software.

1.6 Conclusions

In the different sections of this chapter, it was presented the zeolite catalyst and why it has become so relevant in industrial processes. Its characteristics, such as, crystallinity, microporosity and acidity where carefully described in order to understand the main roles that participate in a heterogeneous catalytic reaction. In fact, different reactions were presented where zeolite is widely used due to its outstanding performance. There, it was seen a very important concept, the effective diffusivity, and how strongly it can influence the outcome of the reaction using zeolites.

With this in mind, this Thesis makes an important connection between academic and industrial research. Indeed, zeolites have been widely studied and several strategies have been proposed in order to increase their performance in many applications. However, the majority of these studies have focused only in powder zeolites having little interest in industry. In the following chapters, it will be presented the work performed on zeolite technical bodies, moreover, the attempt to understand and improve the effective diffusivity in this type of materials.

Chapter 2 – Literature background

Abstract

Herein, the literature background on the zeolite shaping technology currently implemented is carefully reviewed. The different strategies, the materials used, as well as the interactions between the binder and the zeolitic structure are presented.

Then, the main drawbacks of the shaping technology on zeolite are reminded. An innovative strategy, being later on detailed in the Thesis, attempts to solve the diffusion limitations associated to this process. A literature overview is given herein regarding those aspects.

This chapter can be found in Bingre et al., *Catalysts* **2018**, *8*, 163.

2.1 The shaping technology

Concerning heterogeneous reactions, these processes involve the use of fixed-bed or fluidized-bed reactor technologies. Fluidized-bed reactors are required for processes like fluid catalytic cracking (FCC) and oxychlorination of ethane to chloroethane, for instance, where it is necessary to lift the catalyst material in its fluid state. Although synthetic zeolites are obtained in the form of a fine powder, the crystallites are too small to be used directly in such kind of reactor technology. In this way, the catalyst is shaped by spray-drying methods to give birth to abrasion-resistant particles of 60 to 100 µm in diameter. Additionally, in cases where the process requires a fixed-bed reactor technology, the major problem relies on the fact that powder exhibits poor mechanical strength that can lead to damage or degradation of the catalyst, thus creating fines and debris at the reactor outlet. Indeed, the presence of small particles can lead to dramatic consequences on both the reactions and the equipment. The required mechanical strength may be conferred by shaping the zeolite, for example in a pellet or extrudate form: the best choice being conditioned by hydrodynamic considerations (Figure 15). Hence, mass and heat transfer limitations and pressure drop issues have to be fixed to perfectly design the reactor. The final material should possess significant physical strength and, therefore, being fracture resistant during loading and transfer. Reactions that are performed in this case are, for example, the reforming of naphtha fraction and toluene disproportionation.

Figure 15: Different industrial catalysts morphologies

The zeolite shaping is usually performed in the presence of a binder or matrix. Common binders are clays, such as kaolin, attapulgite, boehmite, aluminas, and / or silicas or combinations of these materials. These additives have to be added in quantities which are generally higher than 20% in weight to reach the desired mechanical strength, forming a homogeneous and plastic mixture. Then, the latter mix can be extruded into the desired shape, dried to evaporate the water and calcined at high temperatures to confer the targeted mechanical and textural properties. However, one should consider that the high-pressure forming process can alter the physico-chemical properties if the pore size is too large, like mesoporous materials, or if the framework is fragile.

2.1.1 Silica and Alumina Binders

Several studies devoted to the different strategies to produce zeolites extrudates are given in the following paragraphs. First, Perego et al.[45] reported a procedure to design an extruded catalyst based on silica / alumina gel. In this approach, the gel was blended with boehmite or pseudoboehmite prior to the ageing step (occurring after extrusion). To facilitate this extrusion step, methyl cellulose and glacial acetic acid were added. The authors observed a mechanical strength raging from of 90 to 280 kg/cm^2 and a specific area close to 500 m^2/g.

However, the addition of binders can significantly alter the zeolite properties, in terms of structure or acidity. For instance, Chu et al.[46] measured a quasi-inexistent acidity with an activity similar to high silica-containing ZSM-5 zeolite with a Si/Al > 1600 by allowing its reaction with a solid binder in the presence of water. Those binders were materials exhibiting high aluminium content, such as alumina, along with silica, titania, silica-alumina, etc. It was claimed a possible improvement of the activity of crystalline silicate materials with little or no acidity by mixing them with the aforementioned materials for acid catalysis purposes. By considering the influence of active sites, Martin et al.[47] performed a bounding system between HZSM-5 and boehmite. They observed that boehmite, although partially neutralizing Brønsted acid sites, may induce supplementary weak and strong Lewis acid sites. Additionally, the latter boehmite can act as a catalyst for coke formation, preserving the sites of the zeolite activity, thus leading to higher alkene yields in the n-butane cracking reaction.

Wu et al.[48] performed a study to analyse the influence of alumina and silica binders on the acidity of ZSM-5 and Y zeolites. Regarding alumina, an increase in the number of Brønsted acid sites was observed for alumina-bound Y that might be explained by the reaction of free SiO_2 (non-frame silica) present in the zeolite with the binder at high temperature. This phenomenon may either occur during calcination or by an easier insertion of alumina into Y zeolite than ZSM-5. In contrast, Liu et al.[49] observed a decrease in the total acidity after blending ZSM-5 with colloidal silica, due to possible neutralization. Wu et al.[48] also demonstrated, for silica-bound zeolites, particularly for Y zeolite, a general decrease in the total acidity. Although the same phenomenon between silica from the binder and extra-framework species forming new Brønsted acid site occurred, the presence of sodium ions in Ludox HS-40 (silica binder used) may have neutralized them. This was corroborated by Lee et al.[50] after blending HZSM-5 zeolite with silica, alumina, and / or aluminophosphate solution together with hydroxylethylcellulose. Upon testing the samples in the conversion of methanol to propylene, they also reached the conclusion that the best procedure would be the addition of silica or alumina with aluminophosphate solution, conferring high bulk crush strength and similar propylene selectivity to the one achieved over HZSM-5. In those three studies, both pore volume and surface area of the zeolite were observed to diminish after the binder addition.

[45] Perego C, Bassi G, Girotti G. Extruded catalyst based on silica/alumina gel. European Patent, 0 665 055 A1, **1995**.
[46] Chu P, Garwood W. Catalytic composition from reaction of high silica zeolites with binder. US Patent, 4 563 435, **1986**.
[47] Martin, A.; Berndt, H.; Lohse, U.; Wolf, U. *J. Chem. Soc. Faraday Trans* **1993**, *89*, 1277–1282.
[48] Wu X, Alkhawaldeh A, Anthony RG. In *Studies in Surface Science and Catalysis 143*, ed Elsevier, 217–225, **2002**.
[49] Liu, G.; Guo, J.; Meng, F.; Zhang, X.; Wang, L. *Chinese J. Chem. Eng.* **2014**, *22*, 875–881.
[50] Lee, K. Y.; Lee, H. K.; Ihm, S. K. *Top. Catal.* **2010**, *53*, 247–253.

Likewise, Kasture et al.[51] established correlations between BEA zeolite composition containing different percentages of alumina binder along with the shape of the final composite catalyst and the performance in isopropylation of benzene to produce cumene. An increase in the benzene conversion was achieved when the content of alumina was enhanced, being caused by an increase in the total acidity of the catalyst with alumina. The catalyst pellet appeared as an optimal formulation over catalyst extrudates (Figure 16).

Figure 16: Homemade catalyst extrudate

A new concept appeared along with the study of Kong et al.[52] devoted to the inter-crystalline mesoporosity generation by the addition of binders. They observed an increase of mesopores formed by intercrystalline voids of alumina crystallites leading to a better performance of Ni / ZSM-5 zeolite in the hydrodeoxygenation of cyclohexanone. However, it also caused a lower metal dispersion hiding the conversion of this compound, hence leading to set an optimal loading of 30 wt% of the alumina binder. For the same reaction and catalyst, Du et al.[53] reached the same conclusions: the total mesoporous volume and average pore diameter were the highest for an extruded catalyst with alumina, although the surface area and microporous volume diminished after the addition of binders. Pérez-Uriarte et al.[54] while investigating the effects of bentonite and boehmite on the performance of ZSM-5 zeolite in the transformation of DME into olefins, observed that although the BET surface area and microporous volume diminished after the addition of the binders, it conferred a remarkable volume of mesopores and higher acidity, but weak acid strength. This led to high selectivity towards propylene at low conversion.

An alternative for alumina binder has been proposed by several groups consisting in modified pseudo-boehmite by adding P through phosphoric acid to the binder, thus forming an amorphous AlPO phase[55]. Freiding et al. confirmed that aluminium phosphate-bound extrudates exhibit no acidity due to interaction of phosphates species with the acid sites. However, the original acidity could be restored by

[51] Kasture, M. W.; Niphadkar, P. S.; Bokade, V. V.; Joshi, P. N. *Catal. Commun.* **2007**, *8*, 1003–1008.
[52] Kong, X.; Liu, J. *PLoS One* **2014**, *9*, 5–10.
[53] Du, X.; Kong, X.; Chen, L. *Catal. Commun.* **2014**, *45*, 109–113.
[54] Pérez-Uriarte, P.; Gamero, M.; Ateka, A.; Diaz, M.; Aguayo, A. T.; Bilbao, J. *Ind. Eng. Chem. Res.* **2016**, *55*, 1513–1521.
[55] a) Chen, D.; He, L.; Shang, S. *Mater. Sci. Eng. A* **2003**, *348*, 29–34; b) Lee, Y. J.; Kim, Y. W.; Viswanadham, N.; Jun, K. W.; Bae, J. W. *Appl. Catal. A* **2010**, *374*, 18–25; c) Freiding, J.; Patcas, F. C.; Kraushaar-Czarnetzki, B. *Appl. Catal. A* **2007**, *328*, 210–218; d) Freiding, J.; Kraushaar-Czarnetzki, B. *Appl. Catal. A* **2011**, *391*, 254–260.

means of repeated ion-exchange-calcination steps. This characteristic was considered to be essential to study as, in the mechanism of methanol-to-propylene, the key step for an effective conversion of methanol lies in controlling the reaction at the olefin formation stage, where the acidity of the catalyst plays a crucial role. For this reason, the authors analysed the advantages of using aluminium phosphate as a binder to ZSM-5. Although the micropore volume decreased after the addition of the binder it allowed creating a macroporous system in the matrix, which may be beneficial to avoid pore diffusion resistance. Likewise, since no insertion of Al species from the binder into the zeolite framework occurs, it allowed an optimization of the Si/Al ratio. Therefore, the results showed an improved selectivity in C_2-C_4 olefins, particularly towards propylene.

In terms of silica as a binder, its nature (acid, basic or neutral) can strongly influence the acidic properties of the zeolite. Liu et al.[49] observed that HZSM-5 extruded with colloidal silica showed higher acidic properties, but also rapid deactivation attributed to the coke formed over the zeolite catalyst; which may block the acid sites and channels. It could also be attributed to changes in the mesoporous structures during alkali treatment. Whiting et al.[56] suggested that although SiO_2 lacks acid sites able to take part in acid-catalysed processes, its intimate contact with impregnated zeolite can induce solid-state ion exchange, with loss of Brønsted acidity as a result of zeolite framework dealumination.

In contrast, if the objective is to maintain the acidity of the catalyst, the binding of zeolites with silica can be made as shown by Bowes[57] with ZSM-5 zeolite, but Ghosh et al.[58] developed a method for producing Ge-ZSM-5 shaped body with silica binder. In this case, the silica binder was comprised of solid silica and colloidal silica containing other non-silica oxides, such as Al_2O_3, MgO, Fe_2O_3, CaO, etc. The silica binder was used because it is barely acidic, which provides no significant acid-cracking side reaction(s) producing fewer light hydrocarbons, thus resulting in an enhanced selectivity towards higher hydrocarbons. It can be included an extrusion aid of a partially hydrolysed polyvinyl alcohol to the zeolite and binder mixture since it has been shown that this compound greatly enhanced the mechanical or crush strength of the extrudate made from the zeolite and silica binder.

However, this is not viable in the case of bi-functional hydrocracking catalysts where the metal dispersion is known to be crucial. With that in mind, Keville et al.[59] performed the preparation of high-silica Y zeolite with improved resistance to the alumina binder. It involved the zeolite treatment to reduce the amount of silanol groups prior to the blend with alumina binder and water followed by extrusion. In the latter case, Y zeolite with high silica content and high mechanical resistance provided by alumina was obtained. Table 1 presents an overview of alumina and silica binders, their characteristics, and their impact on the overall acidity.

[56] Whiting, G. T.; Meirer, F.; Mertens, M. M.; Bons, A. J.; Weiss, B. M.; Stevens, P. A.; De Smit, E.; Weckhuysen, B. M. *ChemCatChem* **2015**, *7*, 1312–1321.
[57] Bowes E. Extrusion of Silica-rich solids. US Patent, *4 582 815*, **1986**.
[58] Ghosh A, Mihut C, Simmons M. Method of forming zeolite shaped body with silica binder. US Patent, *9 180 441 B2*, **2015**.
[59] Keville K, Timken H, Ware R. Method for preparing catalysts comprising zeolites extruded with an alumina binder. US Patent, *5 500 109*, **1995.**

Table 1: Selected examples of alumina and silica binders, their characteristics, and influence on the zeolite acidity

Reference	Catalyst	Binder	S_{BET} (m^2/g)	Mechanical Strength (kg/cm^2)	Influence on acidity
45	Amorphous silica/alumina	AlO(OH)	608	249 (10wt% binder)	
47	ZSM-5	SiO_2 or AlO(OH)			Maintained with SiO_2, but decreased with AlO(OH)
49	ZSM-5	SiO_2	210-350		Decreased
50	ZSM-5	SiO_2 or AlO(OH)	320-450	1.4 (10wt% SiO_2) – 4.8 [20wt% AlO(OH)]	Decreased
51	BEA	Al_2O_3	400-500		Increased
52	ZSM-5	Al_2O_3	235-275		Decreased
53	ZSM-5	Al_2O_3 or SiO_2 or kaolin	200-260		Decreased
54	ZSM-5	Al_2O_3	200-300		Decreased
55b	ZSM-5	AlPO	315-370		Decreased
55c	ZSM-5	AlPO		81 (25wt% binder) – 907 (75wt% binder)	Maintained after ion-exchange
56	ZSM-5	SiO_2 or Al_2O_3	350		Decreased

2.1.2 New Binders Approaches

Silica and alumina are the most common binders to shape catalyst bodies. They are cheap and expected to induce beneficial effects in the catalytic properties. However, other ways for shaping zeolites have been studied. In 1992, Plee[60] used siliceous earth as a binder, to produce a paste with the zeolite powder together with an aqueous solution formed by the dissolution of hydrated alumina in sodium hydroxide. The shaped zeolite was obtained by means of extrusion, but other methods could also be used to produce agglomerates. The authors assessed the feasibility of this process for A, X and Y zeolites in petrochemistry, for air conditioning in cars or as desiccants in insulating double windows.

Additionally, Timken[61] prepared a method to design titania-bound zeolite catalysts. It consists in a homogeneous mixture of ZSM-5, low acidity titania binder and an aqueous slurry of titanium oxide hydrate to provide a shapable and extrudable mass. These catalysts exhibit lower binder activity than alumina-bound zeolites, which is useful in hydrocarbon conversion processes with reduced coke formation, improving the catalyst lifetime. After calcination, the material can be subjected to other operations, such as alkaline exchange, dealumination, steaming, and impregnation with catalytically

[60] Plee D. Zeolite granules with zeolitic binder. US Patent, *5 132 260*, **1992**.
[61] Timken H. Method for preparing titania-ound zeolite catalysts. US Patent, *5 430 000*, **1995**.

active metal(s). It is noted that low-acidity refractory oxide binders, such as titania, do not interact with molecular sieves (zeolite) to enhance the acid catalysis activity but they maintain their structural integrity at low pH, thus implying possible treatment with an acid to modulate dealumination phenomenon.

Verduijn[62] suggested a process for producing shaped zeolites without any need of binder addition. For that, silica binder can be converted into zeolite phase (MFI, KFI, FAU, BEA, …) by ageing the bound zeolite in an ionic solution. This solution should contain hydroxyl anions with an initial molar ratio of OH/SiO_2 up to 1.2. This discovery may solve the problem of obtaining a bound zeolite aggregate with lower adsorption properties than the zeolite powder. Note that binder-free refers to zeolites containing less than 10 wt% (based on the total weight) of non-zeolitic binder. The preparation procedure occurs, therefore, in a usual way: synthesis of a zeolite mixture and ageing prior to crystallization. The as-obtained solid is washed, dried, and optionally calcined to produce zeolite powder; the zeolite powder is mixed with a silica sol together with an extrusion aid to form a thick, smooth paste. The paste is then extruded to form silica-bound extrudate which is dried and calcined; the extrudates are mixed with the ionic solution, aged in autoclave, washed, dried, and calcined.

Recently, some studies have highlighted the fact that the introduction of a binder in the zeolite led to the formation of agglomerates which can significantly reduce the intercrystalline diffusivities and also affect the adsorption equilibrium; indeed, these materials demonstrated different adsorption properties for hydrocarbons. Sun et al.[63] evaluated the effects of the binder in the adsorption of n-paraffins on 5A molecular sieves. Experiments realized under the same conditions revealed that binderless 5A zeolite pellets led higher adsorption capacities for four paraffins than pellets (with a binder). The authors attributed this difference to two aspects: a dilution effect, as well as a main aperture blocking effect. It is also possible to directly synthesize zeolite monoliths; however, they exhibit reduced mechanical strength. The advantage relies on the fact that the addition of binders enhances the risk of pore blockage and hindered accessibility to the active sites. Similarly, Zhang et al.[64] aimed to develop one-pot hydrothermal synthesis of monolithic zeolites in the absence of any organic template and binder that might avoid the high-temperature template removal and post-moulding process. In addition, this strategy should allow the direct use of the zeolite products. MOR monolith was prepared by an unconventional acid hydrolysis route using neither organic templates nor binders. It was observed that TEOS as the silica source was the key factor for the generation of the monolith. The same zeolite used to make monoliths was also mixed with colloidal silica as binder. A catalyst with lower surface area and pore volume was obtained. This can be explained by partial pore blockage due to the addition of the binder as discussed in the former section. The MOR-monolith exhibited the largest micropore size and maximum micropore content among all as-prepared samples.

In the previous section, the influence of bentonite and boehmite was reported by Pérez-Uriarte et al.[54]. Likewise, Jasra et al.[65] studied the effect of a clay binder, as bentonite and attapulgite on the sorption and catalytic properties of zeolite X, Y, and MOR pellets. An increase in the heat of adsorption values

[62] Verduijn J. Process for producing substantially binder-free zeolite. US Patent, *5 460 769*, **1995**.
[63] Sun, H.; Shen, B.; Liu, J. *Sep. Purif. Technol.* **2008**, *64*, 135–139.
[64] Zhang, J.; Mao, Y.; Li, J.; Wang, X.; Xie, J.; Zhou, Y.; Wang, J. *Chem. Eng. Sci.* **2015**, *138*, 473–481.
[65] Jasra, R. V.; Tyagi, B.; Badheka, Y. M.; Choudary, V. N.; Bhat, T. S. G. *Ind. Eng. Chem. Res.* **2003**, *42*, 3263–3272.

upon pelletization was highlighted, which may be explained by the migration of clay cations within the zeolite cavities, thus decreasing the surface activity. This means, solid-state ion-exchange of Na^{+}, Mg^{2+} in the zeolite may occur, thus reducing the Brønsted acid site density. The same conclusion was reached by the group of Dorado et al.[66] while studying the influence of bentonite on the acidity and performance of BEA and ZSM-5 zeolites.

Shams et al.[67] prepared 5A zeolite monolith granular extrudates using firstly metakaolin as silica and alumina sources, kaolin and carboxymethylcelullose (CMC) as binder agents. Different percentages of those compounds were used, with a higher purity and better adsorption properties when 30 wt% of kaolin and small amount of CMC were added. The authors attributed the effect on the adsorption properties to the de-clogging of the pores caused by the gasification of CMC during the final calcination of the extrudates. However, data related to the mechanical strength of the material were missing in this study. Uphade et al.[68] presented a shaped Ga-ZSM-5 zeolite. In order to extrudate the catalyst, La modified kaolin was added as a binder in a weight percentage comprised between 30% and 35%. The authors noticed that the zeolite binder catalyst led appreciable alkane conversion, to good overall yield in aromatics and to lower deactivation rate than other catalysts containing Ga and/or silica or alumina as binders. However, Du et al. [53] showed that the specific surface area and micropore volume diminished after kaolin binder addition. Its structure is ruled by weak van der Waals interactions that can be induced by water entering the interlayer, potentially reducing ZSM-5 pore blocking.

A flash-calcined hydrotalcite (HT) binder for MFI zeolite was suggested by Lee et al.[69] as a strategy to maintain its intrinsic acidity. For that, basic trihydroxide was calcined for a few seconds to form flash-calcined HT. This product was blended to MFI zeolite in quantities up to 20 wt% along with a minimal quantity of water to make the paste for granulation. The crushing strength of the MFI zeolite granule was measured and found comparable to commercially available MFI granules containing alumina as a binder. The authors confirmed that the MFI zeolite granule prepared using flash-calcined HT could be used as an acid catalyst. In contrast, the use of SiO_2 and Al_2O_3 failed in either shaping the spherical granule or in obtaining sufficient mechanical strength. According to TPD measurements, the acidity changed when alumina was used, but not when flash-calcined HT was used as a binder.

In order to evaluate the performance of the catalyst, 1-butene isomerization and methanol-to-olefins (MTO) reactions were selected. The results, when compared with a MFI reference catalyst, suggested no influence of the flash-calcined HT as a binder in the first mentioned reaction. In the case of MTO, although the conversion was maintained, a slightly different product distribution was obtained, being attributed to pore blockage by the HT presence. In conclusion, there were no adverse effects due to the presence of the flash-calcined HT in the granule and the catalytic activity could be preserved.

[66] a) Sánchez, P.; Dorado, F.; Fúnez, A.; Jiménez, V.; Ramos, M. J.; Valverde, J. L. *J. Mol. Catal. A Chem.* **2007**, *273*, 109–113; b) de Lucas, A.; Valverde, J. L.; Sánchez, P.; Dorado, F.; Ramos, M. J. *Ind. Eng. Chem. Res.* **2004**, *43*, 8217–8225; c) Dorado, F.; Romero, R.; Caizares, P. *Appl. Catal. A Gen.* **2002**, *236*, 235–243.
[67] Shams, K.; Mirmohammadi, S. J. *Microporous Mesoporous Mater.* **2007**, *106*, 268–277.
[68] Uphade, B.; Gopal, S. Zeolite-Binder Catalyst Composition. US Patent, *2010/0029999 A1*, **2010**.
[69] Lee, H.; Kim, J. H.; Park, D. W.; Cho, S. *Appl. Catal. A* **2015**, *502*, 42–47.

Zeolites can also be shaped by means of a hydraulic binder as affirmed by Bazer-Bachi et al.[70]. The hydraulic binder can be high-alumina cement, sulphoaluminate cements, plaster, cements containing phosphate, blast furnace slag cements and mineral phases selected from alite (Ca_3SiO_5), belite ($CaSiO_4$), alumina-ferrite, tricalcium aluminate ($Ca_3Al_2O_6$), and calcium aluminates such as monocalcium ($CaAl_2O_4$) and calcium hexoaluminate ($CaAl_{12}O_{18}$). The material obtained had 10-95% of zeolite; 0-5% of source of silica; 0-7% of one organic adjuvant; and 1-20% of hydraulic binder.

One advantage remains the successful design of a material with improved mechanical strength and high thermal resistance, being potentially useful for processes involving steam or solvents. In this process there is no need for calcination step after the shaping that has no effects on the properties of the final material and can be carried out irrespectively of the zeolite content. Table 2 presents an overview of alternative binders used for zeolite shaping along with some remarks observed during these studies.

Table 2: Summary of the alternative binder strategies

Reference	Zeolite	Binder	Observations
60	A, X and Y	Siliceous earth	
61	ZSM-5	Titania	Lower binder activity
62,64	Several	Binder-free	Adsorption properties similar to zeolite powder No evidence of pore blocking
65,66	X, Y, MOR, BEA, ZSM-5	Bentonite and attapulgite	Solid-state ion-exchange of Na^+, Mg^{2+}: decrease in Brønsted acid site density
69	MFI	Hydrotalcite	Preservation of the acidity Crush strength similar to commercial MFI granules
70	Several	Hydraulic binders (cements, plaster, aluminates, …)	High mechanical strength High thermal resistance

[70] Bazer-Bachi D, Harbuzaru B, Lecolier E. Zeolite formed by extrusion and pelleting with a hydraulic binder having improved mechanical properties and process and preparing same. US Patent, *2016/0288109A1*, **2016**.

2.2 Hierarchical alumina as a binder

As reported in the previous section, zeolites must be shaped into centimetre-sized bodies to be used in industry, such as in reactors or columns. In some reactions, the diffusion of reactants plays a major role in the activity of the catalyst. Indeed, mass transfer limitations inside the zeolite particle may hamper the catalyst performance. This implies that upon the formation of larger molecules, their diffusion to the pores exit is not facilitated, leading to pore blockage and deactivation of the catalyst by coke formation. When the zeolite is mixed with a binder in order to be extruded, this diffusion problem is further amplified, as the possibility of pore blockage by the binder is greater, thus implying that the molecules cannot reach the active sites. Generally, the binder possesses a smaller specific surface area, and rather small or even no pores. This creates a layer between the reaction medium and the surface of the zeolite, inducing severe mass transfer limitations.

γ-alumina possess a crystalline framework and can be ascribed to both high thermal stability and moderate Lewis acidity[71]. Additionally, it is known for the high chemical and mechanical stability making it ideal for applications in automotive and petroleum industries, as well as in catalysis[72]. Usually, boehmite appears as the binder of choice for shaping zeolite bodies, while transforming its structure to alumina by calcination. Boehmite is an inexpensive material widely used in industry characterized by a low specific surface area, and presence of small pores. This may lead to the problem referred before. It is, therefore, necessary to introduce meso- and / or macropores to guarantee a fast diffusion of the molecules from the reaction medium to the surface of the catalyst.

A review of the different strategies to generate hierarchical porosity in alumina found in the literature will be presented in the following paragraphs. It will be mostly focused on the procedures to synthesize those aluminas and the main outcome given.

2.2.1 Ordered mesoporous aluminas

To synthesize aluminas with an ordered mesostructure, several authors proposed the use of amphiphilic block copolymers through an evaporation-induced self-assembly process (EISA) that was first reported by Brinker and Ozin[73]. In this case, it consists of an assembly of partially condensed Al species in the ethylene oxide blocks of the structure-directing co-polymer via weak coordination bonds. Then, a slow solvent evaporation must be performed, as the organic template prevents the mesoporous structure to collapse during the drying step. Finally, through calcination of the powder, the organic template is removed, leaving a void constituting the mesopores (Figure 17).

One of the first studies related to this method involving alumina is the one from Zhao et al.[74]. Indeed, mesoporous aluminas were synthesized by using inorganic aluminium salts (nitrate or sulphate) as an alumina source and polyethylene glycol 1540 as an organic template. The samples exhibited a surface area of about 300 m^2/g and uniform pore size of 6 nm. However, the prominent conclusion of the

[71] Hartmann, S.; Sachse, A.; Galarneau, A. *Materials.* **2012**, *5*, 336–349.
[72] Trueba, M.; Trasatti, S. P. *Eur. J. Inorg. Chem.* **2005**, *17*, 3393–3403.
[73] Yang, H.; Coombs, N.; Sokolov, I.; Ozin, G. A. *Nature*. **1996**, *381*, 589–592.
[74] Zhao, R.; Guo, F.; Hu, Y.; Zhao, H. *Microporous Mesoporous Mater.* **2006**, *93*, 212–216.

authors was that mesoporous alumina can be obtained by self-assembly through templating, but not by precipitation from inexpensive inorganic alumina salts.

Later, Yuan et al.[75] proposed an easier procedure using amphiphilic block copolymers, such as Pluronic P123. Combining aluminium isopropoxide with nitric acid, ethanol, and the referred template, drying it slowly at 60°C for 48h and calcining it for 4 h at 400°C, produced samples with a well-ordered and crystalline pore network, evidenced by TEM images and XRD analysis. From nitrogen adsorption – desorption, samples with surface area of 434 m^2/g and pore diameters up to 6 nm were formed. The authors highlighted the presence of strong Lewis acidity, provided by aluminium atoms, proving those ordered mesoporous aluminas to be ideal supports for heterogeneous catalysis purposes. The same method was used by Grant et al.[76] but using Pluronic F127. This copolymer formed cage-like mesopores with eight interconnecting cages, having a width of up to 8 nm and specific surface area value of 338 m^2/g.

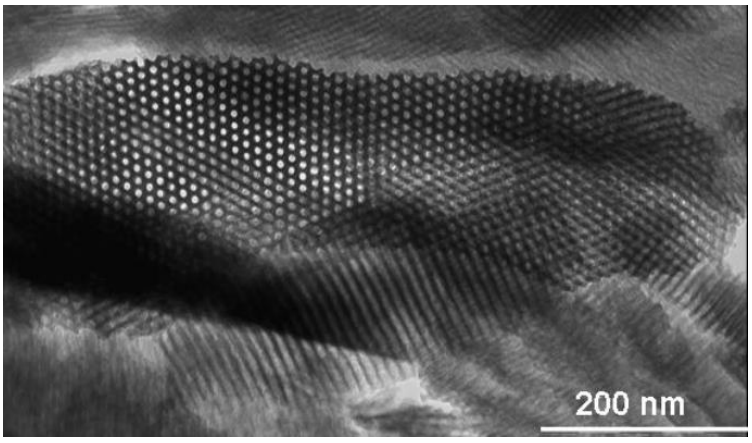

Figure 17: Ordered mesostructure obtained by Grant et al.

A slight modification in the synthesis method of mesoporous aluminas by hydrolysis of aluminium isopropoxide with Pluronic P123 was proposed by Wu et al.[77]. In this study, the authors replaced ethanol with water, allowing the introduction of an active component of potassium species to the alumina after the one-pot synthesis pathway, instead of using common synthesis methods like impregnation. The pore sizes of the samples prepared were up to 2.9 nm linked to a surface area of 261 m^2/g. This led to higher biodiesel yields over the mesoporous aluminas with higher surface area, pore volume and superior pore sizes, being attributed to reduced mass transfer limitations.

Wu et al.[78] developed a double templating technique consisting in an addition of trimethylbenzene (TMB) with Pluronic P123. In this case, the surfactants were dissolved in ethanol, while aluminium isopropoxide was mixed with HCl and citric acid. The samples calcined at 500°C did not exhibit any diffraction peaks, suggesting an amorphous framework, but a further calcination at 900°C showed peaks

[75] Yuan, Q.; Yin, A.-X.; Luo, C.; Sun, L.-D.; Zhang, Y.-W.; Duan, W.-T.; Liu, H.-C.; Yan, C.-H. *J. Am. Chem. Soc.* **2008**, *130*, 3465–3472.
[76] Grant, S. M.; Vinu, A.; Pikus, S.; Jaroniec, M. *Colloids Surfaces A Physicochem. Eng. Asp.* **2011**, *385*, 121–125.
[77] Wu, W.; Wan, Z.; Chen, W.; Yang, H.; Zhang, D. *Adv. Powder Technol.* **2014**, *25*, 1220–1226.
[78] Wu, Q.; Zhang, F.; Yang, J.; Li, Q.; Tu, B.; Zhao, D. *Microporous Mesoporous Mater.* **2011**, *143*, 406–412.

matching with γ-alumina structure. The authors tentatively explained that alumina oligomers can interact with hydrophilic PEO segments from Pluronic P123 by hydrogen-bonding, forming a rigid and robust 2D mesostructure after solvent evaporation at 60°C with surface areas up to 309 m^2/g and pore size of 7.5 nm.

Yuan et al.[79] developed a method to synthesize ordered mesoporous alumina monoliths. Firstly, the EISA method was implemented with hydrolysis of aluminium isopropoxide in the presence of P123 surfactant in ethanol. After a slow evaporation of the solvent and calcination of the powder, it was mixed with acrylamide (cross-linker), ammonium persulfate, and water to form a gel easily shaped into various types of monoliths. TEM images showed highly ordered hexagonal cylindrical channels, however, the surface area and pore size diminished from pristine to shaped sample (307 to 282 m^2/g and 9.5 to 7.5 nm, respectively). On the other hand, Bejenaru et al.[80] successfully prepared ordered mesoporous aluminas using P123 dissolved in ethanol and hydrochloric acid. In this latter case, the aluminium precursor aluminium-tritert-butoxide allowed to generate a 2D hexagonal pore structure with a surface area of 393 m^2/g and pore size of 6.7 nm. However, the sample remained amorphous after calcination.

Liu et al.[81] applied the same method of slow solvent evaporation of gels prepared with an alumina source and P123 as a structure-directing agent. However, in this case, the source of alumina consisted of the main raw material in industry, boehmite, largely used for the preparation of alumina catalysts and supports. Pre-formed boehmite nanocrystals were observed which could act as “building blocks” to form the mesostructure with crystalline framework walls. The interactions between boehmite particles and the surfactant were not strong enough to destroy the intrinsic boehmite crystalline structure, but could effectively direct the loose stacking of the boehmite particles, leading to mesostructured aluminas with pore sizes of 11 nm and surface areas of 339 m^2/g. Fulvio et al.[82] came to those conclusions by using the same method. They observed samples with a specific surface area of 300 m^2/g and pore size of 16 nm, demonstrating better characteristics as crystallinity, thermal stability, etc., than mesoporous aluminas obtained with an alkoxide precursor.

Zhang et al.[83] although also used boehmite as aluminium precursor while implementing Tergitol as non-ionic surfactant. This led to samples formation with pore diameter of 15 nm with a specific surface area of 321 m^2/g. In the past, the same group successfully prepared mesoporous aluminas with surface areas of 350 m^2/g and pore size of 6.7 nm, using several pluronic surfactant types along with different aluminium precursors, such as $AlCl_3.6H_2O$, $Al(NO_3)_3.9H_2O$ and aluminium chlorohydrate[84].

Bleta et al.[85], used different quantities of Pluronic F127 to evaluate the influence of the polymer quantity on the formation of mesopores. Using aluminium tri-sec-butoxide (ABS) to prepare boehmite colloids, it was observed a pore size increase up to 14 nm for an EO/Al ratio comprised between 0.6 and

[79] Yuan, X.; Xu, S.; Lü, J.; Yan, X.; Hu, L.; Xue, Q. *Microporous Mesoporous Mater.* **2011**, *138*, 40–44.
[80] Bejenaru, N.; Lancelot, C.; Blanchard, P.; Lamonier, C.; Rouleau, L.; Payen, E.; Dumeignil, F.; Royer, S. *Chem. Mater.* **2009**, *21*, 522–533.
[81] Liu, Q.; Wang, A.; Wang, X.; Gao, P.; Wang, X.; Zhang, T. *Microporous Mesoporous Mater.* **2008**, *111*, 323–333.
[82] Fulvio, P. F.; Brosey, R. I.; Jaroniec, M. *ACS Appl. Mater. Interfaces* **2010**, *2*, 588–593.
[83] Zhang, Z.; Pinnavaia, T. J. *Langmuir* **2010**, *26*, 10063–10067.
[84] Zhang, Z.; Pinnavaia, T. J. *J. Am. Chem. Soc.* **2002**, *124*, 12294–12301.
[85] Bleta, R.; Alphonse, P.; Pin, L.; Gressier, M.; Menu, M.-J. *J. Colloid Interface Sci.* **2012**, *367*, 120–128.

1.2 and a specific surface area of 450 m^2/g, which can be associated to micelles formation. This means, the copolymer adsorbs on boehmite nanoparticles when its concentration remains low, but with a higher content in copolymers, the formation of micelles occurred, acting as space fillers, hence preventing the compaction of boehmite nanoparticles.

Other techniques than EISA method can be found in the literature for the preparation of mesoporous aluminas. Taking into account the needs of the material and the resources locally available, they can be considered more or less simple than the method described above. In the following paragraphs, an overview of the implemented methods is addressed.

A green way to produce mesoporous aluminas is presented by Zhang et al.[86] who found a way to use methylcellulose (MC), able to be recovered up to 60% after the synthesis. The samples prepared by aluminium chloride and sodium aluminate and templated by MC exhibited surface areas of 315 m^2/g and pore sizes of 8 nm with an organized mesostructure. Cardoso et al.[87] presented an original strategy to synthesize mesoporous alumina by introduction of biomass. Sugar cane bagasse was hydrolysed with a strong base, recovering after filtration the liquid and the remaining solids. The pristine bagasse, the hydrolysis of bagasse and the fibres remaining after the hydrolysis step were then mixed with bayerite separately and subjected to a hydrothermal treatment. After calcination, the samples prepared with fibres from hydrolysis exhibited lower BET surface area but larger pore diameter than the sample prepared with pristine bagasse. In contrast, the use of biomass hydrolysate had no influence on the structure of alumina. It was then concluded that the presence of biomass (the nature rather than its amount) strongly affected the self-assembly process of the crystals.

Kumar et al.[88] investigated the effect of peptization agents, additives and binder on the mesopore size distribution of alumina powder. Boehmite was peptized with nitric acid and added to polyvinyl alcohol, polyethylene glycol, and carbon black. They observed that an increase in the concentration of nitric acid led to diminish the surface area and enhance the pore volume, the optimal concentration being 1.5%. They were able to control the pore size in the range of mesoporosity. Polyvinyl alcohol showed to be more effective in the increase of mesopores than polyethylene glycol, although both were able to create macroporosity. Likewise, carbon black raised the mesoporosity, but did not affect the macroporosity.

An important note should be added here concerning the peptization of boehmite with an acid. It was found that boehmite particles adsorb protons on the surface hydroxyl groups and repel each other to form colloidal particles when the acid / alumina ratio was kept low. Using more hydrochloric acid, large amounts of chloride anions cause compression of the boehmite diffusion layer, resulting in boehmite coalescence. It was then found an optimum acid / alumina ratio of 0.11 resulting in the smallest dispersed boehmite particles.[89]

[86] Zhang, Y.; Zhong, L.; Chen, F.; Zhang, Y. *Microporous Mesoporous Mater.* **2011**, *142*, 740–744.
[87] Cardoso, C. S.; Licea, Y. E.; Huang, X.; Willinger, M.; Louis, B.; Pereira, M. M. *Microporous Mesoporous Mater.* **2015**, *207*, 134–141.
[88] Kumar, M.; Lal, B.; Singh, A.; Saxena, A. K.; Dangwal, V. S.; Sharma, L. D.; Dhar, G. M. *Indian J. Chem. Technol.* **2001**, *8*, 157–161.
[89] Zheng, Y.; Song, J.; Xu, X.; He, M.; Wang, Q.; Yan, L. *Ind. Eng. Chem. Res.* **2014**, *53*, 10029–10034.

Deng et al.[90] used Pluronic 64L together with aluminium ABS in butanol giving birth to pore sizes up to 11 nm and surface areas of 470 m^2/g. The samples demonstrated thermal stability after template removal, but also to prolonged heating at elevated temperature.

An important study from Yue et al.[91] shows the importance of the use of hydroxyl polyacids to enhance the interaction between aluminium species and surfactant, thus promoting the directing function of the template. The procedure consisted of a hydrothermal treatment of $Al(NO_3)_3.9H_2O$ and $NaAlO_2$ with CTAB and citric acid dissolved in water. Several characterization techniques confirmed that the samples with CTAB or citric acid could not alter the structure of alumina upon the hydrolysis process. The same was observed in another study from the same group[92]. The reason more likely proposed by the authors suggests that CTAB cationic surfactant hardly interacted with neutral aluminium hydroxides. However, in samples subjected to double templating in both studies presented surface areas close to 400 m^2/g associated with pore sizes up to 6.2 nm.

Su et al.[93] prepared mesoporous alumina with a lamellar structure using sodium aluminate and aluminium sulfate together with polyethylene glycol with an average molar weight of 6000 g/mol. Samples with specific surface areas of 280 m^2/g and pore diameters of 12 nm were obtained with the addition of PEG6000. The authors suggested that the dispersion of the surfactant in a polar medium, inducing the oxide groups to form at the outer surface of micelles, became in close contact with the polar medium. Then, boehmite crystallites grew in the direction parallel to the corrugated surface due to strong bonding between the oxide group of the surfactant and boehmite surface.

Liu et al.[94] analysed the introduction of mesopores by adding only hydro-carboxylic acids (HCA) as structure-directing agents. For that, the normal procedure was performed by peptizing boehmite with nitric acid, followed by additional citric acid, or DL-malic acid, tartaric acid, or lactic acid. Samples with specific surface areas up to 380 m^2/g and pore sizes of 27 nm calculated by mercury intrusion were obtained. The authors observed different pore structures due to coordination interactions and the steric effect of the HCA.

In principle, these techniques are of easy implementation, but originate relatively small pore sizes and volumes, and specific surface areas. This is due to the fact that aforementioned methods are very sensitive to the mixture preparation conditions. Moreover, one of the main drawbacks remains the large amount of organics that have to be eliminated resulting in low yields. Table 3 presents a summary of the strategies reported to synthesize ordered mesoporous aluminas.

[90] Deng, W.; Bodart, P.; Pruski, M.; Shanks, B. H. *Microporous Mesoporous Mater.* **2002**, *52*, 169–177.
[91] Yue, M. B.; Jiao, W. Q.; Wang, Y. M.; He, M. Y. *Microporous Mesoporous Mater.* **2010**, *132*, 226–231.
[92] Yue, M. B.; Xue, T.; Jiao, W. Q.; Wang, Y. M.; He, M. Y. *Solid State Sci.* **2011**, *13*, 409–416.
[93] Su, A. P.; Zhou, Y.; Yao, Y. H.; Yang, C. M.; Du, H. *Microporous Mesoporous Mater.* **2012**, *159*, 36–41.
[94] Liu, Q.; Wang, A.; Wang, X.; Zhang, T. *Microporous Mesoporous Mater.* **2006**, *92*, 10–21.

Table 3: Summary of the techniques used for the synthesis of ordered mesoporous alumina

Reference	Al Source	Template	Surface Area (m^2/g)	Pore Diameter (nm)
74	Aluminium salts	Polyethylene glycol 1540	300	6
75,77,79,80	Aluminium isopropoxide; aluminium titert-butoxide	Pluronic P123	261 – 434	2.9 – 9.5
76,85	Aluminium isopropoxide	Pluronic F127	338 – 450	8 – 14
78	Aluminium isopropoxide	Pluronic P123 + trimethylbenzene	309	7.5
81,82	Boehmite	Pluronic P123	300 – 339	11 – 16
84	Boehmite	Tergitol	321	15
86	Aluminium chloride + sodium aluminate	Methylcellulose	315	8
87	Bayerite	Sugar cane bagasse	209	7.8
90	Aluminium tri-sec-butoxide	Pluronic 64L	470	11
91,92	Aluminium nitrate	CTAB + hydroxylpolyacids	400	6.2
93	Sodium aluminate + aluminium sulphate	PEG 6000	280	12
94	Boehmite	Hydro-carboxylic acids	380	27

2.2.2 Disordered mesoporous aluminas

If the desired application does not require a well-ordered mesoporous alumina phase, the synthesis of disordered mesoporous materials can be more convenient and efficient. The following method is easily scaled-up, in contrast to the previous synthesis of EISA that requires an expensive structure-directing agent. It consists of a one-step, easy, and fast method to obtain disordered mesoporous γ-Al_2O_3 by using 2-butoxyethanol as a solvent and as controlling agent for the $Al(Osec)Bu_3$ hydrolysis[71]. This method led to designed materials with a crystalline alumina phase with high specific surface area of 338 m^2/g and mesopore size of 11 nm (Figure 18). Surprisingly, the authors suggested that this method provides better yields as only 30% of the raw materials consisted in inorganics needed to be eliminated during the calcination process.

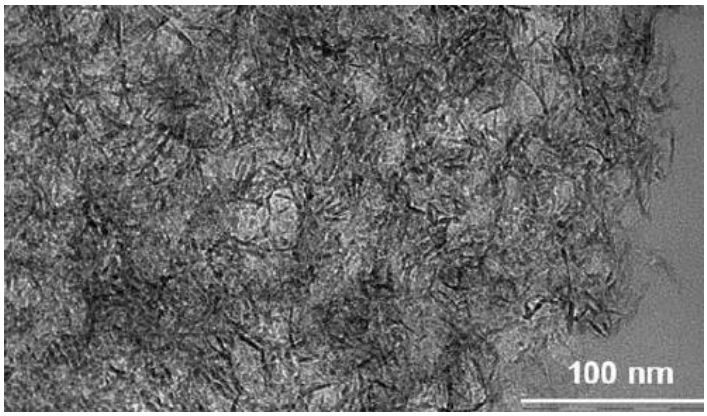

Figure 18: Disordered mesoporous alumina prepared by Xu et al.

A different template can be used for mesoporosity generation in aluminas as suggested by Xu et al.[95]. Indeed, glucose was chosen as structure-directing agent upon the hydrolysis of aluminium isopropoxide yielding specific areas of 422 m^2/g and pore size of 5.1 nm. TEM analysis showed a wormhole-like appearance, but no significant pore ordering. XRD patterns confirmed the amorphous nature of the samples calcined at 600°C. It was necessary to raise the temperature up to 800°C to evidence mesoporous γ-Al_2O_3, thus showing that the thermal stability of mesoporous alumina by this method is very high.

A study performed by Bejenaru et al.[80] evaluated several techniques for a proper introduction of mesopores in alumina that could be used as supports for CoMo HDS catalysts. One of the techniques was the sol-gel method, where tri-sec-butoxide was dissolved in 2-butanol with further addition of butan-1,3-diol. After evaporation of the solvent and calcination of the samples, a specific surface area of 349 m^2/g and pore size of 10.7 nm were achieved. Another strategy consisted of using a cationic surfactant that could be mixed to aluminium-tri-sec-butoxide dissolved in ethanol with CTAB, or aluminium nitrate and P123, or aluminium-trisec-butoxide with P123 together with butanol. All the samples exhibited a disordered mesostructure with specific surface areas ranging between 343 and 423 m^2/g associated to pore sizes of 5.3 to 11.6 nm. Table 4 summarizes the different approaches selected to produce disordered mesoporous aluminas.

Table 4: Summary of the strategies to design mesoporous aluminas

Reference	Al Source	Method	Surface Area (m^2/g)	Pore Diameter (nm)
71	Aluminium tri-sec-butoxide	Sol-gel	338	11
95	Aluminium isopropoxide	Glucose templating	422	5.1
80	Aluminium tri-sec-butoxide	Sol-gel	349	10.7

[95] Xu, B.; Xiao, T.; Yan, Z.; Sun, X.; Sloan, J.; González-Cortés, S. L.; Alshahrani, F.; Green, M. L. H. *Microporous Mesoporous Mater.* **2006**, *91*, 293–295.

2.2.3 Macrostructured Aluminas

In this last section, few methods for the preparation of hierarchical macro-/mesoporous aluminas are presented. Materials with macropores possess the advantage to allow high mass transfer with low pressure drop and high specific surface areas for a good dispersion of the active sites. For example, Dacquin et al.[96] discovered a route to design highly organized macro-mesoporous aluminas. For that, pure mesoporous aluminas were prepared according to an EISA procedure using Pluronic P123. This strategy yielded a well-resolved hexagonal pore structure with pore sizes of 5.1 nm. To obtain macroporous-mesoporous solids, monodispersed latex spheres of controlled size were added to the former solution. From SEM analysis, it was possible to observe a long-range structural ordering imparted by a polystyrene template resulting in a macroporous skeleton with macropores of 320 nm and a specific surface area of 249 m^2/g. However, XRD analysis did not evidence any crystalline alumina phase. This suggests that the framework comprised transitional alumina between hydroxide or oxyhydroxide and γ-Al_2O_3.

Li et al.[97] found a way to prepare highly ordered 2D hexagonal mesopores in the walls of macroporous materials. The general synthesis strategy was based on a simple sol-gel process using the polyurethane (PU) foam replication method combined with P123 as the mesoporous structure-directing agent. For that, aluminium isopropoxide, nitric acid, and P123 were dissolved in ethanol. After the addition of PU, the sol solution entered into interconnected macropore voids by capillary and wetting driving forces. Then the cross-linked aluminium species could assemble with P123 to form the ordered mesophases on the inner surface of the PU, resulting in a solvent-evaporation-induced coating and self-assembly process. The samples exhibited mesopores of 3.4 nm, macropores of 600 µm and specific surface area of 300 m^2/g (Figure 19). Through the same sol-gel method, Tokudome et al.[98] investigated the formation of meso-macroporous Al_2O_3 monoliths from aerogels and xerogels in the presence of propylene oxide and poly(ethylene oxide) (PEO). Indeed, they observed that samples with different PEO content can lead to a tailored range of pores ranging from 400 nm to 1.8 µm. This is caused by the distribution of PEO in the fluid phase separation, while the interstices between the secondary particles of the gel skeleton work as mesopore structures. Samples with surface area up to 511 m^2/g and mesopores of 5.4-33.1 nm were produced, depending on the type of gel used: aerogel versus xerogel.

[96] Dacquin, J. P.; Dhainaut, J.; Duprez, D.; Royer, S.; Lee, A. F.; Wilson, K. *J. Am. Chem. Soc.* **2009**, *131*, 12896–12897.
[97] Li, L.-L.; Duan, W.-T.; Yuan, Q.; Li, Z.-X.; Duan, H.-H.; Yan, C.-H. *Chem. Commun.* **2009**, 6174–6176.
[98] a) Tokudome, Y.; Fujita, K.; Nakanishi, K.; Miura, K.; Hirao, K. *Chem. Mater.* **2007**, *13*, 3393–3398; b) Tokudome, Y.; Nakanishi, K.; Kanamori, K.; Fujita, K.; Akamatsu, H.; Hanada, T. *J. Colloid Interface Sci.* **2009**, *338*, 506–513.

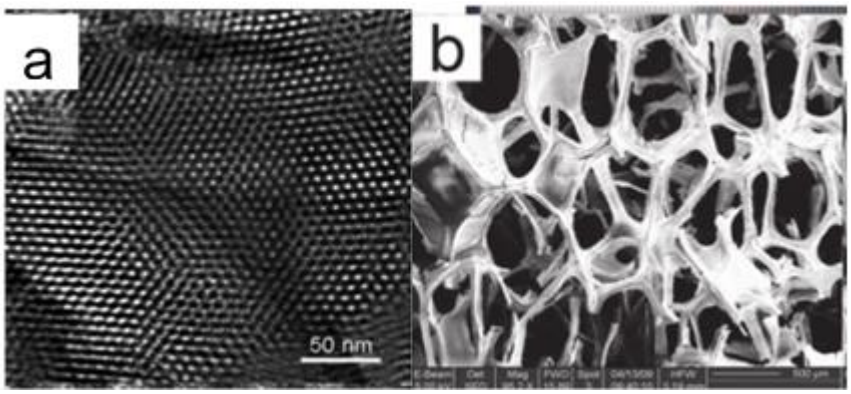

Figure 19: a) Ordered mesoporous walls of the materials obtained by TEM ; b) macropores of the material visible by SEM. Samples prepared by Li et al.

Finally, Ma et al.[99] proposed the use of bio-templates to form meso-macroporous aluminas. The template used in the study was a yeast aqueous solution added to a solution of $Al(NO_3)_3.9H_2O$ and triethanolamine. SEM images showed a macroporous structure with pore sizes between 1.5-3 µm, whose walls were impregnated by mesopores between 3-4.5 nm as determined by N_2 adsorption/desorption isotherms, also giving birth to surface area values of nearly 340 m^2/g. A raise in the calcination temperature hardly increased the quantity of mesopores, suggesting a structure with high thermal stability. Table 5 summarizes the strategies encountered to design macroporous alumina materials.

Table 5: Strategies undertaken for the synthesis of macroporous alumina

Reference	Al Source	Template	Surface Area (m^2/g)	Pore Diameter (nm)
96	Aluminium isopropoxide	Latex spheres	249	0.3
97	Aluminium isopropoxide	Polyurethane foam	300	600
98	Aluminium chloride	Poly(ethylene oxide)	511	0.4-1.8
99	Aluminium nitrate	Yeast	340	1.5-3

2.3 Conclusion

The catalysts shaping technology has been developed for many decades due to its crucial role in industrial applications. As seen in the previous sections, several scientists have proposed different materials as binders to better reach the desired specifications, as to confer high mechanical stability and inertia to the process. However, many studies report secondary effects that can deteriorate the catalyst performance, such as, loss of conversion, change in the selectivity, and reduced catalyst lifetime. These impacts are often caused by migration of cations from the binder into the zeolite structure which may change the acidity, pore blockage hindering the diffusion of the molecules towards and from the active sites, or creation of a new phase in the system. As a consequence, this chapter presented several proposals of different research groups on the use of *green* binders, not only as a biomass valorisation but

[99] Ma, Y.; Wei, Q.; Ling, R.; An, F.; Mu, G.; Huang, Y. *Microporous Mesoporous Mater.* **2013**, *165*, 177–184.

also as potential solvers of the problems found before. However, the latter implies an increase of the process cost and difficult implementation at a larger scale.

As the main goal of this thesis relies on the improvement of the effective diffusivity of shaped zeolites, the introduction of additional porosity on the binder might be an interesting strategy to overcome diffusion limitations. Due to that, it was decided to use boehmite as a binder since this material will suffer transformation upon the calcination step to form γ-alumina, a very strong material characterized by a low acidity, cheap, and widely available. The last section was dedicated to the summary of the different procedures already existent to form meso- and/or macropores in the alumina structure.

Chapter 3 - Experimental part

Abstract

This chapter describes in detail the materials and methods as well as the equipment used during this Thesis. The procedure of synthesis and shaping of zeolites are described along with the characterization techniques: N_2 physisorption, mercury intrusion porosimetry, X-ray diffraction, scanning electron microscopy, transmission electron microscopy, mechanical strength measurements, NH_3 adsorption, pyridine FT-IR, pulsed-field gradient NMR, inverse gas chromatography, gravimetric method. Later on, the set-ups used for toluene adsorption, n-hexane cracking, n-butylcyclohexane cracking and methanol-to-hydrocarbons reaction are briefly described.

3.1. Preparation of the materials

3.1.1 Reactants and catalysts

For the shaping of the catalysts, the following starting materials were used: NH_4-ZSM-5 (Zeolyst CBV3020-E, Si/Al = 15), boehmite (Sasol Disperal P2), nitric acid 70% (Fisher Chemical), and Methocel * K4M Premium CR Hydroxypropyl Methylcellulose (Dow Chemicals). For the introduction of porosity in the zeolite bodies, the following reagents were added separately during the process: acrylic glass Porlat K 85 (Zschimmer & Schwarz), micro powders Propyltex 325S – 100S (Kromachem GmbH), poly(ethylene glycol)-*block*-poly(propylene glycol)-*block*-poly(ethylene glycol) Pluronic P123 (Sigma Aldrich), cellulose fibers Arbocel (J. Rettenmaier & Söhner – JRS), cellulose nano-crystals (CelluForce), and oxidized lignin (kindly provided by Prof. Aleksander Vasilyev from the Department of Chemistry of the Saint-Petersburg State University).

The ammonium form of the catalyst was calcined at 550°C for 15h with a heating ramp of 1h to get the proton form to be used in the catalytic experiments. All the other materials and reactants were used as-received.

The synthesis and treatment of zeolites were performed with the following reactants: sodium aluminate anhydrous ($NaAlO_2$, Riedel de Haën), tetrapropylammonium hydroxide (TPAOH 20-25 wt% in water, TCI), tetraethyl orthosilicate (TEOS 99%, Sigma-Aldrich), sodium chloride (NaCl, AnalaR NORMAPUR), sodium hydroxide (NaOH 97%, Alfa Aesar), hydrochloric acid (HCl 37%, Sigma-Aldrich), and ammonium nitrate (NH_4NO_3 98%, Acros Organics).

3.1.2 Shaping method

The typical procedure for the preparation of the catalyst bodies consisted in the mix of 80wt% zeolite with 20wt% boehmite with a kitchen robot (Kenwood KM244). A small weight percentage of methocel (~1wt%) could be added to facilitate the extrusion of the paste. This product is composed by water-soluble derivatives of methylcellulose, capable to retain water, providing a plastic character to the system, thus facilitating the extrusion. After homogenization, an aqueous solution of HNO_3 (4 wt%) was slowly added to the mix while stirring vigorously. Small yellow spheres of the previous mix should be formed, indicating that the paste is ready to be extruded. For that, the chamber of a Walnut Hollow Clay Extruder was filled with the previous paste and pressure was applied until the exit of the material in the opposite orifice with a diameter of 2 mm.

Upon extrusion, the wires were let to dry at room temperature for 24 h to slowly evaporate the water allowing the preservation of the chemical structure. After, each wire was cut into a cylinder with 4 mm in length, placed in a ceramic crucible and calcined at 600°C for 4h with a heating ramp of 1°C/min. This calcination method allows burning off the pore formers agents leaving the voids that constitute the hierarchical porosity, to obtain the proton form of the zeolite as described in the previous subsection, and to transform the boehmite into γ-Al_2O_3.

All the procedure was adapted from Saint-Gobain methodology and performed by the author at the Institut de Chimie et Procédés pour l'Energie, l'Environnement et la Santé (ICPEES) – UMR7515 – CNRS of the University of Strasbourg.

3.1.3 Synthesis of zeolites

The general synthesis method consisted in the dissolution of 0.110 g of $NaAlO_2$ and 0.350 g of NaCl in 40 mL of distilled water. Then, 3.1 mL of TEOS and 17.7 mL of TPAOH were slowly added to the previous solution marking the initial synthesis time. Different masses of oxidized lignin were added right after (100, 300 and 500 mg). The gel with the following mole ratios: $NaAlO_2$: TEOS : TPAOH : NaCl : H_2O = 1 : 10 : 15 : 4 : 3100 was stirred for 2h at room temperature and placed in an autoclave at 170ºC for 48h. Approximately 1 g of solid was obtained after filtration, washing, drying overnight and calcination at 550ºC for 15h to remove the organics: both the TPA template and the oxidized lignin. These samples were named zxLO, x being the mass of oxidized lignin added.

3.1.4 Desilication of zeolites

The commercial zeolite was subjected to an alkaline treatment to remove part of silica species from the framework, leaving voids called mesopores, and named BAW. 6 g of CBV3020E were mixed with 200 mL of 0.2M of NaOH at 65ºC for 30 min. After filtration, washing, and drying, the sample was treated with 0.1M of HCl at 70ºC for 6h to remove the extra-framework species. After filtration, washing and drying, the sample was exchanged with 1M of NH_4NO_3 for 1h, repeated three times, and finally calcined to obtain the proton form at 550ºC for 15h (1 h heating ramp).

3.2 Characterization methods

3.2.1 N_2 adsorption-desorption

The Brunauer-Emmet-Teller (BET) theory consists in the adsorption of gas molecules to determine the surface area of the sample and its pore diameter.

The isotherms are obtained by following the quantity of nitrogen adsorbed with an increase in the relative pressure as also as the reverse operation (desorption of the gas when the relative pressure diminishes).

The isotherms can be linearized by Eq. 18:

$$\frac{(P/P^0)}{V_m(1-P/P^0)} = \frac{1}{n_m C} + \left[\frac{(C-1)}{n_m C}\right]\left(\frac{P}{P^0}\right) \quad (18)$$

where V_m represents the quantity of nitrogen adsorbed, n_m is the monolayer capacity, C an empirical constant, P the adsorbate pressure, and P^0 the adsorbate vapour pressure at the measuring temperature.

The surface area can be calculated by the capacity of the monolayer obtained from the slope and interception of the previous equation, by the Avogadro Number, N, and by the molecular cross-sectional area, σ_N, (0.162 nm^2 for N_2)[100] as in Eq. 19.

$$S_{BET} = n_m N \sigma_N \quad (19)$$

[100] Ertl, G.; Knözinger, H; Schüth, F.; Weitkamp J. In *Handbook of Heterogeneous Catalysis Vol 1*, Wiley VCH, **2009**, 723–726.

Assuming that close to a relative pressure of 1, the pores are fully filled with liquid nitrogen, it is possible to determine their volume, V_{pore}, with the volume of liquid nitrogen at 77K (34.65 cm^3/mol). The pore diameter, d_{pore}, can then be calculated through:

$$d_{pore} = \frac{4V_{pore}}{S_{BET}} \tag{20}$$

This technique was performed using a ASAP2420 instrument (Micromeritics) at 77K. The samples were previously degassed under vacuum at 250°C overnight. The specific surface area, S_{BET}, was determined from the isotherm branch in the range of relative pressure P/P^0=0.05-0.25, the mesopore surface area, S_{meso}, and micropore volume, V_μ, were determined by the t-plot method, and the pore profile was evaluated from the desorption branch of the isotherm using the Barrett-Joyner-Halenda (BJH) method.

This technique was performed by the author at ICPEES of the University of Strasbourg.

3.2.2 Mercury Intrusion Porosimetry

Hg intrusion porosimetry (MIP) is a technique widely used in materials to investigate the pores profile between 3.5 nm and 500 µm. This analysis measures the volume of liquid metal that penetrates in the structure. Since mercury is a non-wetting liquid for most materials (its contact is greater than 90°) a continuous applied pressure is required. By assuming a cylindrical pore geometry, it is possible to use a modified Young-Laplace equation (commonly referred as Washburn equation) that relates the pressure difference across the curved mercury interface (r_1 and r_2) to the corresponding pore size (r_{pore}) using the surface tension of mercury (γ) and the contact angle (θ) between the solid and mercury.

$$\Delta P = \gamma\left(\frac{1}{r_1} + \frac{1}{r_2}\right) = \frac{2\gamma cos\theta}{r_{pore}} \tag{21}$$

This analysis was performed in an AUTOPORE IV 9500 instrument (Micromeritics) working at a pressure range from 0.5 to 3000 Psi. The samples were first kept in an oven at 100ºC overnight to eliminate any residual water, followed by a degasification procedure under vacuum at room temperature for 5 min.

This technique was kindly performed by Béatrice Rivière at the Centre de Recherche d'Etudes Européens (C.R.E.E.) of Saint-Gobain Provence in Cavaillon.

3.2.3 X-Ray Diffraction

X-ray diffraction is a non-destructive technique widely used to reveal detailed information about the chemical composition and crystallographic structure of a solid.

A crystal lattice is a regular three-dimensional distribution (cubic, orthorhombic, etc.) of atoms arranged in space to form a series of parallel planes separated from another by a distance, d, which varied according to the nature of the material. In any crystal, these planes exist in a number of different orientations, each with its own specific d-spacing.

When a monochromatic X-ray beam with a wavelength λ is projected onto a crystalline material at an angle θ, diffraction occurs only when distance travelled by the rays reflected form successive planes differs by a complete number n of wavelengths (Bragg's law).

$$n\lambda = 2d(hkl)\ sin\theta \quad (22)$$

By varying the angle θ, the Bragg's law conditions are satisfied by different d-spacings in polycrystalline materials. Plotting the angular positions and intensities of the resultant diffracted peaks of radiation produces a pattern, which is characteristic of any sample. When a mixture of phases is present, the resultant diffractogram is formed by the addition of the individual patterns.

The equipment used was Bruker AXS D8 Advance. The analyses were performed with a source of X-rays of Cu (λ=1.5418Å) and detector LynxEye (filter of nickel that allows the passage of the Kα of copper). The angle 2θ was varied between 5 and 60º, with a step of 0.01 and with 0.04 s per step. The patterns were processed with the software EVA by Bruker and compared with data base ICDD.

This technique was performed by the author at ICPEES of the University of Strasbourg.

3.2.4 Scanning Electron Microscopy

The morphology of the zeolite crystals, their sizes and shapes, degree of aggregation, and presence of other phase could be observed by scanning electron microscopy (SEM). This technique consists of scanning the surface of the sample with a focused electron beam, accelerated by a 10 to 20 kV voltage. Then, by analysing the interactions between the beam and the atoms from the matter it is possible to produce various signals that can be detected and that contain information about the sample surface topography and composition. The SEM image can be obtained by two types of interactions: secondary electrons or back-scattered electrons emitted from the area irradiated by the scanning electron probe. The contrast is mainly due to the difference in the electron collection efficiency depending on the angle of emission and surface roughness, but it also depends on the atomic number of elements.[101]

The surface of the sample should be electron conducting, which in most cases requires that the specimen surface has to be covered with a conducting metal layer. For that, the samples were maintained with an adhesive tape in carbon and they were covered with a thin layer of carbon in order to increase their electric conductivity. SEM images on a scale of 100 µm to 100 nm were recorded on a JEOL FEG 6700F microscope working at 9 kV accelerating voltage. In some cases, micrographs of resin-embedded extrudates were acquired on a microprobe JEOL FEG JXA8530F with spectrometers WDS and EDS JEOL. The samples were metallised with Au for 60s.

This technique was kindly performed by Thierry Romero at ICPEES of the University of Strasbourg and by Maxime Mayer at C.R.E.E. in Cavaillon.

3.2.5 Transmission Electron Microscopy

The distinction between zeolite and alumina of the samples were visible by transmission electron microscopy (TEM). This can be achieved by passing the beam through the sample deposited on a thin

[101] Ertl, G.; Knözinger, H; Schüth, F.; Weitkamp J. In *Handbook of Heterogeneous Catalysis Vol 1*, Wiley VCH, **2009**, 756.

metal grid typically coated with a thin layer of carbon and reaches the detector. The image collected in bright field imaging mode gives information regarding the contrast of the sample. Thicker areas or areas with higher atomic number will be darker and vice versa. The choice of specimen support is important for high resolution TEM, since thicker support film decreases the resolution and may render difficult the detection of lattice fringes. TEM images and elemental composition of the materials were acquired over a Hitachi HF-3300kV instrument. The sample preparation was done by ultrasonic dispersion of the sample in ethanol, placing a drop over a copper grid coated with an amorphous carbon film, and then drying under open air conditions.

This technique was kindly performed by Prof. Shanmugan Sangaraju at the Daegu Gyeongbuk Institute of Science and Technology (DGIST) in South Korea.

3.2.6 Mechanical strength measurements

Mechanical strength is an important characteristic of the extrudates. In this Thesis, the impact of porosity introduction in the mechanical stability of the samples was verified. The most common method, as the one used during this Thesis, is the standard ASTM international test.

This method is a mean of determining the crushing strength of a catalyst bed. Techniques to measure the crushing strength of a shaped catalyst particles is limited to crushing individual particles, which may not be related to how the catalyst will crush in a reactor or bed. For some catalysts, such as granules, this technique may be the only viable method for obtaining crushing strength. The production of fines in a reactor is not desired because of the potential of bed compacting and the pressure drop created in the reactor.

The measurements were performed by placing 15 extrudates individually in the sample holder of a mechanical press from Shimadzu AGS-X and applying pressure. During the process, this pressure is measured and plotted in function of the distance covered. When the extrudates crushes, the applied force decays drastically and the procedure finishes. The maximum force applied is the maximum stress, given in Newton.

This technique was performed by the author at C.R.E.E. in Cavaillon.

3.2.7 NH_3 adsorption

Temperature-programmed desorption (TPD) is one of the most widely used and flexible techniques for characterizing the acid sites on zeolites. In this case, ammonia was used as a basic probe due to its simplicity. Also, this molecule has a small size allowing its penetration into all pores of the solid and its basicity may even titrate weak acid sites which may not contribute to the activity of the catalysts.

The analysis was performed in a chemisorption analyser AutoChem II from Micromeritics, where the sample was firstly activated under 500°C to eliminate any adsorbed water and other impurities. Then, the adsorption step occurred at 100°C where the sample was saturated under a continuous flow of ammonia. After, the desorption was performed by ramping the temperature up to 1000°C. During this process, a built-in thermal conductivity detector (TCD) monitored the concentration of the desorbed species.

By plotting the concentration of desorbed species as a function of the temperature of desorption, it is possible to determine the quantity of ammonia adsorbed on the catalyst surface by an integration of the signals. In addition, the temperature recorded at the peak maximum provides useful information concerning the strength of the adsorption.

This technique was performed by the author at C.R.E.E. in Cavaillon.

3.2.8 Pyridine - FTIR

Infrared spectroscopy was used to characterize the nature of hydroxyls and the acidity of the samples. For that, it is necessary to know qualitative information of the acid sites nature, and quantitative information of their strength and density. The basicity of the probe molecule, its size (to penetrate into the pores), its spectral response (intensity of the bands and vibration frequency sensibility) are important parameters. The molecule should be easily adsorbed and stable on the catalyst surface, and it should neither be hydrolysed nor oxidized. In this Thesis, pyridine was used as probe molecule.

Prior to analysis, samples were pressed at approximately 1 ton.cm^{-2} into thin wafers of ca. 10 mg.cm^{-2} and placed inside the IR cell. Before pyridine adsorption/desorption experiments, the wafers were calcined in static conditions at 400°C for 1 h in O_2 (15 kPa) and then outgassed under secondary vacuum at 400°C for 1h. These wafers were contacted at 150°C with gaseous pyridine (67 Pa) via separate cell containing liquid pyridine. The spectra were then recorded following desorption from 150 and 300°C with a Bruker Vector 22 spectrometer (resolution 4 cm^{-1}, 64 scans). The reported spectra were obtained after subtraction of the spectrum recorded before pyridine adsorption. The amount of Brønsted and Lewis acidic centres titrated by pyridine was obtained using a molar adsorption coefficient value of ε = 1.14 cm.µmol^{-1} for the ν_{19b} vibration of protonated pyridine (Py-H$^+$) at ~1545 cm^{-1} and of ε = 1.76 cm.µmol^{-1} for the ν_{19b} vibration of coordinated pyridine (Py-L) at ~1455 cm^{-1}.

This technique was kindly performed by Dr. Thomas Onfroy from the Laboratoire de Réactivité de Surface of the Paris-Sorbonne University.

3.2.9 Pulsed-Field Gradient NMR

The samples previously prepared were subjected to a PFG-NMR technique which allows performing diffusion studies via diffusion ordered nuclear magnetic resonance spectroscopy (DOSY). This technique consists in a short time-pulsed that creates a phase shift depending on the spatial position of the spins. Then, the DOSY spectrum is obtained by an application of the inverse Laplace transform to process the NMR data, being the output a two-dimensional (2D) map form of NMR data. One dimension represents the chemical shift information, while the other represents the diffusion coefficient[102].

To perform this technique, a given mass of the sample was crushed and transferred to a small flask to be premixed with the liquid probe molecule (toluene). For each sample, a determined volume of this liquid was added to guarantee the loading of 2 molecules per unit cell (molec. / u.c.). Considering that the samples are the result of a mixture between zeolite and alumina with a mass percentage of 80 and 20%, respectively, a pondered average of the volume necessary to load 2 molec. / u.c. of the zeolite and

[102] Pagès, G.; Gilard, V.; Martino, R.; Malet-Martino, M. *Analyst* **2017**, *142*, 3771–3796.

alumina was used. After 1h agitation, the premixed samples were transferred to a NMR-tube, to which a capped capillary tube containing d_4-CD_3OD was added. As-prepared tubes were capped and sealed to avoid any evaporation of the probe molecules.

The analysis was performed on a Bruker 600 MHz spectrometer – Avance III, equipped with a high strength z gradient probe DOTY Scientific, developing a pulse field gradient of 50 G/cm/A. The gradient coil was cooled by air flow and the sample was thermostated at 298K. The gradient strength varied linearly between 16 and 302 G / cm in 40 experiments.

Diffusion NMR data were acquired using Simulated Echo pulse sequence with bipolar z gradients. The diffusion time and the duration of the sinusoidal gradients were optimised for each sample. Typically, the diffusion time was set between 2 and 100 ms and the half-gradient delay between 400 and 700 µs. The gradient recovery delay was set to 200 µs. A recycling delay of at least 3.5 s was respected between scans.

This technique was kindly performed by Bruno Vincent at the NMR common service from the Institut de Chimie of the University of Strasbourg.

3.2.10 Inverse Gas Chromatography

The theory of this technique was given in the introduction.

The analysis was performed in a gas chromatograph Clarius 500 from Perkin Elmer. The samples were crushed into particles with 0.160 < diameter < 0.200 mm and filled a column of stainless-steel tube with 0.2 cm of inner diameter and 2.8 cm of length. The samples were treated *in situ* at 110°C overnight under a flow of 15 mL/min to eliminate any adsorbed water and other impurities. The temperature of the column was then increased to 350°C to perform the analysis at different flows as explained before, and the treatment of the data in Adscientis software.

This technique was performed by the author at C.R.E.E. in Cavaillon.

3.2.11 Gravimetric Method

The theory of this technique was given in the introduction.

The samples were tested in extrudate form or crushed into particles with 0.074 < diameter < 0.1 mm. They were placed in the TGA plate (Figure 20) and calcined at 550ºC for 1h with a heating ramp of 10ºC/min under a flow of 40 mL/min of N_2. Then, the temperature was reduced to 35ºC, and the gas was switched for toluene at a concentration of 0.28 mg/min, supplied by a gas bottle of 2000 ppm from Beijing Ruizhi Hanxing Technology. The mass of the sample was recorded during all the process until saturation.

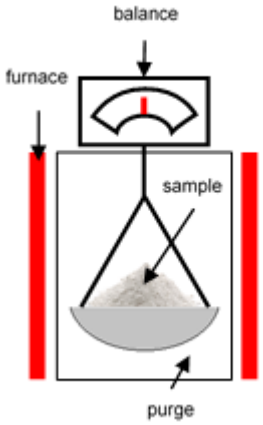

Figure 20: Scheme of the experimental setup of the gravimetric method

This technique was performed by the author, during her 2 months-stay, at the College of Environmental Science and Engineering of the Beijing Forestry University in the group of Prof. Qiang Wang.

3.3 Applications

3.3.1 Toluene adsorption

Prior to use, 200 mg of catalyst were calcined at 600°C for 1h. Toluene adsorption in VOC removal conditions was performed in a fixed bed reactor at 40ºC. The flow consisted in 400 ppm of toluene in the presence of O_2 and Argon in a total of 100 mL/min. The outlet was analysed by gas chromatography equipped with a flame ionization detector (FID) and a column Agilent 125-7062 DB-Wax 60m x 530µm x 1µm. The GC program consisted in an increase of temperature from 150ºC until 195ºC at 15ºC/min to eluate the toluene.

This technique was performed by the author at the College of Environmental Science and Engineering of the Beijing Forestry University.

3.3.2 n-hexane cracking

Prior to use, catalysts were crushed into particles with an average diameter of 0.5 mm and calcined at 500°C for 30 min. The cracking of n-hexane was performed in a fixed bed reactor at 500ºC. 0.1 mL/min of the reactant was injected into the reactor by means of a SyringePump from New Era Pump Systems (NE-1000), being *a priori* evaporated and mixed with 230 mL/min of N_2. After 5, 20 and 35 min of reaction, the outlet was analysed by gas chromatography equipped with a flame ionization detector (FID) and a column Agilent HP-Al/KCl 50m x 0.32mm x 8µm. The GC program consisted in an isothermal at 130ºC for 13 min. The activity of the samples was expressed in terms of n-hexane conversion, calculated from the difference between inlet and outlet concentrations of reactant. The selectivity was obtained by the mole ratio of each product referred to the moles of converted n-hexane. The mass of catalyst was optimized in each experiment in order to guarantee isoconversion.

This technique was performed by the author, during her 2 months-stay, at the Laboratório de Catálise e Energia Sustentável (LACES) leaded by Prof. Marcelo Maciel Pereira from the Institute of Chemistry of the Federal University of Rio de Janeiro.

3.3.3 n-butylcyclohexane cracking

Prior to use, catalysts were crushed into particles with an average diameter of 0.5 mm and calcined at 500°C for 30 min. The cracking of n-butylcyclohexane was performed in a fixed bed reactor at 500ºC. 0.1 mL/min of the reactant was injected into the reactor by means of a Syringe Pump from New Era Pump Systems (NE-1000), being *a priori* evaporated and mixed with 90 mL/min of N_2. After 5 min of reaction, the outlet was analysed by gas chromatography equipped with a flame ionization detector (FID) and a column Agilent DB-1 30m x 0.32mm x 3µm. The GC program consisted in an isothermal at 35ºC for 5 min, followed by an increase of 10ºC/min until 120ºC and 5ºC/min until 250ºC. The activity of the samples was expressed in terms of n-butylcyclohexane conversion, calculated from the difference between inlet and outlet concentrations of reactant. The selectivity was obtained by the mole ratio of each product referred to the moles of converted n-butycyclohexane. The mass of catalyst was optimized in each experiment in order to guarantee isoconversion.

This technique was performed by the author at LACES of the Federal University of Rio de Janeiro.

3.3.4 Methanol-to-hydrocarbons reaction

Prior to use, catalysts were calcined at 550°C for 1h under argon flow. 2 g of zeolite bodies with an equivalent diameter of 2.8 mm were placed in a tubular quartz reactor with inner diameter of 1.5 cm (ratio between reactor and particle diameter is around 5, which avoids wall effects) and packed between two quartz wool plugs, resulting in a catalytic bed length of 7 cm (ratio between reactor length and its diameter around 5, ensuring a plug-flow regime). A determined constant argon flow was flown through a methanol saturator, heated to 45°C by oil bath, to achieve WHSV= 2.0 $g_{MEOH}/g_{cat}.h^{-1}$. The reactant was subsequently fed to the reactor containing the catalyst at 450°C. The products at the outlet were analysed every hour by GC equipped with a 50 m capillary column (PONA) and a flame ionization detector (FID). The GC program consisted in an isothermal at 40ºC for 7 min, followed by an increase of 20ºC/min until 280ºC and an isothermal at this temperature for 10 min. The activity of the samples was expressed in terms of methanol and dimethyl ether (DME) conversion, calculated from the difference between inlet and outlet concentrations of methanol and DME. The selectivity was obtained by the mole ratio of each product referred to the moles of converted methanol and DME.

This technique was performed by the author at ICPEES of the University of Strasbourg.

Chapter 4 - Porosity design of a shaped zeolite

Abstract

The detailed procedures for the preparation of the samples are described herein. An in-depth characterization of the structure of the materials and their main features are presented, such as specific surface area, pore volumes and diameters, XRD patterns, SEM images, acidity measurements, and mechanical strength.

This chapter can be partially found in Bingre et al., *Catalysts* **2019**, *9*, 545.

4.1 The birth of a new catalyst

4.1.1 Mesoporous aluminas

The introduction of hierarchical porosity in alumina has been widely studied during the past decades. Many scientists reported several applications of these materials in catalysis, such as active phase, catalytic promoter or support. However, no study up to date dealt with the use of hierarchical aluminas as a binder for extruded zeolites. With that in mind, some of the procedures described in Chapter 2 were adapted and reproduced in this work. Herein, the detailed procedures of the samples' preparation are presented.

- *Al_P123_Wu*: 1.2 g of boehmite was dispersed in a 0.2 M HNO_3 solution for 12 h. Then, 2.1 g of P123 was added to the solution and stirred for another 12 h. The solution was then let to dry for 48 h at 60°C to obtain the mesoporous boehmite powder (adapted from Wu et al.[77]);
- *Al_P123_Grant*: 2 g of P123 was first dissolved in 40 mL of EtOH for 4 h at room temperature. Then, 1 g of boehmite and 0.8 mL of HNO_3 70% were added to the solution and mixed for 5 h. The gel was let to dry for 48 h at 60°C to obtain the powder form of mesoporous boehmite (adapted from Grant et al.[76]);
- *Al_P123_Liu*: peptization of 2 g of boehmite in equal volumes of 30 mL of water and 1M HNO_3 at 80°C for 6 h. Then, the gel was cooled to room temperature, and 2 g of P123 was added and mixed for 3 h. Evaporation of the solvent occurred for 48 h at 60°C (adapted from Liu et al.[81]);
- *Al_P123_Fulvio*: 2 g of P123 was first dissolved in 20 mL of EtOH for 2 h at room temperature. In parallel, 2 g of boehmite was dispersed in 30 mL of distilled water and 30 mL of 1M HNO_3 for 1 h at 80°C. Then, both solutions were mixed at room temperature for 5 h. The gel was allowed to dry for 48 h at 60°C to obtain the mesoporous boehmite in its powdered form (adapted from Fulvio et al.[82]);
- *Al_CTAB_Grant*: 2 g of CTAB was first dissolved in 40 mL of EtOH for 4 h at room temperature. Then, 1 g of boehmite and 0.8 mL of HNO_3 70% were added to the solution and mixed for 5 h. The gel was dried for 48 h at 60°C to obtain the powder of mesoporous boehmite (adapted from Grant et al.[76]);
- *Al_BH_Louis*: 2 g of sugarcane bagasse was treated with 100 mL of 0.5 M NaOH at 130°C for 1 h. The solution was filtered, and the liquid was recovered. Meanwhile, 3 g of boehmite was dispersed in 7.5 mL of distilled water. 64 mL of the bagasse hydrolysate was added and mixed. The solution was transferred to a teflon-lined autoclave and placed in oven at 150°C for 16 h. The solid was filtered, washed and dried overnight (adapted from Cardoso et al.[87]);
- *Al_PEO_Tokudome*: 2 g of boehmite and 0.09 g of PEO were dissolved in a mixture of 5.5 mL of EtOH and 4.0 mL of distilled water. 3.8 mL of propylene oxide (PO) was added to the latter solution at room temperature. The solution was let to age for 24 h at 40°C in a closed vessel and the product was obtained by evaporation of the solvent at 60°C for 48 h (adapted from Tokudome et al.[98]).

All the samples were calcined at 600ºC for 4 h with a heating ramp of 1ºC/min. The diffraction patterns of calcined boehmite show that this treatment is adequate to transform the boehmite in γ-Al_2O_3

structure (Figure 21). It must also be kept in mind that, during this step, the proton is obtained from the ammonium form of the zeolite and the boehmite used as binder is transformed into more stable structure of alumina, crucial to provide the required mechanical strength.

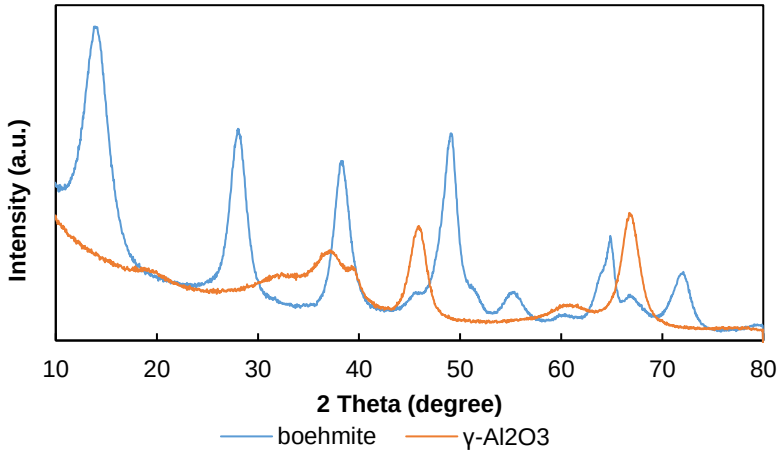

Figure 21: XRD patterns of boehmite and γ-alumina (obtained after calcination at 600ºC during 4 h)

Isotherms of nitrogen adsorption-desorption were obtained, allowing to determine the specific surface area of the alumina and its pore diameter. It was possible to verify which procedures led to the formation of meso- or macroporous aluminas and, consequently, which recipe can be followed during the preparation of extruded catalysts. Table 6 presents the textural properties of as-prepared alumina materials.

Table 6: Structural properties of as-prepared hierarchical aluminas

Sample	S_{BET} (m^2/g)	V_{pore} (cm^3/g)	D_{pore}[a] (nm)
Al_P123_Wu	227	1.17	23
Al_P123_Grant	357	1.01	23
Al_P123_Liu	204	0.93	32
Al_P123_Fulvio	198	1.14	20
Al_CTAB_Grant	225	0.63	8
Al_BH_Louis	149	0.46	9
Al_PEO_Tokudome	187	0.57	10

[a]obtained by BJH method.

The surfactant P123 revealed to be the most efficient pore former agent in boehmite, forming mesopores up to 32 nm. Surprisingly, the four methods were successfully implemented to generate the creation of a hierarchical porosity in boehmite. Unfortunately, bagasse of sugar cane, CTAB, and PEO, although increasing slightly the size of the pores, did not have the same efficiency as the surfactant P123.

In the literature, it is commonly reported that the latter compound, having a hydrophobic part, is capable to form micelles. As the solvent is slowly evaporated, the structure of boehmite adjusts itself around these spheres, which upon calcination, when the structure transforms to γ-alumina and the surfactant is decomposed, leaves voids or the so-called mesopores. In stark contrast, the other reagents used do not have this capacity to form micelles, being totally dispersed in the boehmite. This may justify the fact that there is a slight increase in the pore size but not as significant as the experiments performed with P123.

4.1.2 Hierarchical zeolite bodies

Prior to the introduction of mesoporosity in the zeolite bodies, some samples were prepared to be used as references. Pure boehmite and pure commercial ZSM-5 were separately extruded and named boeh_ext and ZSM-5_ext, respectively. Then, both compounds were mixed and extruded according to typical procedure described in the experimental part (Catal_ref).

Regarding the creation of mesopores in the catalytic body, the methods described before were used when a creation of pore sizes up to 32 nm was achieved. First, the gels were prepared according to the procedures and let to dry slowly. At the end of this ageing step, when remained only the solid, the zeolite and HNO_3 were added, and the extrusion was performed. One of the first observations made was the fact that the extrudable paste did not present the plastic character as the reference one. Indeed, the extrusion revealed to be difficult to perform, as the powder seemed not to be able to agglomerate. The extrudates obtained exhibited poor mechanical strength and were easily crushed. The samples were named Catal_XX, where *XX* relates to the reference where the procedure was based (Grant, Liu, and Fulvio – see section 4.1.1).

Besides the implementation of these methods, one extrusion was also performed where Pluronic P123 and boehmite were directly added to the zeolite without previous treatment. After wetting with an aqueous solution of HNO_3, the extrusion was achieved. Again, the extrudates were not as resistant as the reference one. In this case, the sample was simply named Catal_P123. Here, a question related to the interaction between Pluronic and boehmite arises: to allow the formation of hierarchical porosity after the burning off of the pore former agent, it is necessary that the molecule interacts with boehmite. This is achieved when ethanol and / or nitric acid is / are used. In this case, the acid is in fact employed but in much smaller mass ratio than described in several aforementioned references. One of the reasons may be that this acid is capable of favouring the bonding between P123 and boehmite, consisting in the peptization of the particles of boehmite when the acid / alumina ratio is around 0.11.[89] In the other side, the presence of ethanol results in the formation of an outer surface of micelles by the oxide groups of the polymer, being in contact with the polar medium. Then, the boehmite self-assembles around the ethylene oxide blocks via week coordination bonds.[93] However, ethanol was not used in this method, leaving the doubt that micelles were actually formed during the mixing step.

In the previous section, it was observed that the use of Pluronic P123 exhibited no capacity to form macropores in the alumina. Indeed, all the studies reporting the use of this surfactant do not mention pore sizes greater than few dozens of nanometres. Some pore formers are industrially well-known to create macropores, such as Propyltex and Porlat K85. The first compound is characterized by micronized

polypropylenes, having a particle size up to 149 µm, while Porlat K85 is acrylic glass particles of maximum 150 µm. It was then performed the addition of 10 wt% of these materials during the mixing process of the zeolite with boehmite (samples label: Catal_10Propyl and Catal_Porlat). To verify the influence of the quantity of pore former agent, two additional samples were prepared with 5 and 20 wt% of Propyltex and named Catal_5Propyl and Catal_20Propyl, respectively. Other compounds were used during the extrusion step, such as lignin oxidized extracted and treated from biomass waste of Russia (Catal_lignin), nanocrystals of cellulose that are able to self-assemble, thus creating bigger structures to create meso- or macropores from CelluForce (Catal_CNC) and cellulose fibres Arbocel (Catal_Arbo).

Industrially, the current strategy for improving the effective diffusivity within the zeolite consists in a demetalation of the framework. In order to compare this method with the one developed in this Thesis, CBV3020E was subjected to a desilication treatment to form mesopores in its structure. Part of the sample was further extruded in the same way as Catal_ref and named (BAW for the powder and BAW_ext for the body).

4.2 Interesting features

4.2.1 Structural properties

Through the analysis of the XRD patterns of the samples prepared, it is possible to confirm the sole presence of MFI structure (see representative samples in Figure 22). All the bodies prepared exhibited the same crystallinity than pristine commercial zeolite, meaning that the process of extrusion and the alkaline treatment did neither induce loss of crystallinity, nor the formation of a new crystalline phase. However, one can barely distinguish the peaks associated to the alumina binder in the extrudate samples. In fact, as the ratio used during the extrusion process is relatively small, the intensity of the former is expected not to be detected. However, as it was observed in the previous section, the calcination conditions implemented are appropriate to allow the transformation of boehmite into γ-Al_2O_3.

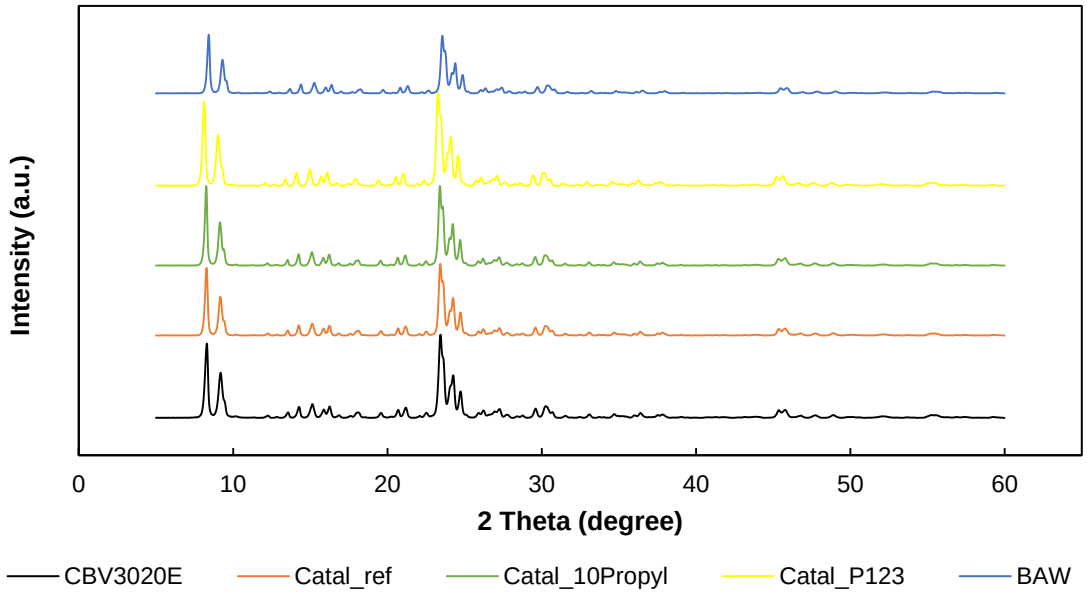

Figure 22: Comparison of the XRD patterns of representative as-synthesised samples

In order to assess the textural properties of the samples, nitrogen adsorption-desorption was performed (Figure 23). The sample boeh_ext exhibited a Type IV isotherm with H1 hysteresis loop, indicating mesopores that can be associated to the interspace formed by the close stacking of the spherical secondary particles. For pure zeolite – CBV3020E – it is observed a Type I isotherm with an associated H4 hysteresis loop. This is typical of microporous materials such as zeolites. The loop describes the behaviour of a wide range of narrow slit-like nanopores.[101]

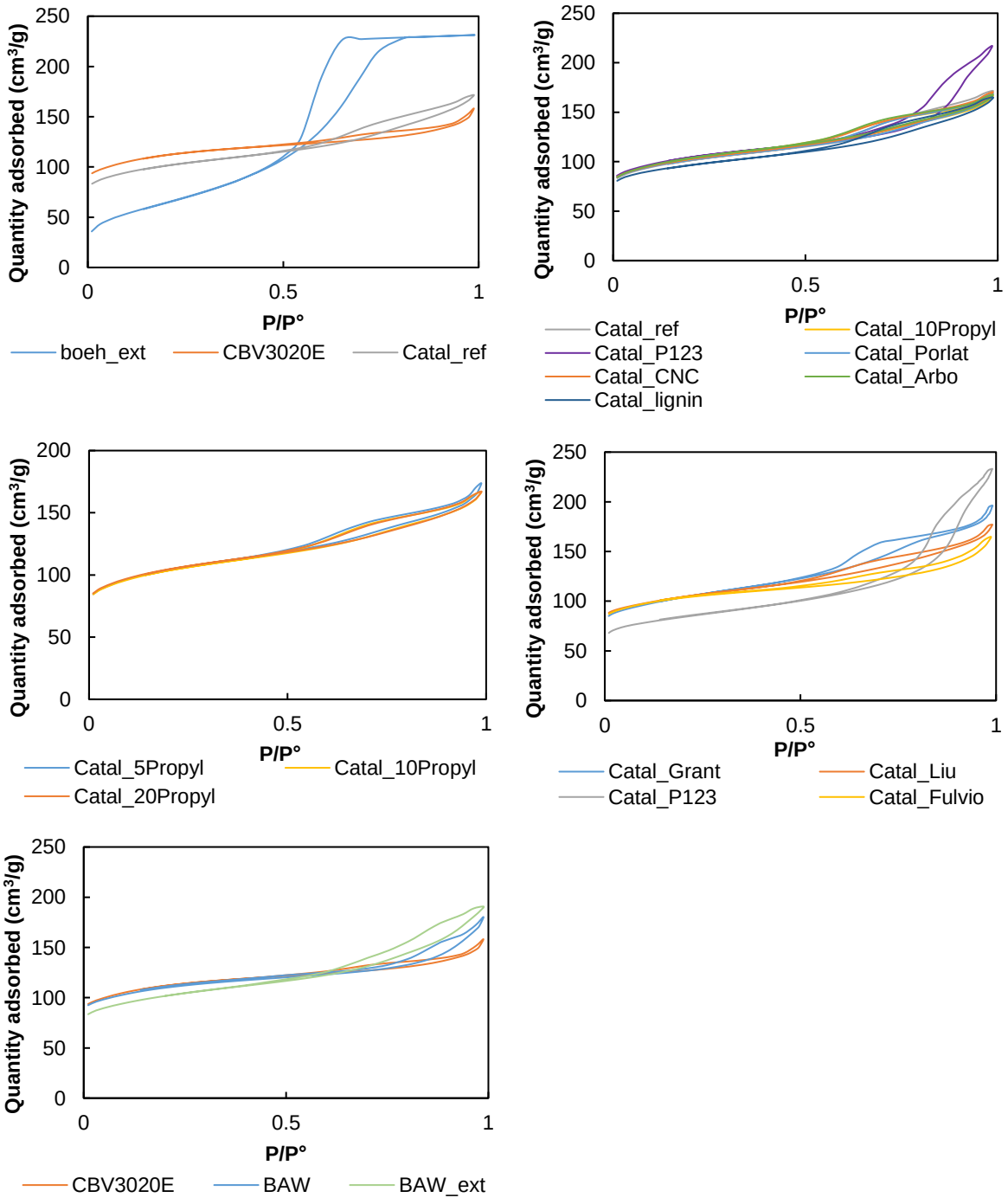

Figure 23: Isotherms of N_2 adsorption-desorption of the samples prepared in this study

Regarding the remaining samples, those results suggest an increase of the total quantity of nitrogen adsorbed upon extrusion. In fact, the sample with sole boehmite presence possesses a higher capacity of nitrogen adsorption. This means, that the addition of the binder leads to an increase in the total pore volume associated to the higher capacity of γ-alumina to adsorb nitrogen. This was verified in all extruded samples with or without the presence of pore former agents (including BAW_ext), except Catal_P123. From the isotherm of this sample, it is possible to observe a higher nitrogen uptake in comparison with the remaining samples. Reminding that the inclusion of Pluronic P123 is expected to create mesopores, this may be a first indication of hierarchical porosity formation.

To further analyse the pore characteristics, the pore profile by BJH method was plotted (Figure 24). For the sample boeh_ext, only one type of pores is found, with a size of 4.5 nm, characteristic of γ-alumina, and justifying the type of isotherm discussed above.[82,94,100] For the remaining samples, it is always observed two main pores at around 3.5 and 6.5 nm. These pores are believed to be associated to intercrystalline mesopores, commonly present in nanocrystals. The absence of further peaks reveals the absence of creation of mesoporosity for most samples, except Catal_P123 that exhibits pores around 11 nm. However, the samples prepared with mesoporous boehmite (Catal_Grant/Liu/Fulvio) did not exhibit the same peak as Catal_P123, although in section 4.1.1, the methods revealed the formation of mesopores. It is possible that the extrusion step somehow collapsed the mesoporous structure due to the application of high pressure, or the quantity of mesopores formed is not enough to be detected among the zeolite structure. In the case where surfactant Pluronic P123 is directly added to the extrudable paste, the material agglomerates itself with the zeolite and boehmite, forming micelles that will leave voids in the structure after being burned off upon calcination. Also BAW and BAW_ext revealed the presence of mesopores having roughly 13 nm in size, confirming that the alkaline treatment of pristine zeolite was successful. The mesopores are maintained even upon extrusion, only with a slight decrease in their surface area and micropore volume due to the presence of the binder, as discussed above. As this technique is limited to the range of 30 to 40 nm, it is not possible to determine the presence of macropores in the material. For that, a complementary mercury intrusion porosimetry (MIP) is needed to verify the presence of pores up to 500 µm, providing a complete profile of the pores profile (Figure 25).

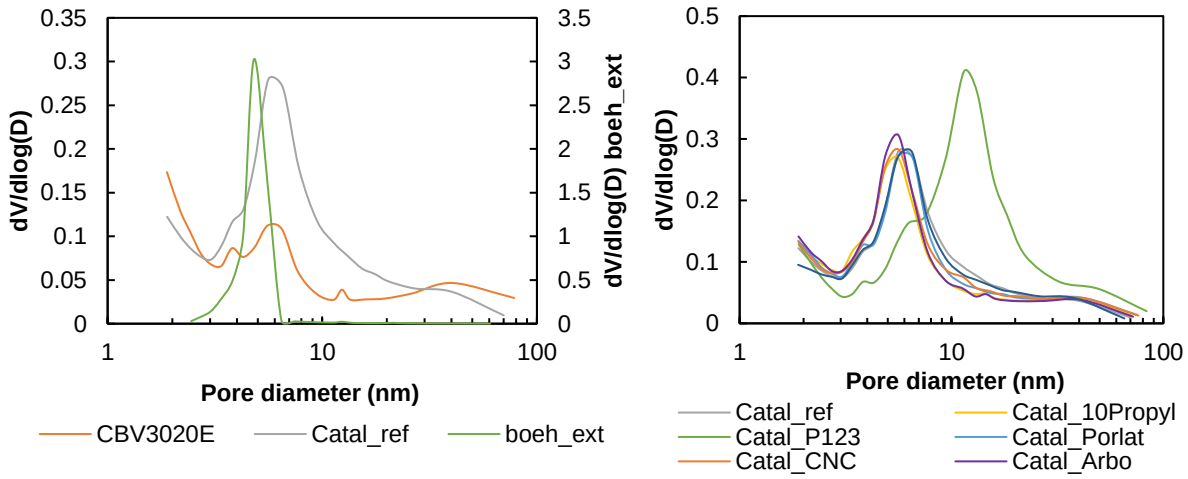

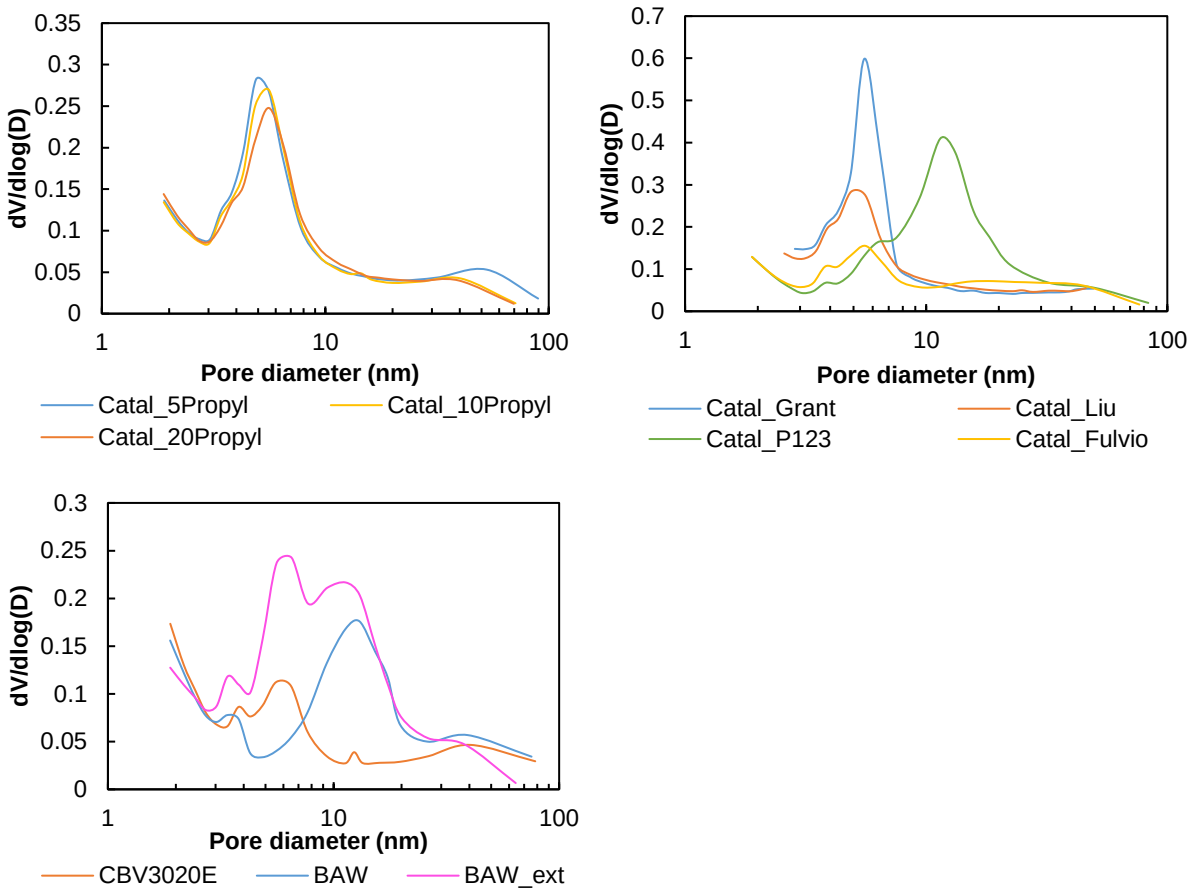

Figure 24: BJH pore profile of the samples prepared in this study

The technique of mercury intrusion porosimetry was implemented in a certain set of samples to assess the presence of macropores. At this point, Catal_Grant / Liu / Fulvio are discarded from the following characterization, since there was no evidence of the presence of mesopores, and it is known that Pluronic P123 does not have the capability to form macropores. At the first sight, the cumulative intrusion curves (Figure 25 A and B) reveal higher amounts of mercury intruded around 0.1 µm in all samples, that it is associated to the macroporosity between zeolite agglomeration with γ-alumina crystals.[103] However, the samples with the presence of pore former agents were able to adsorb higher amounts of mercury in the range of 0.1 to 10 µm in comparison with Catal_ref, thus suggesting the presence of some macropores. Further analyses of the incremental intrusion (Figure 25 C and D) confirm this observation with deeper focus on the samples prepared with Propyltex. The latter materials exhibit peaks around 0.5 to 1.8 µm with an increase of the intensity of peak with a raise in the quantity of Propyltex used during the extrusion step. It seems fair to conclude that this material was able to form macropores in the catalytic bodies, being affected by the amount of mass added.

[103] a) Mitchell, S.; Michels, N.-L.; Pérez-Ramírez, J. *Chem. Soc. Rev.* **2013**, *42*, 6094–6112; b) Michels, N. L.; Mitchell, S.; Pérez-Ramírez, J. *ACS Catal.* **2014**, *4*, 2409–2417.

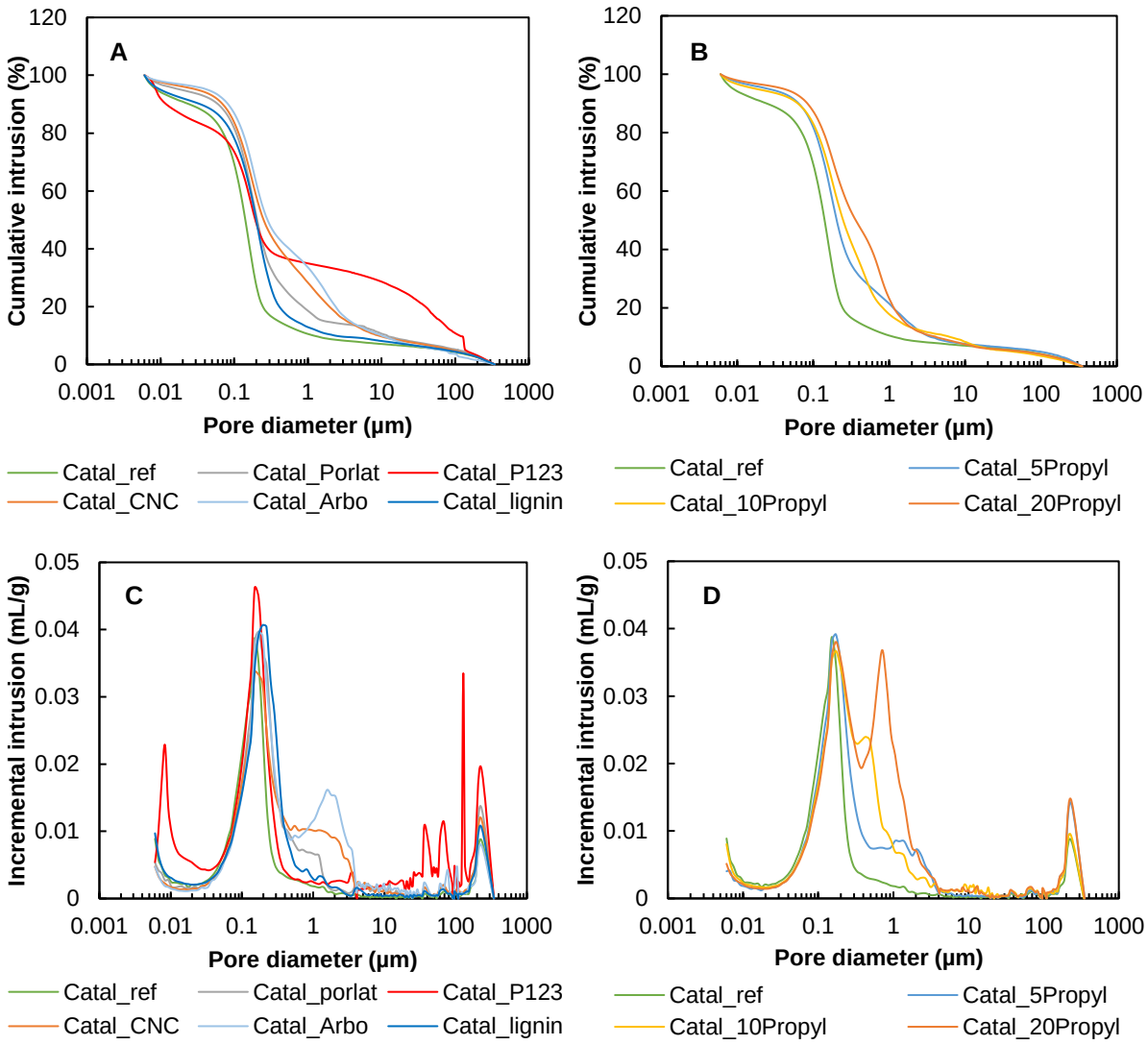

Figure 25: Cumulative (A and B) and incremental (C and D) Hg intrusion of the samples

Regarding Catal_P123, no mercury uptake is observed in the range of 0.1 to 10 µm which is in agreement with the previous observations that Pluronic P123 does not induce macropores formation. However, this is not the case between 10 and 300 µm that it is associated to possible fissures and cracks present in the catalytic body. It was mentioned before, that this method led to poor efficient extrusion, producing fragile bodies that are easily crushed by hand. This is not the case for the remaining samples where the extrusion process occurred smoothly, and the resulting bodies presented elevated mechanical strength. Table 7 summarizes the main features obtained by the two techniques. It is possible to observe that the external surface area did not change upon extrusion, however this is not the case for the samples prepared with different pore former agents. In fact, the external surface area increases what further confirms the creation of additional porosity in the binder that allows better access to the external surface of the zeolite. On the contrary, Catal_lignin had a considerably reduction in this parameter which suggests that the introduction of this material in the extrusion step improves the interaction between binder and zeolite, creating a more connected system that hinders the arrival of the nitrogen molecules to the zeolite structure.

Table 7: Parameters obtained by N_2 adsorption - desorption and MIP of the samples

Sample	S_{BET}[a] (m^2/g)	S_{ext}[a] (m^2/g)	V_{pore}[a] (cm^3/g)	V_{micro}[a] (cm^3/g)	$V_{intrusion}$[b] (cm^3/g)	D_{pore}* Mesopores[a] (nm)	D_{pore}* Macropores[b] (µm)	Porosity[b] (%)
Boeh_ext	237	-	0.36	-	-	-	-	-
CBV3020E	368	147	0.23	0.11	-	-	-	-
Catal_ref	336	148	0.26	0.09	0.43	-	-	43
Catal_5Propyl	347	159	0.25	0.09	0.56	-	1.8	41
Catal_10Propyl	345	156	0.25	0.09	0.65	-	0.5	53
Catal_20Propyl	348	155	0.25	0.09	0.78	-	0.7	58
Catal_Porlat	339	149	0.25	0.09	0.57	-	0.9	48
Catal_P123	348	154	0.32	0.09	0.81	11	-	60
Catal_Arbo	345	159	0.25	0.09	0.67	-	2	53
Catal_CNC	342	152	0.25	0.09	0.61	-	2	52
Catal_lignin	319	129	0.25	0.09	0.55	-	-	48
BAW	362	144	0.26	0.11	-	13	-	-
BAW_ext	338	156	0.28	0.09	-	11	-	-

[a]obtained by N_2 adsorption – desorption; [b]obtained by MIP.
*NOTE: in the table it is presented the diameter of the pores formed by the pore former agents, excluding intercrystalline mesoporosity and macroporosity characteristic of the zeolite and extruded materials.

In order to assess the observations made by the previous techniques related to textural properties, SEM images were recorded for the samples. In Figure 26 (left), it is possible to observe the nanocrystals of the commercial zeolite used in the preparation of the pellets. This justifies the presence of intercrystalline mesopores, as the nanocrystals are susceptible to create mesoporosity during their stacking. Besides, the alkaline treatment kept the crystallinity of BAW with the addition of a certain degree of intracrystalline mesoporosity as verified by nitrogen adsorption-desorption.

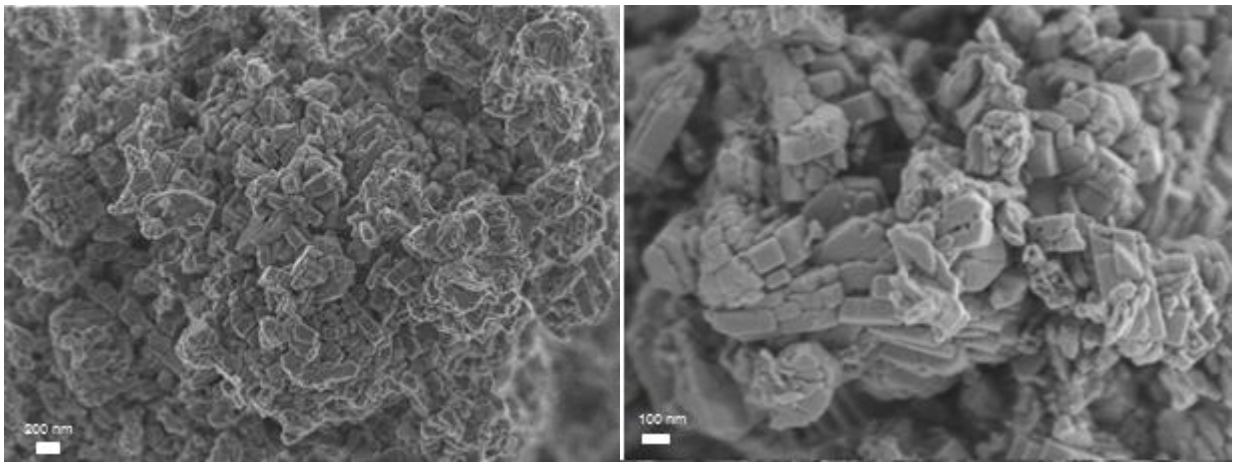

Figure 26: SEM image of CBV3020E (left) and BAW (right)

The samples comprising pure boehmite and boeh_ext were also analysed by this technique (Figure 27). In the former, a “donut-like” shape can be observed with around 20 µm in diameter. For the second one, very large crystals are found with a size in the scale of dozens of µm. The difference is associated with the structure transition from boehmite into γ–alumina due to the calcination process.

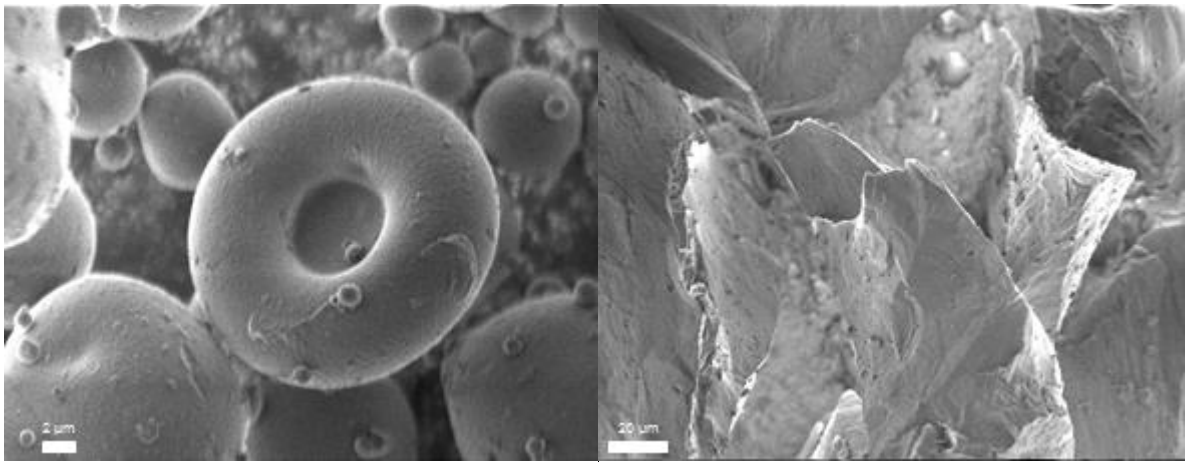

Figure 27: SEM image of boehmite Sasol P2 (left) and γ-alumina (right)

As a first trial for the extruded zeolites, the images were obtained from a tabletop microscope Hitachi TM3030, efficient enough to detect the presence of macropores, where the bodies can be analysed directly in the equipment without the need to crush. In this wat, the images are captured at a lower zoom range (dozens of µm) being possible to observe some characteristics of the whole extrudate that may not be visible at the scale of the nm. Figure 28 shows those micrographs and confirms the presence of macropores in the samples.

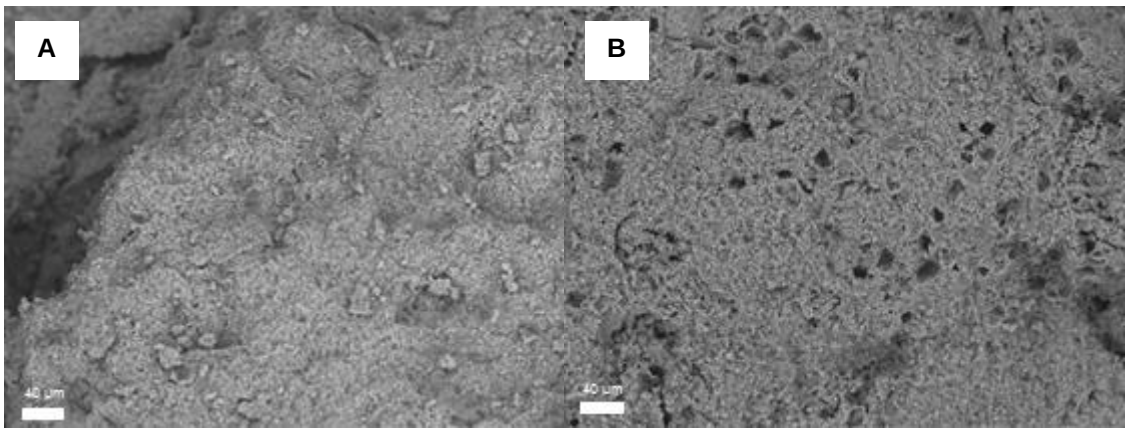

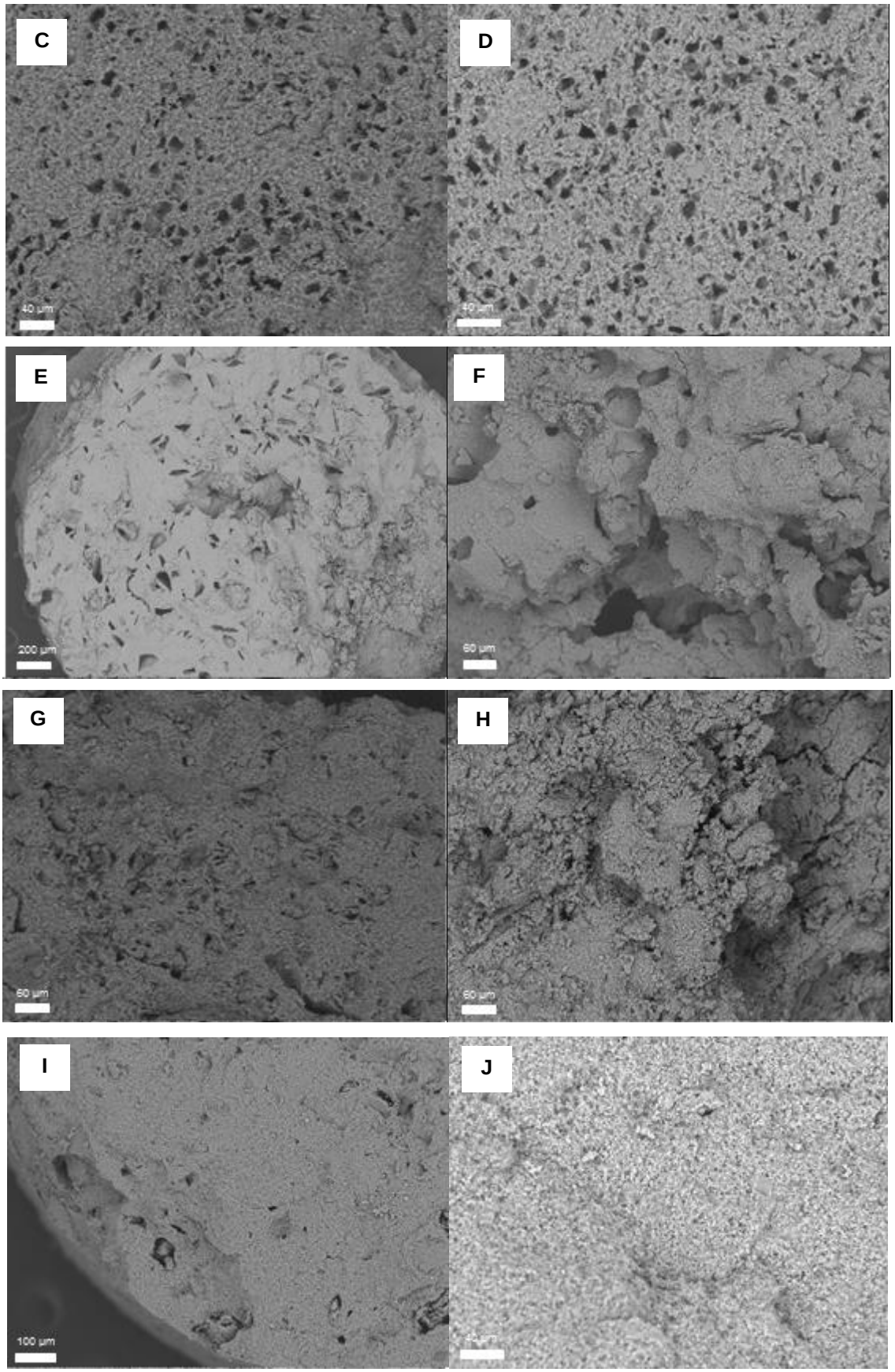

Figure 28 : Tabletop SEM images of the samples: A) Catal_ref; B) Catal_5Propyl; C) Catal_10Propyl; D) Catal_20Propyl; E) Catal_Porlat; F) Catal_P123; G) Catal_Arbo; H) Catal_CNC; I) Catal_lignin; J) BAW_ext

The samples prepared with different quantities of Propyltex exhibit circular voids of regular size in their surface that it is not visible in Catal_ref, which displays a smooth surface without the presence of macropores. Moreover, it seems that the density of macropores increases with an increase of the amount of this pore former agent, being thus in line with the results of Hg porosimetry that indicated an increase in the intrusion volume. These images also explain the higher pore volume of the remaining samples in comparison with Catal_ref, as each one of them presents a determined type of pore. Also, as expected, Catal_P123 possesses giant voids in the extrudate caused by cracks and fissures. Finally, BAW_ext presents the same surface characteristics as Catal_ref, being associated to the absence of macropores.

To further characterize the extrudates, one important analysis was performed that consisted in the mapping of the elements present in the samples. For that, images of resin-embedded extrudates were recorded at the microscope coupled with a microprobe (Figure 29 and Figure 30). Figure 29 shows a good extrusion procedure, in terms of water content, and plastic character of the extrudable paste, as no imperfections could be observed, such as fissures and great voids caused by the presence of air. The mapping of Si and Al elements suggests a relatively homogeneous distribution of the binder in the catalytic body. This is crucial to ensure an even mechanical strength in all the bodies prepared, avoiding zones weaker than others.

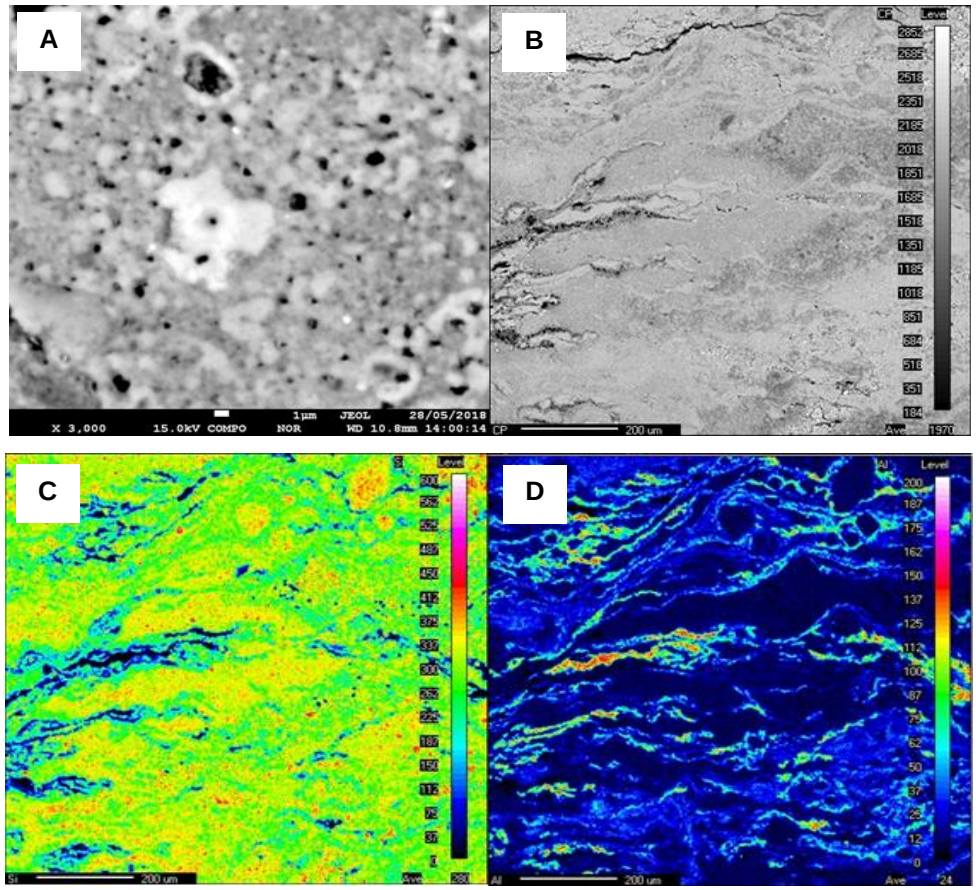

Figure 29: SEM image coupled with microprobe of Catal_ref at two different scales: A) clear visualisation of two different phases of Al_2O_3 and SiO_2; B) morphology of the catalyst at 200 µm; mapping of the Si (C) and Al (D) elements present in Catal_ref

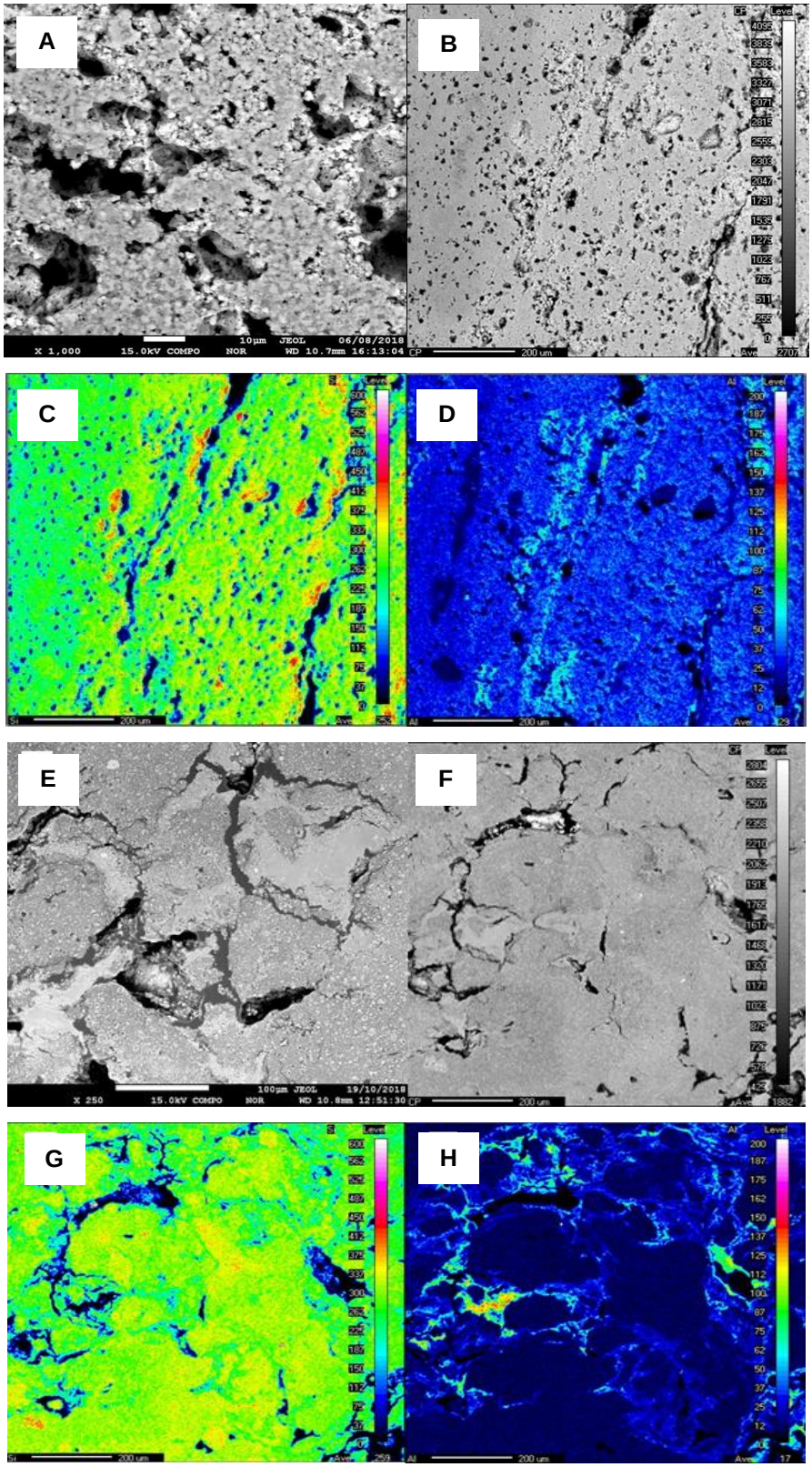

Figure 30: A) clear visualization of macropores in Catal_10Propyl; B) morphology of Catal_10Propyl at 200 µm; mapping of the (C) Si and (D) Al elements present in Catal_10Propyl; (E) clear visualization of macropores in Catal_P123; (F) morphology of Catal_P123 at 200 µm; mapping of the (G) Si and (H) Al elements present in Catal_P123

On the other side, the macropores of Catal_10Propyl and Catal_P123 measured by MIP and evidenced by table-top microscope are clearly visible (Figure 30). The sample is characterized by a homogeneous distribution of macropores of nearly identic size. Evidently, the formation of these macropores has been caused by the presence of Propyltex, that upon calcination, is removed leaving the voids that constitute “highways” in the catalytic body. Moreover, while observing the mapping of the elements, there is a better distribution of the binder in all the extrudate, compared with Catal_ref. This represents similar structural characteristics in the whole sample, conferring a homogeneous influence for further catalytic testing.

TEM images of Catal_ref and Catal_10Propyl were recorded in Figure 31. Two distinct structure morphologies are clearly visible, one being attributed to the ordered microporosity of zeolite and the other has been previously observed by Paglia et al.[104] The latter is typical of γ-Al_2O_3 formed from calcination of boehmite at 600ºC showing a disordered mesoporosity, as predicted by N_2 adsorption-desorption measurements.

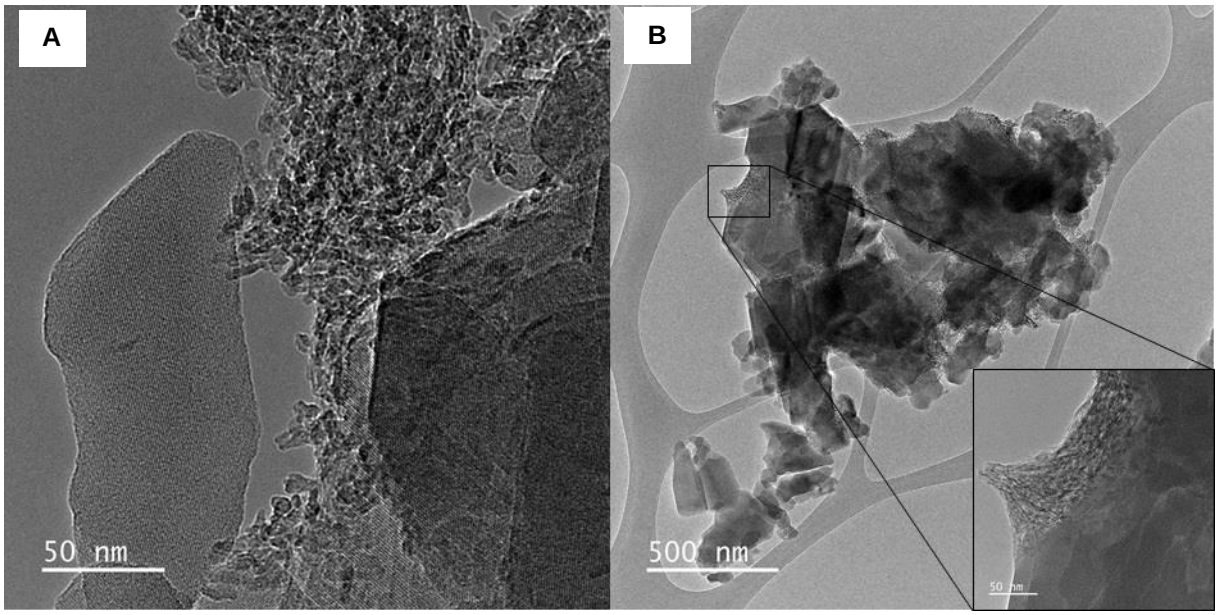

Figure 31: TEM image of a) Catal_ref and b) Catal_10Propyl *with a close look at the interface between zeolite and alumina*

4.2.2 Acidity and mechanical strength

After checking the structural properties of the samples, it is obviously necessary to measure the acidity of these zeolite bodies. The nature of the interactions (and their influence) involved in the binding process has been discussed in the first part of this manuscript. Many studies reported alterations in the Brønsted and Lewis acid sites due to presence of alumina in the extrudate. As this aspect is crucial for the catalytic activity of the zeolites, one has to study it carefully.

[104] Paglia, G.; Buckley, C. E.; Rohl, A. L.; Hart, R. D.; Winter, K.; Studer, A. J.; Hunter, B. A.; Hanna, J. V. *Chem. Mater.* **2004**, *16*, 220–236.

The desorption of ammoniac by an incremental increase of the temperature was performed in the samples. This technique is a powerful tool to determine changes in the acidity of the material. At first, NH_3 adsorbs onto the sample until saturation with different strengths, i.e., as much stronger is the acid site, higher energy is necessary to desorb it from the structure. It is known that Lewis acid sites are weaker than Brønsted sites, which justifies the presence of two peaks at 220 and 550°C in the TPD spectra (Figure 32).

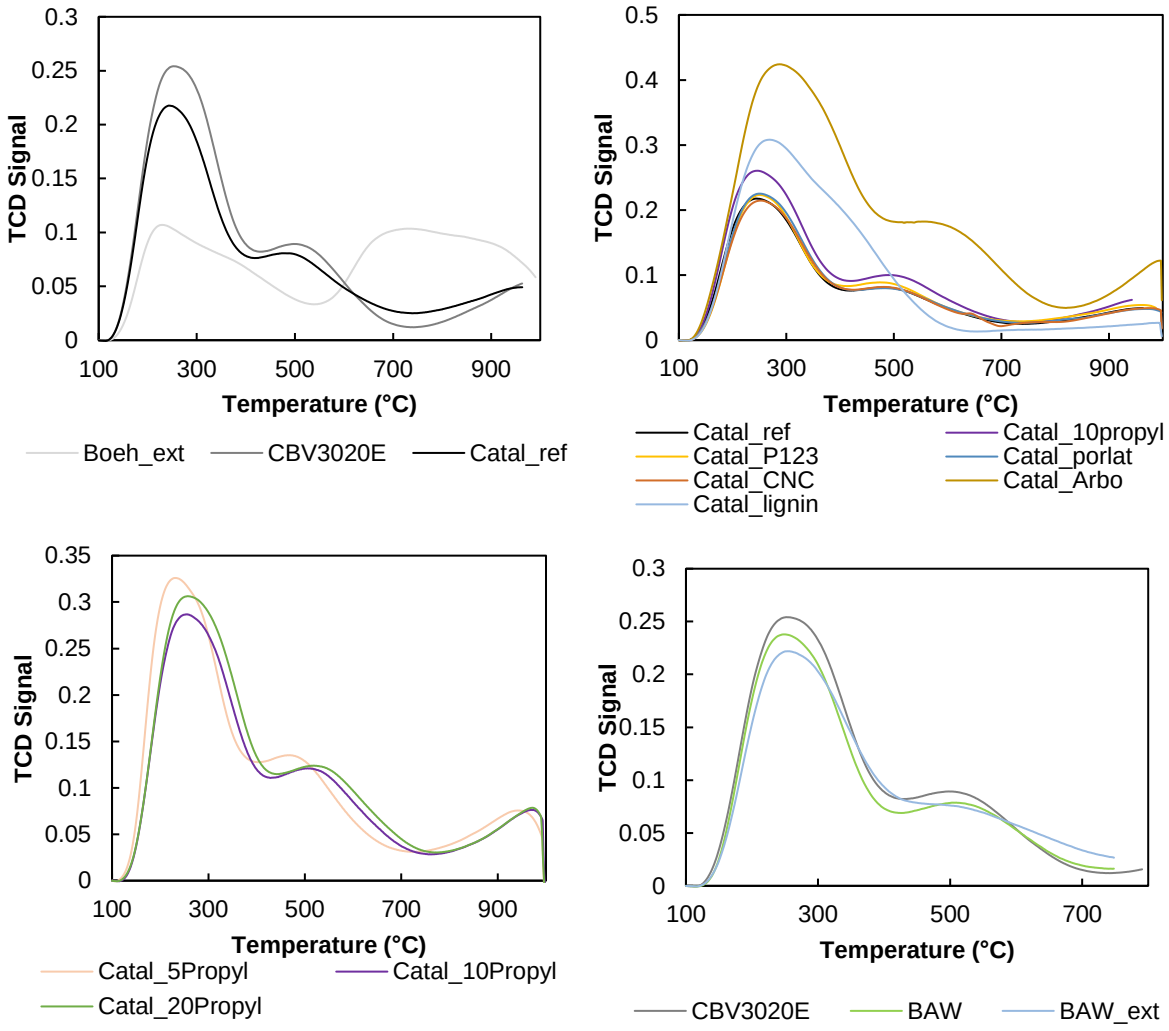

Figure 32: Desorption profile of NH_3 recorded for selected samples.

By integration of the high-temperature peak, the concentration of strong acid sites could be estimated (Table 8). The acidity profile of boeh_ext revealed the presence of mainly weak acid sites, being located at 220°C. This shows that the presence of the binder in the zeolite extrudates did not induce additional acidity, as the total acidity of the samples corresponds approximately to 80% of the total acidity of CBV3020E (quantity of zeolite used in the extrusion process). All samples exhibit similar NH_3 desorption profiles, suggesting that the extrusion procedure did not alter significantly the acidity of these materials, with the exception of Catal_Arbo and Catal_lignin. The first presents a higher amount of probe molecule adsorbed, however its values presented in Table 8 are similar with the remaining

samples. Concerning Catal_lignin, a peak at higher temperatures can be barely observed, which may imply that the presence of lignin as pore former agent somehow impacted the acidity of the sample. One possible explanation relies in high exothermicity of lignin combustion upon the calcination step; it is known that the presence of high amounts of steam at high temperature is capable to dealuminate the zeolite framework, resulting in a decrease of the number of Brønsted acid sites.[105] On the other side, it is noteworthy that no shift of the peak at higher temperatures could be evidenced among the different samples. In contrast to previous studies showing a higher desorption temperature, hence a higher acid strength[106], the strategy presented herein did not induce changes in the acidity of the material. This is extremely important for acid catalytic purposes.

Table 8: Quantification of sample's acidity by NH_3-desorption and pyridine FT-IR

Samples	Low acidity by NH_3-TPD (µmol/g)[a]	Strong acidity by NH_3-TPD (µmol/g)[b]	Lewis acid sites by pyridine-IR (µmol/g)[c]	Brønsted acid sites by pyridine-IR (µmol/g)[d]
Boeh_ext	328	-	-	-
CBV3020E	817	249	90	350
Catal_ref	642	223	110	340
Catal_5Propyl	854	278	-	-
Catal_10Propyl	781	287	120	270
Catal_20Propyl	833	279	-	-
Catal_P123	641	218	90	320
Catal_Porlat	653	188	-	-
Catal_Arbo	849	210	-	-
Catal_CNC	651	251	-	-
BAW	872	276	-	-
BAW_ext	800	243	-	-

a) obtained by integration of the low-temperature peak of NH_3-desorption analysis; b) obtained by integration of the high-temperature peak of NH_3-desorption analysis; c) obtained by integration of the peak correspondent to coordinated pyridine in pyridine FT-IR; d) obtained by integration of the peak correspondent to protonated pyridine in pyridine FT-IR.

For a better characterization of the acidity of the samples, a selected group was subjected to adsorption of pyridine followed by FT-IR allowing the determination of the quantity of Lewis and Brønsted acid sites (Table 8). IR spectra (Figure 33) present 6 bands at: (i) 1634 and 1544 cm^{-1} characteristic of the ν_{8a} and ν_{19b} vibration modes of pyridinium ions; (ii) 1622 and 1611 cm^{-1} characteristic of the ν_{8a} vibration mode of coordinated pyridine Al in tetrahedral and octahedral environments, respectively; (iii) 1455 cm^{-1} characteristic of the ν_{19b} vibration mode of coordinated pyridine; and (iv) 1498 cm^{-1} characteristic of the ν_{19a} vibration mode of coordinated and / or protonated pyridine. By integration of the peaks at 1544 and 1455 cm^{-1}, it is possible to determine the Brønsted and Lewis acid sites, respectively.

[105] Romero, M. D.; Calles, J. A.; Rodríguez, A.; De Lucas, A. *Microporous Mater.* **1997**, *9*, 221–228.
[106] a) Hidalgo, C. v.; Itoh, H.; Hattori, T.; Niwa, M.; Murakami, Y. *J. Catal.* **1984**, *85*, 362–369; b) Katada, N.; Igi, H.; Kim, J.-H. *J. Phys. Chem. B* **1997**, *101*, 5969–5977.

As seen in the aforementioned ammonia desorption analysis, there is a decrease of the acidity due to dilution of the zeolite phase by the binder presence. However, although the total amount of Brønsted acid sites did not drastically change, there is a significant decrease in Catal_10Propyl. This was not observed by NH_3-desorption, that showed in fact a slightly higher density of strong acid sites, however one must keep in mind the different techniques used and a certain degree of uncertainty of the analysis (15% to NH_3-desorption and 3% for pyridine FT-IR). In general, it may be admitted low changes in the acidity of the samples, confirming the previous observations, although contradicting the results obtained by Coralie Demaret.[107] In her thesis, it was deeply studied the interactions of the binder with the structure of the zeolite, showing considerable changes in the acidity of the samples prepared with 50 wt% of binder. The presence of alumina as a binder led to alumination of the zeolite structure, reducing the quantity of Brønsted acid sites. This was not observed during this Thesis, probably due to the lower quantity of binder used and the absence of the peptization step during the preparation.

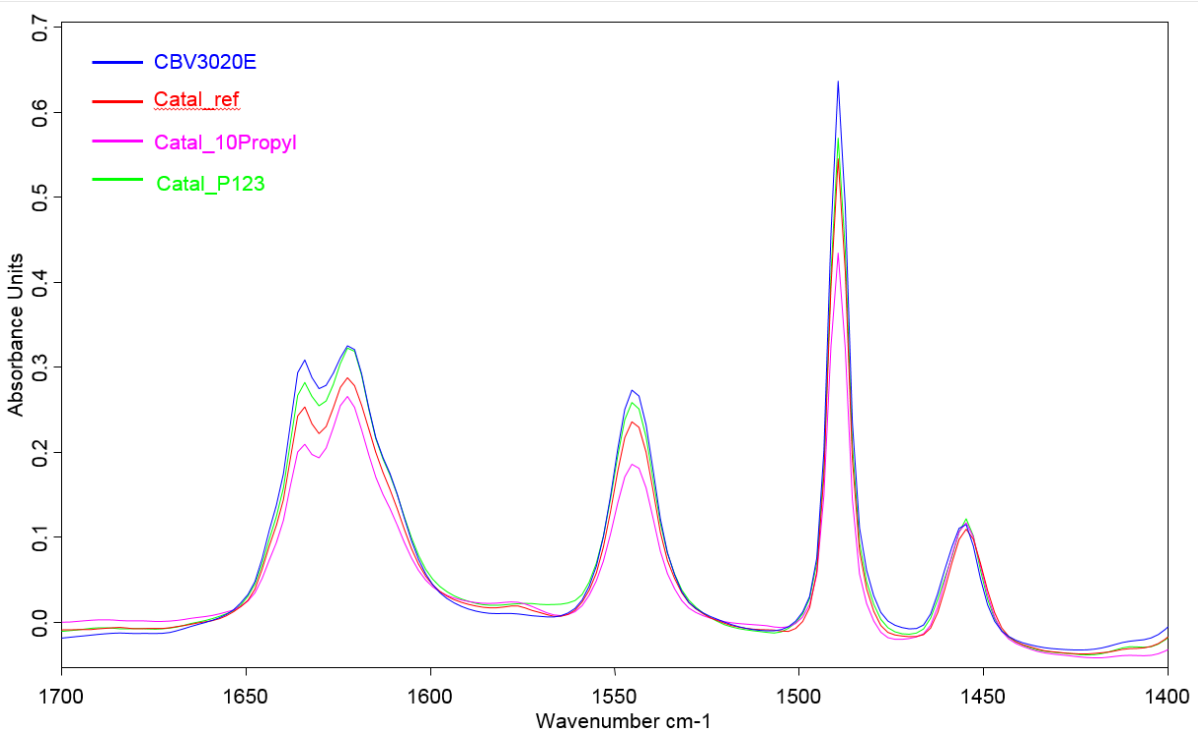

Figure 33: IR spectra of adsorbed pyridine on selected samples

Finally, as seen in the introductory section, the mechanical strength of extrudates is an important parameter in industrial equipment as the lower layers of catalyst must be able to resist the weight of tons of materials without crushing. The mechanical stability of selected samples was assessed, and the results are given in Table 9.

[107] Demaret, C. *Mise en forme de zéolithes : Contrôle des propriétés acides des zéolithes et description de l'interface zéolithe / liant*, Ph.D. Dissertation, **2019**.

Table 9: Pressure applied to the extrudates where crushing occurred. The table presents the maximum, minimum, and average of this force over an experiment with 15 extrudates.

	Catal_ _ref	Catal_ _5Propyl	Catal_ _10Propyl	Catal_ _10Porlat	Catal_ _Arbo	Catal_ _lignin
Average strength (N)	16.5	5.5	6.5	13.9	7.3	15.5
Maximum	22.5	8.7	8.4	28.8	10.1	34.7
Minimum	10.8	1.1	5.3	6.1	3.9	5.0

As expected, the introduction of porosity in the material results in a decrease of the mechanical stability. The creation of pores and "highways" implies that less quantity of materials is supporting the pressure applied, which results in a lower resistance to crush forces. However, the porosity is not the only factor that influences the mechanical stability of zeolite extrudates. The efficiency of the extrusion process plays, perhaps, the biggest role in this parameter. The author risks affirming that the introduction of meso- or macropores diminished only slightly the capability of the material to support high pressures as it is seen in the case of Catal_10Propyl. For example, Catal_lignin shows mechanical stability very similar to Catal_ref, by the fact that, as it was mentioned before, the presence of lignin had a positive effect during the extrusion process, according to experimental observations. In contrast, Catal_P123 exhibited a low mechanical stability (not represented) below 1N, being thus easily crushed by hand. This is not attributed to the presence of mesopores but by poor extrusion efficiency, as a result of the use of Pluronic P123 that did not lead to high homogeneity in the solids and providing a very thick gel paste to be extruded.

4.3 Conclusion

In this chapter, a strategy to design different types of porosity without, at the first sight, compromising the zeolite structure was achieved. The pores created by the voids left after burning off the pore former agents were present homogeneously in the extrudates. In fact, the structure of boehmite (AlOOH) suffered transformation at high temperatures by dehydrating, to form γ-Al_2O_3 that is characterized by an elevated mechanical strength and crystallinity. Since this transformation occurs in the presence of the pore former agents, the structure will arrange around these components, maintaining the hierarchical porosity. In addition, no major changes in the structure of the zeolite could be observed at elevated temperatures.

Nonetheless, it is important to consider the possibility of some degree of dealumination of the zeolite due to the high exothermicity of pore formers combustion. The quantity of water vapour produced during this reaction may be capable to extract some aluminium species from the framework leading, consequently, to a decrease of the Brønsted acid sites. Moreover, a decrease of the mechanical stability was also observed. These two factors, due to different reasons, are important parameters to take into account in industrial processes, and, particularly the acidity, will be considered further in this Thesis for the catalytic reactions.

Chapter 5 – Catalytic performances

Abstract

This chapter presents the performance of as-synthesized zeolite bodies with different porous systems in three catalytic reactions and in an adsorption process. The catalyst lifetime and the selectivity in the methanol-to-hydrocarbons reaction are presented and discussed. To better understand the influence of additional porosity in the zeolite bodies, cracking of n-butylcyclohexane (model for naphtha fraction) was performed and further analysed. The cracking of n-hexane allowed the assessment of the acidic characteristics of the samples. Finally, toluene adsorption in VOC removal conditions is also presented.

This chapter can be found in Bingre et al., *Catalysts* **2019**, *9*, 545.

5.1 Methanol-to-hydrocarbons reaction

The methanol-to-hydrocarbons (MTH) reaction has received great attention by academic researchers due to its large range of valuable products, being either olefins, primary blocks in the production of plastics and polymers, either fractions of heavier molecules, nearly ready gasoline. For the first part, two types of zeolites have shown outstanding performance: SAPO-34 (CHA type) and ZSM-5 (MFI type), exhibiting higher selectivity towards light olefins, such as ethylene and propylene. However, in recent decades, the demand in propylene has greatly increased due to the use of cheaper natural gas over oil as a feedstock by North America petrochemical producers. As a result, the co-product of region's steam-crackers (propylene) is significantly decreasing, which leads to the desire of reaching higher selectivity towards this molecule.[108]

ZSM-5 having pores with diameters of 5.1 – 5.6 Å and crossed 10-member ring channels and channel intersections[109] allows the exit of larger molecules, giving products in the range of C_1-C_{10}. SAPO-34, on the other side, possesses narrow pores with a diameter of 3.8 Å, large cages and narrow 8-member ring openings[109], which although large aromatic hydrocarbons are capable to be formed inside, the narrow pores inhibit them from escaping, giving a product distribution between C_1-C_5. An accumulation of large aromatic species on the surface induces a faster catalyst deactivation than ZSM-5. Nonetheless, the deposition of coke in the ZSM-5 zeolite pores is still significant and many researchers have proposed the introduction of hierarchical porosity and the design of nanocrystals to increase the diffusion of these larger molecules outside the microstructure, leaving the active sites *clean*.

The group of Pérez-Ramírez[110] has greatly contributed with reports devoted to study the influence of binders in the performance of hierarchical ZSM-5 zeolites in the MTH reaction. Frequently, there can be alterations to the catalyst lifetime and / or products selectivity caused by either cation migration from the binder to the zeolite structure, or the creation of intercrystalline meso / macroporosity, or even pore blocking issues already discussed in Chapter 2.

5.1.1 Catalytic activity

As discussed before, this Thesis describes the development of a new strategy to improve the effective diffusivity within shaped zeolites without changing their structure. The samples prepared and characterized in Chapter 4 were tested in the conversion of methanol and are represented in Figure 34. The first observation worthy to describe is the significant decrease of Catal_ref lifetime compared with the pristine commercial zeolite CBV3020E. After 24 h on stream, the extruded samples exhibited a conversion of around 75%, indicating a fast deactivation. In fact, the sample is only capable to maintain

[108] a) https://www.businesswire.com/news/home/20161028005216/en/Global-Propylene-Market-Witness-Growth-2020-Owing (accessed on May 6, 2019); b) https://www.chemicals-technology.com/news/newsworldwide-demand-for-propylene-to-rise-to-130-million-tonnes-by-2023-says-ihs-4356137/ (accessed on May 6, 2019); c) https://www.economic-plant.com/18-news/70-increasing-global-demand-for-on-purpose-production-of-propylene.html (accessed on May 6, 2019).

[109] http://www.iza-structure.org/databases/(accessed on May 29, 2019)

[110] a) Mitchell, S.; Michels, N. L.; Kunze, K.; Pérez-Ramírez, J. *Nat. Chem.* **2012**, *4*, 825–831; b) Gueudré, L.; Milina, M.; Mitchell, S.; Pérez-Ramírez, J. *Adv. Funct. Mater.* **2014**, *24*, 209–219; c) Michels, N. L.; Mitchell, S.; Milina, M.; Kunze, K.; Krumeich, F.; Marone, F.; Erdmann, M.; Marti, N.; Pérez-Ramírez, J. *Adv. Funct. Mater.* **2012**, *22*, 2509–2518; d) Michels, N. L.; Mitchell, S.; Pérez-Ramírez, J. *ACS Catal.* **2014**, *4*, 2409–2417.

the conversion at 100% during 4 h of reaction. In contrast, CBV3020E exhibits nearly 100% of conversion even after 24 h on stream, thus having a relatively slower deactivation rate.

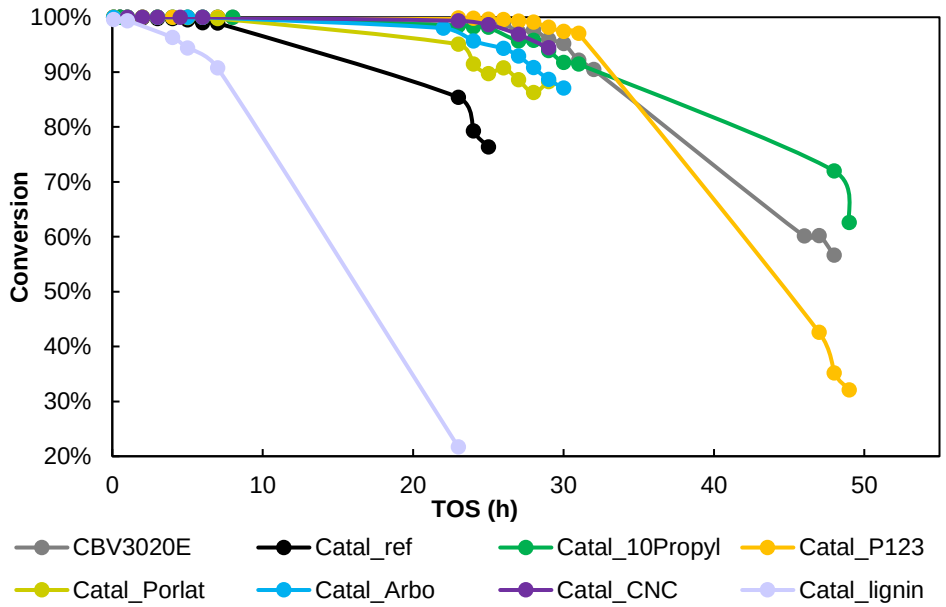

Figure 34: Methanol and dimethyl ether conversion over the samples prepared with different pore former agents

Regarding the different samples synthesised with additional pore former agents, two of them showed performances comparable with the powder zeolite: Catal_10Propyl and Catal_P123. These two samples retain the conversion at nearly 100% for 24 h of reaction, although Catal_P123 was able to convert for longer time than CBV3020E and Catal_10Propyl. Recording to the previous chapter, the latter exhibited regular and homogeneous macropores, while Catal_P123 was the only sample where mesopores where created, although at the cost of cracks and fissures formation during the extrusion process. Catal_Porlat, Catal_Arbo and Catal_CNC exhibited higher catalyst lifetime than Catal_ref although not as important as the samples described before.

In contrast, Catal_lignin although reaching 100% of conversion during the first hour of reaction, a rapid deactivation occurred after that. This was expected as the addition of lignin as pore former agent did not lead to the formation of meso- or macropores and greatly diminished the strong acidity of the sample (assessed by NH_3-TPD, see Figure 32). The key role of acidity in the MTH reaction is well known, as the active sites are responsible for the conversion of methanol into the products. It seems obvious that an extensive decrease of the latter will negatively affect the catalytic performance of the sample.

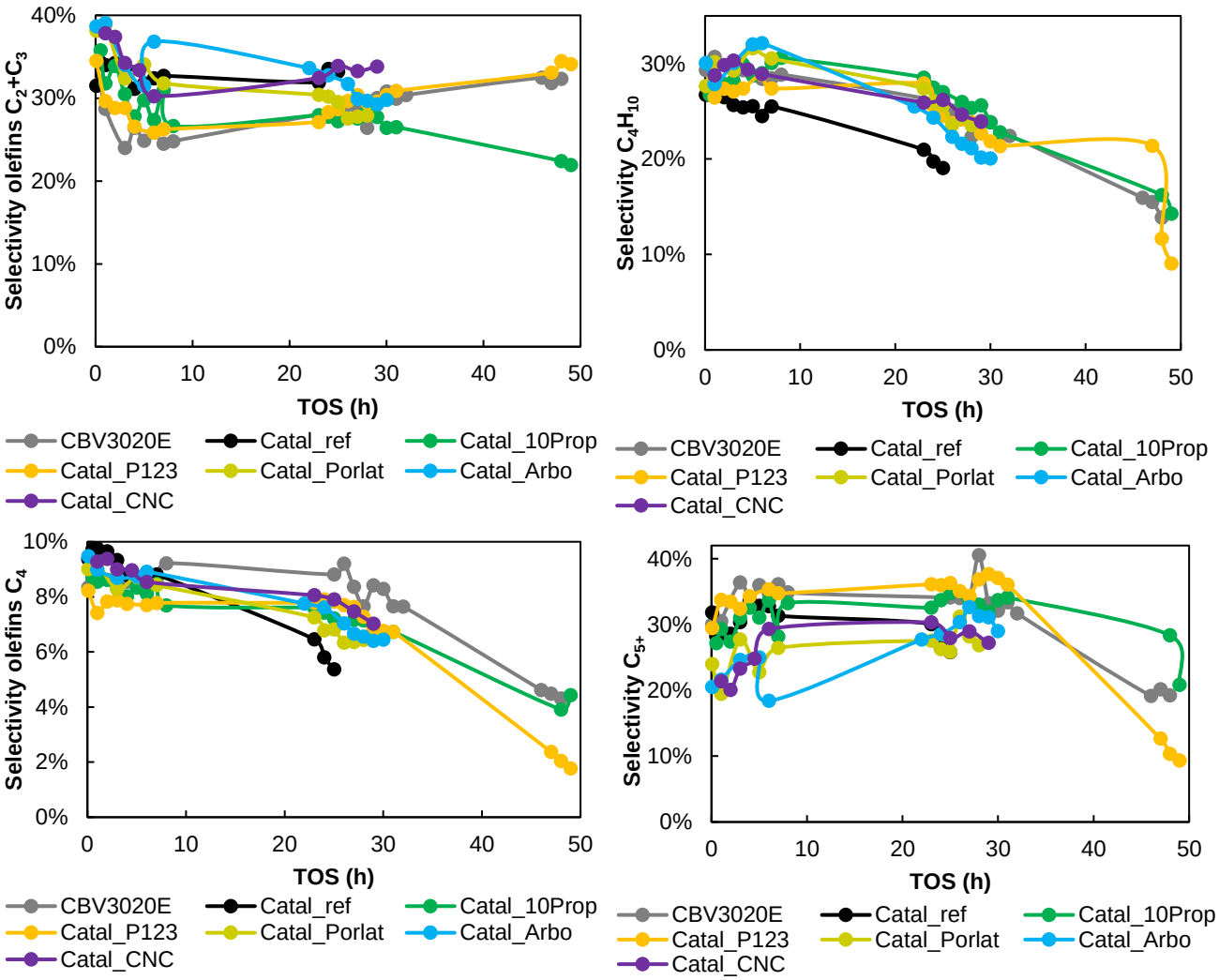

Figure 35: Selectivity in light olefins C_2+C_3 (ethylene and propylene), butylenes (C_4), isobutane (C_4H_{10}), and compounds with 5 carbons or more (C_{5+}) over the samples prepared with different pore former agents

Table 10: Selectivity in ethylene (C_2H_4), propylene (C_3H_6), butylenes (C_4H_8) and compounds with 5 carbons or more (including aromatics – C_{5+}) after 1 h reaction of the samples

Samples	$\%S_{C2H4}$	$\%S_{C3H6}$	$\%S_{C4H8}$	$\%S_{C5+}$
CBV3020E	3	26	9	30
Catal_ref	6	28	10	29
Catal_10Propyl	4	28	9	29
Catal_P123	4	26	7	34
Catal_Porlat	6	33	9	19
Catal_Arbo	4	35	9	22
Catal_CNC	5	33	9	21
Catal_lignin	12	20	9	36

Figure 35 shows the selectivity in light olefins, butylenes, isobutane and compounds with 5 carbons or more over the entire reaction. Interestingly, light olefins seem to be little influenced by the

deactivation of the catalyst, while the remaining products start to decrease when the conversion of oxygenates decreases. This may due to the fact that deactivation is caused by a poising of the active sites by coke molecules that can also block the pore entrance. In this way, the products diffusion will be hindered, causing a decrease in the selectivity. However, as light olefins exhibit low diffusional limitations, the pore blockage seems to not affect their exit from the cages and channels of the zeolite structure. Observing the products selectivity after one-hour reaction, in Table 10, it is worthy to mention the significant difference of Catal_lignin behaviour. This sample, as shown in the previous chapter, exhibited lower acidity than the remaining catalysts, which plays a key role in the hydrocarbon pool mechanism of this reaction. With this sample, the important requirement of maintaining the catalyst acidity to avoid lower catalyst lifetime and different products distribution is clearly proven.

CBV3020E exhibited higher selectivity in propylene than in ethylene, which is expected considering the topology of the ZSM-5 zeolite. Moreover, this sample has a considerably low Si/Al ratio, which is translated in high Brønsted acid sites density and consequently a product distribution more centred on the gasoline fraction. However, upon extrusion, the selectivity was kept constant which means that only 20 wt% of binder is able to affect the catalyst lifetime but not the distribution of the products. It is not surprising that the remaining samples barely show different selectivities towards the products, as the sole difference between them is the meso- and macropore volume. One may only mention a slight increase in the propylene selectivity in Catal_Porlat, Catal_Arbo, and Catal_CNC, which may be attributed to the type of pores present in the bodies: Catal_10Propyl exhibited circular and regular pores well distributed while the other aforementioned samples present bigger and somehow dispersed pores.

In order to verify the influence of the macropore volume, the samples prepared with different quantities of Propyltex were also tested in the conversion of methanol. By MIP, an increase of the total intrusion volume was observed with an increase of Propyltex quantity.

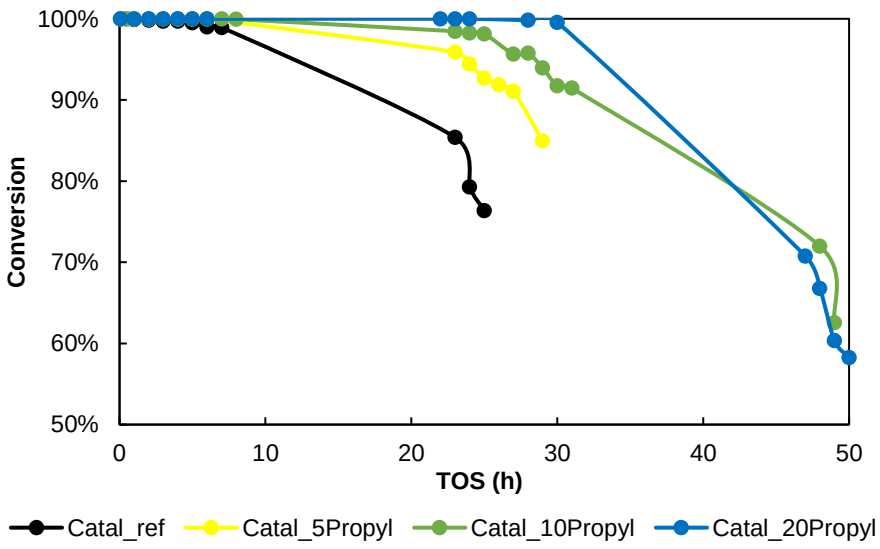

Figure 36: Methanol and dimethyl ether conversion over the samples prepared with different Propyltex quantities

Figure 36 clearly shows a strong influence of the macroporous volume on the catalyst lifetime, i.e., the increase of Propyltex amount added during the extrusion step led to a higher density of macropores represented in Figure 28 B, C and D and, consequently, higher macroporous volume (Table 7). Catal_20Propyl, which represents the sample prepared with 20 wt% of the pore former agent, exhibits higher catalyst lifetime, being able to convert 100% of methanol during 30 h of reaction. This represents a considerable increase in comparison with both Catal_5Propyl and Catal_10Propyl, which at this duration exhibited 85 and 91% of conversion, respectively, while there was a 5 times increase comparing with Catal_ref.

Interestingly, these samples also exhibited an improvement regarding pristine zeolite, CBV3020E, which maintained a conversion at 100% for 25 h, slightly lower than the 30 h of Catal_20Propyl. This may support the idea that the presence of macropores in the binder, allows the deposition of coke outside the micropores, far from the active sites of the zeolite, allowing a longer lifetime. In fact, the increase of 20% is in accordance with the amount of binder used in the extrusion step, clearly demonstrating the influence of the binder present in the catalyst body.

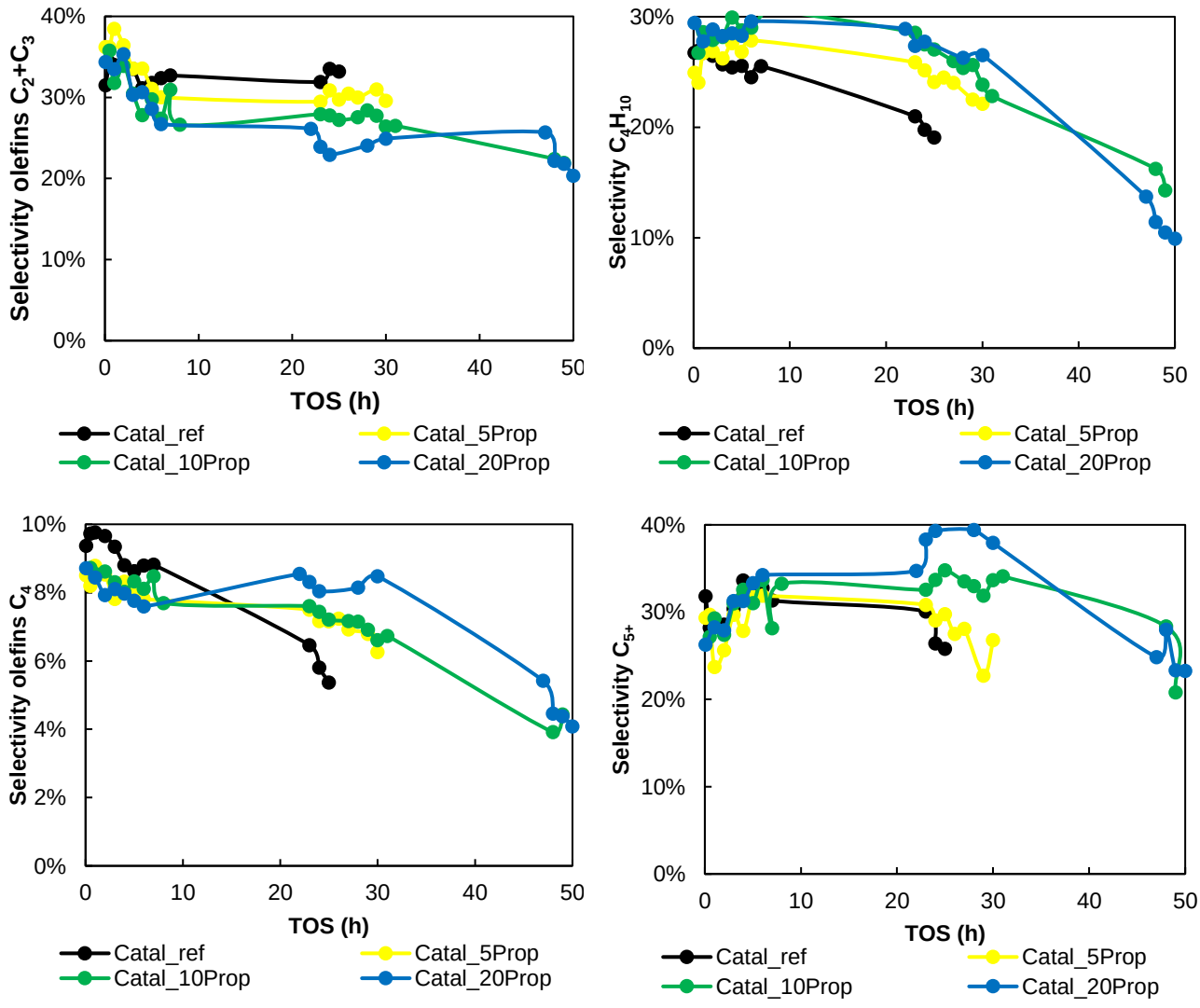

Figure 37: Selectivity in light olefins C_2+C_3 (ethylene and propylene), butylenes (C_4), isobutane (C_4H_{10}), and compounds with 5 carbons or more (C_{5+}) over the samples prepared with different Propyltex quantities

In Figure 37, it is observed the same tendency as the previous samples, with the selectivity in light olefins remaining constant during the whole experiment while the others decreased. However, in this case, it is observed a tendency of the products selectivity with the quantity of Propyltex used in the extrusion step. Light olefins exhibit an increased production with the decrease of the macropore volume, while the remaining products follow the opposite, which is not observed in the first hours of reaction (see For these samples, however, there is no clear decrease in the production of heavier products with the deactivation of the catalyst. BAW sample was able to maintain constant the selectivity towards light olefins and isobutane during all the reaction time, while there is a slight decrease for C4 olefins and C5+ compounds. This shows once again that the presence of additional pathways formed by the presence of meso- and macropores seems to have an effect on the selectivity after few hours of reaction, specially after the catalyst starts to deactivate.

Table 11 – selectivity after one hour reaction). It seems that an increased presence of diffusional paths plays an important role when the catalyst starts to deactivate, as heavier molecules, such as butylenes, isobutane and compounds with 5 carbons or more, are able to exit easier.

In current industry, demetalation is still widely used to overcome the diffusion limitations and often to increase the catalyst lifetime. As a comparison, the performance of desilicated samples, presented and characterized in the previous chapter, is followed.

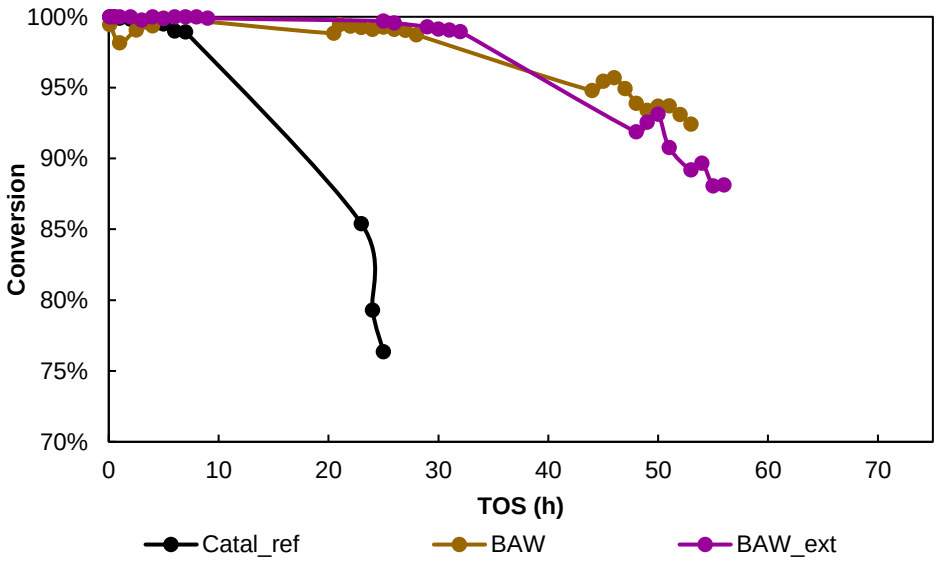

Figure 38: Methanol and dimethyl ether conversion over the desilicated samples

Both BAW and BAW_ext exhibit similar performance regarding lifetime: the conversion remains nearly 100% during roughly 25 h of reaction starting to slowly decrease after that. This suggests that the formation of mesopores by removal of silica species indeed improves the diffusion of products which hinders the deposition of coke that blocks the active sites, hence increasing the lifetime in comparison with Catal_ref. This was observed in other studies, were the introduction of mesoporosity led to longer

catalyst longevity.[110,111] This can be explained by a facilitated diffusion of coke precursors from the micropores to the external surface. This can also be extrapolated to the results where hierarchical porosity was introduced in the binder: the presence of boehmite allows the dispersion of the zeolite crystals exhibiting in that way, a system composed by micro – macro or meso – micropores. Larger molecules encounter short diffusion paths out of the crystals, escaping from the framework and depositing in the macropores of the binder. At this point the molecules are too large to re-enter in the zeolite microstructure, leaving the active sites free for further conversion of methanol. The fast deactivation of those samples comparing with the desilicated ones can be attributed to the fact that the accumulation of coke in the binder will at some point block the zeolite pores neither allowing the exit of products nor the entry of reactant molecules. In desilicated samples, coke is continuously forming in the channels and pores of the zeolite, slowly blocking the active sites, which leads to a slower deactivation rate.

In contrast, the presence of the binder in BAW_ext does not influence the catalyst lifetime as the mesopores were already created and participate in higher diffusion of the molecules. Indeed, it seems that the presence of the binder is not able to block the mesopores and thus not diminishing active sites responsible for the conversion as it happens in Catal_ref that saw its lifetime greatly diminished.

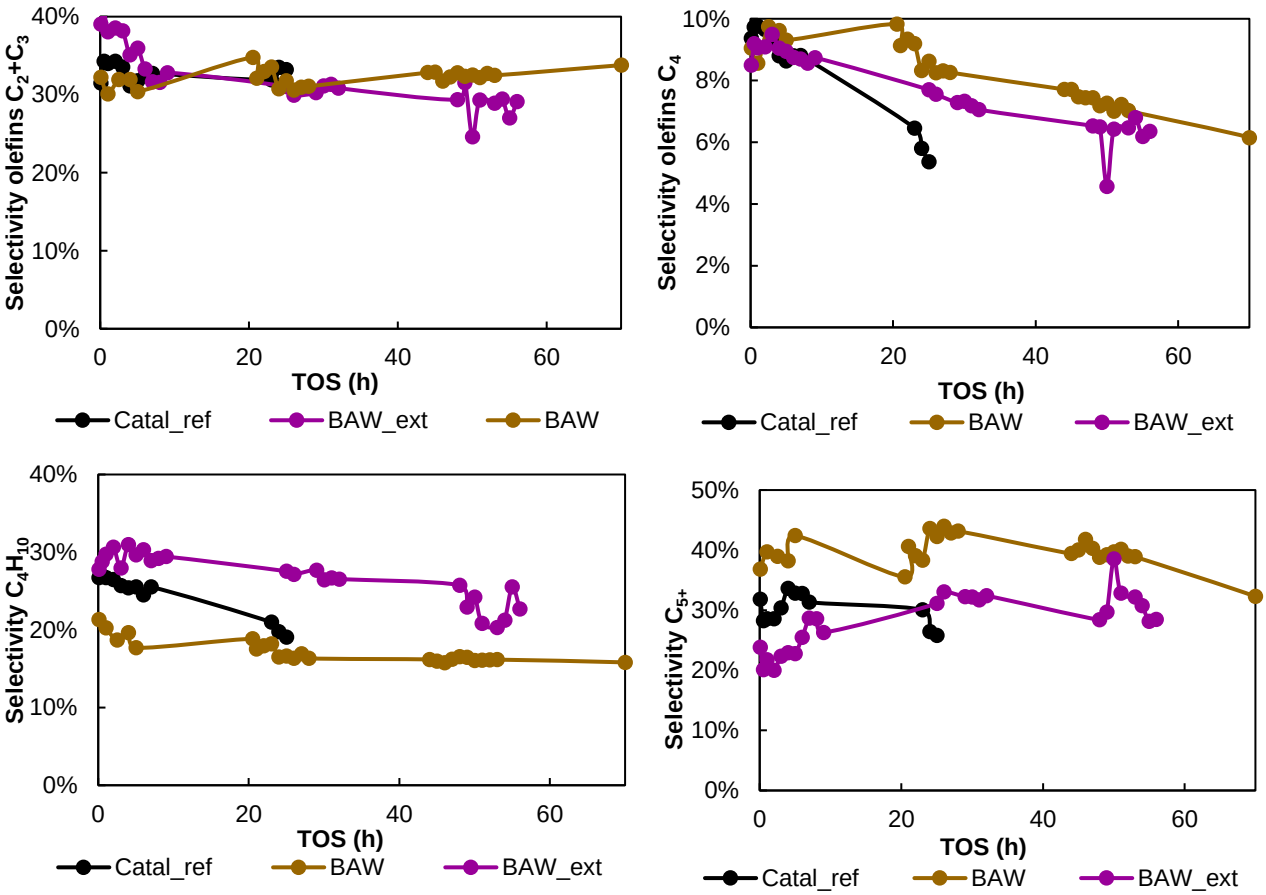

[111] a) Bjørgen, M.; Joensen, F.; Holm, M. S.; Olsbye, U.; Lillerud, K. P.; Svelle, S. *Appl. Catal. A* **2008**, *345*, 43–50; b) Kim, J.; Choi, M.; Ryoo, R. *J. Catal.* **2010**, *269*, 219–228; c) Vennestrøm, P. N. R.; Grill, M.; Kustova, M.; Egeblad, K.; Lundegaard, L. F.; Joensen, F.; Christensen, C. H.; Beato, P. *Catal. Today* **2011**, *168*, 71–79.

Figure 39: Selectivity in light olefins C2+C3 (ethylene and propylene), butylenes (C4), isobutane (C4H10), and compounds with 5 carbons or more (C5+) over the desilicated samples

For these samples, however, there is no clear decrease in the production of heavier products with the deactivation of the catalyst. BAW sample was able to maintain constant the selectivity towards light olefins and isobutane during all the reaction time, while there is a slight decrease for C_4 olefins and C_{5+} compounds. This shows once again that the presence of additional pathways formed by the presence of meso- and macropores seems to have an effect on the selectivity after few hours of reaction, specially after the catalyst starts to deactivate.

Table 11: Selectivity in ethylene, propylene, butylenes and compounds with 5 carbons or more (including aromatics) after 1 h reaction of the samples with different Propyltex quantity and the desilicated samples

Samples	**%S_{C2H4}**	**%S_{C3H6}**	**%S_{C4H8}**	**%S_{C5+}**
Catal_5Propyl	5	34	9	24
Catal_20Propyl	3	30	8	28
BAW	12	18	9	40
BAW_ext	7	31	9	22

The products selectivity of the two last groups of samples after one-hour reaction is presented in For these samples, however, there is no clear decrease in the production of heavier products with the deactivation of the catalyst. BAW sample was able to maintain constant the selectivity towards light olefins and isobutane during all the reaction time, while there is a slight decrease for C4 olefins and C5+ compounds. This shows once again that the presence of additional pathways formed by the presence of meso- and macropores seems to have an effect on the selectivity after few hours of reaction, specially after the catalyst starts to deactivate.

Table 11. As Catal_10Propyl, the two samples prepared with different amounts of the surfactant did not exhibit significant alterations in the selectivity. However, upon desilication of CBV3020E, propylene selectivity diminished while ethylene increased along with the gasoline fractions that can be due to increased diffusion paths, allowing the exit of higher molecules. Upon extrusion, this selectivity returned to same values as the remaining samples, proving once more that the alumina may block the microporous zeolite structure.

5.1.2 Coke analysis

The deactivation of the samples occurs mainly because of the formation and/or deposition of bulky compounds which are not able to desorb under operating conditions. In order to analyse the coke content of the samples after the MTH reaction, they were recovered at the end of the reaction and placed in a TGA equipment. With a temperature increase, under a flow of air, desorption via combustion occurs in the catalyst structure. The percentage of mass loss recorded during the analysis and temperature are plotted versus time (Figure 40).

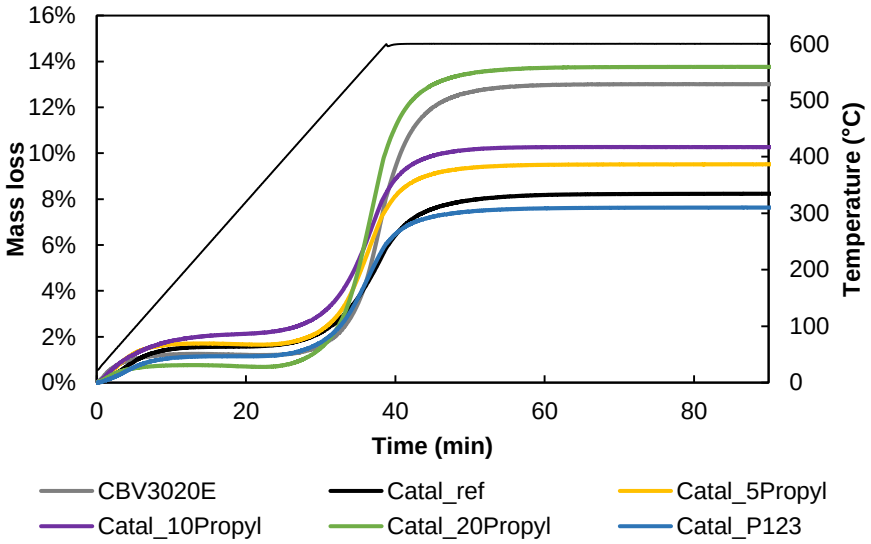

Figure 40: Percentage of samples' mass loss during temperature raise in the TGA equipment

Two distinct desorption processes are visible: (i) at low; and (ii) at high temperatures. Initially, a quick but small loss of mass (1 or 2% for all samples) until around 150ºC can be observed, which can be attributed to the desorption of water accumulated in the pores, during the reaction of methanol dehydration. Then, the mass is kept relatively constant until 450ºC, where a huge loss of mass is recorded. At this stage, it is acceptable to consider that the coke molecules adsorbed in the catalyst are thermally decomposed. As they are probably aromatic molecules, their interactions are stronger and thus higher energy is necessary to favour their combustion. In fact, previous studies showed that the usual coke molecules formed in the MTH reaction are polyalkyl-benzenes, -anthracenes, and –pyrenes that are located in the micropores because no molecules could be recovered by washing. These species are slowly and partially oxidized at low temperatures (150 – 530°C), while around 630°C the combustion is total.[112]

The quantity of coke burned is as big as the amount of reaction time, i.e., the samples with higher catalyst lifetime exhibit higher mass loss. This is acceptable for the samples Catal_ref and Catal_XPropyl, where the lifetime was increased with an increase in the macroporous volume. However, Catal_P123 exhibits less amount of coke than Catal_10Propyl, for example, although having similar lifetime. This may be attributed to the network formed by the presence of meso- and macropores that allowed the exit of coke species, thus inducing less poisoning of the active sites. In fact, Lakiss et al.[112b] showed that silanols and Lewis acid sites play a crucial role in the coke formation, as they are able to trap desorbed products, leading to an accumulation of coke precursors. By having shorter diffusion paths, the coke precursors will reach the external surface easier than remaining in the micropores of the zeolite structure avoiding an autocatalytic reaction of polyaromatics.

[112] a) Hamieh, S.; Canaff, C.; Tayeb, K. Ben; Tarighi, M.; Maury, S.; Vezin, H.; Pouilloux, Y.; Pinard, L. *Eur. Phys. J. Spec. Top.* **2015**, *224*, 1817–1830; b) Lakiss, L.; Ngoye, F.; Canaff, C.; Laforge, S.; Pouilloux, Y.; Qin, Z.; Tarighi, M.; Thomas, K.; Valtchev, V.; Vicente, A.; et al. *J. Catal.* **2015**, *328*, 165–172.

5.2 Cracking of hydrocarbons

The catalytic cracking of hydrocarbons over solid acids consists in breaking one covalent σ-bond in the hydrocarbon chain. This is a highly endothermic reaction, and thermodynamically, it is favoured at high temperatures and low pressures. However, it also involves several parameters and processes, such as the physicochemical characteristics of the catalyst along with the nature of hydrocarbons and the reaction conditions applied in the process (temperature, pressure, time, etc.). A better knowledge of these properties can help the cracking process optimization to obtain specific products.

The study of model reactions representative of oil fractions allows the determination of kinetic parameters, develop reactional mechanisms and design new catalysts according to the market demand.[113] For instance, a model reaction can be used to measure the superficial acidity of a catalyst, if it is solely catalysed by active sites. The cracking of n-hexane (or α test)[114] is considered as a model reaction to characterize strong Brønsted acid sites.[115] It is a useful tool to evaluate the catalytic activity of acid zeolites, since the latter is related to type, quantity and distribution of the active sites and textural properties. The cracking reaction rate in zeolites, for example, is linearly dependent to the tetrahedral aluminium content present in the framework, considering the same activity for all acid sites. In this way, with lower Si/Al ratio, the cracking rate becomes higher, as shown by Haag et al.[116]

On the other side, zeolites are promising catalysts for the cracking of naphtha fraction in oil and several studies concerning the catalytic cracking of C_6-C_8 paraffins have been published.[117] Although naphthenic compounds are important naphtha constituents and affect the products distribution given by the cracking of the reactant, few studies concerning this subject were performed, when compared to the amount of articles dealing with n-hexane. The investigation of naphthenics compounds cracking is an indispensable factor to better understand the naphtha cracking, and studies developed by Konno et al.[118] show that ZSM-5 is an efficient catalyst for the cracking of naphthenic molecules into light olefins. In this way, the cracking of n-butylcyclohexane, with a considerable larger diameter than n-hexane, is able to evaluate the performance of the catalyst in terms of activity and selectivity, as its diffusional limitations are higher.

---

[113] a) Nakao, R.; Kubota, Y.; Katada, N.; Nishiyama, N.; Kunimori, K.; Tomishige, K. *Catal. Letters* **2003**, *89*, 153–157; b) Feng, X.; Jiang, G.; Zhao, Z.; Wang, L.; Li, X.; Duan, A.; Liu, J.; Xu, C.; Gao, J. *Energy and Fuels* **2010**, *24*, 4111–4115.

[114] a) Weisz, P. B.; Miale, J. N. *J. Catal.* **1965**, *4*, 527–529; b) Miale, J. N.; Chen, N. Y.; Weisz, P. B. *J. Catal.* **1966**, *6*, 279–287.

[115] Guisnet, M. R. Model Reactions for Characterizing the Acidity of Solid Catalysts. *Acc. Chem. Res.* **1990**, *23*, 392–398.

[116] Haag, W. O.; Lago, R. M.; Weisz, P. B. *Nature* **1984**, *309*, 589–591.

[117] a) Magnoux, P.; Cartraud, P.; Mignard, S.; Guisnet, M. *J. Catal.* **1987**, *106*, 242–250 ; b) Corma, A.; Gonzàlez-Alfaro, V.; Orchillès, A. V. *Appl. Catal. A, Gen.* **1995**, *129*, 203–215; c) Corma, A.; Melo, F. V.; Sauvanaud, L.; Ortega, F. *Catal. Today* **2005**, *107–108*, 699–706; d) Mochizuki, H.; Yokoi, T.; Imai, H.; Namba, S.; Kondo, J. N.; Tatsumi, T. *Appl. Catal. A Gen.* **2012**, *449*, 188–197; e) Corma, A.; Mengual, J.; Miguel, P. J. *Appl. Catal. A Gen.* **2012**, *421–422*, 121–134; f) Inagaki, S.; Shinoda, S.; Kaneko, Y.; Takechi, K.; Komatsu, R.; Tsuboi, Y.; Yamazaki, H.; Kondo, J. N.; Kubota, Y. *ACS Catal.* **2013**, *3*, 74–78; g) Urata, K.; Furukawa, S.; Komatsu, T. *Appl. Catal. A Gen.* **2014**, *475*, 335–340.

[118] a) Konno, H.; Tago, T.; Nakasaka, Y.; Ohnaka, R.; Nishimura, J. I.; Masuda, T. *Microporous Mesoporous Mater.* **2013**, *175*, 25–33; b) Konno, H.; Ohnaka, R.; Nishimura, J. I.; Tago, T.; Nakasaka, Y.; Masuda, T. *Catal. Sci. Technol.* **2014**, *4*, 4265–4273.

5.2.1 Cracking of n-hexane

A selected group of samples was chosen among the ones prepared previously to be tested in n-hexane cracking. In order to evaluate the influence of the extrusion strategy developed in this Thesis on the acidity of the catalysts, the three samples of Catal_XPropyl and Catal_P123 were considered as a good selection amongst overall samples. The experiment conditions were carefully adjusted to ensure low and iso-conversion to accurately determine the initial cracking rate and compare the products selectivity. The turnover frequency (TOF) was calculated by Eq. 23 and all the results are presented in Table 12.

$$TOF = \frac{moles\ converted\ per\ unit\ time}{number\ of\ active\ sites} \quad (23)$$

being the number of active sites obtained by NH_3-TPD from the previous chapter.

Table 12: n-hexane cracking rate, propane/propylene ratio and selectivity in propylene, and acidity of the samples

Sample	Rate [mmol/(g.min)] (conversion)	$\frac{\text{Propane}}{\text{Propylene}}$	Selectivity (%)		TOF (x 10^{-3} s^{-1})
			Ethene	Propylene	
Boeh_ext	31 (1.4%)[a]	0.90	5	12	-
Catal_ref	522 (6.7%)	0.94	8	27	2.3
Catal_5Propyl	495 (6.3%)	0.94	8	26	1.7
Catal_10Propyl	529 (6.7%)	0.90	8	26	1.8
Catal_20Propyl	543 (6.9%)	1.02	9	25	1.9
Catal_P123	452 (5.7%)	0.89	9	26	2.0

a) experiment made with 35 mg of material.

At a first look, only minor changes (less than 10%) in the reaction rate could be observed among the samples. However, analysing the turnover frequency, it is observed that all the samples exhibit lower activity than Catal_ref following a tendency with the macroporous volume (increased macroporous volume leads to increased activity), with Catal_5Prop having 25% less activity. Knowing that this reaction is highly influenced by the Brønsted acidity of the catalysts, one may conclude that this characteristic changes upon the different extrusion methods implemented. Moreover, the ratio of propane and propene gives a useful insight in the catalytic performance of the materials. The cracking of n-hexane occurs mainly by a β-scission of the chain with three possible reactional pathways at low conversion (Figure 41).

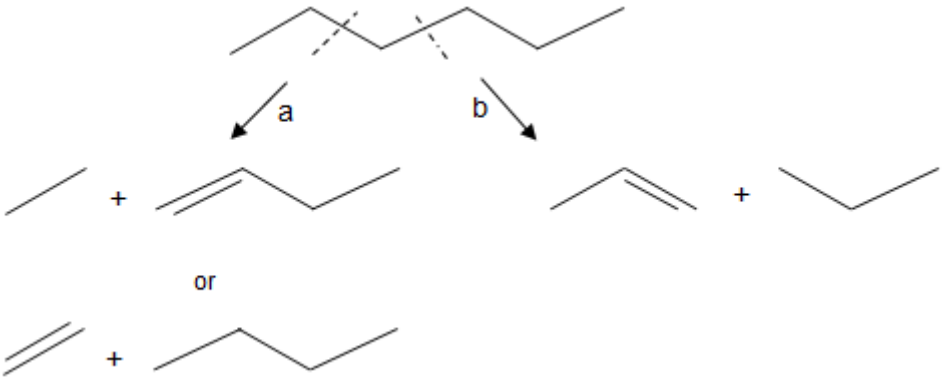

Figure 41: Three possible reactional pathways of n-hexane initial cracking

As the kinetic diameter of n-hexane is 4.3 Å, there are no diffusional limitations in the zeolite pores and channels, which means that the scission of this molecule can occur either via *a* or *b*. As alkenes are more reactive than alkanes, they are more readily transformed via acid-catalysed paths when mass transfer constitutes a limiting factor.[119] Hence, a higher contact time between the reactants/products and the active sites of the framework will favour bimolecular reactions and further conversion into larger molecules, increasing the ratio propane/propylene. However, in this case, the solely responsible for the reaction is the zeolite that remains intact after the extrusion process as considered in the previous chapter. Similar products selectivity among all samples may indicate negligible changes in the acidity, although there were some differences in the activity.

5.2.2 Cracking of n-butylcyclohexane

The further study of the impact of macro- and mesopores in the catalytic bodies was performed by the cracking of n-butylcyclohexane (C_4CC_6). Once it has been excluded significant changes in the acidic characteristics of the samples, it is now investigated if shorter diffusional pathways in the binder may affect the catalytic activity of a molecule with known diffusion constraints. With a kinetic diameter higher than the zeolite pore size, the presence of diffusion *highways* should affect the cracking of this molecule as, for instance, the catalyst cracking preference towards the alkyl or naphthenic group.

Few publications are found concerning the cracking of naphthenics with high alkyl chains, and the main possible reaction pathways extracted were dealkylation and secondary reactions resulting from the products formed.[120] For the first, the main observations were: butene as the main constituent of C_4 fraction; formation of cyclopentanes(enes); medium-low concentration of aromatics as they are secondary products; the presence of the alkyl chain promotes ring opening; and low concentration of naphthenics. For the secondary reactions, it was concluded that subsequent ring opening by β-scission occurs, forming mainly olefins and light paraffins, and hydrogen transfer from the cracking products into a C_6 ring, increasing the concentration of C_8-C_{10} aromatics.

[119] a) Zhang, X.; Cheng, D. Guo; Chen, F.; Zhan, X. *Chem. Eng. Sci.* **2017**, *168*, 352–359; b) Ji, Y.; Yang, H.; Yan, W. *Mol. Catal.* **2018**, *448*, 91–99.
[120] a) Watson, B. A.; Klein, M. T.; Harding, R. H. *Int. J. Chem. Kinet.* **1997**, *29*, 545–560; b) Kubička, D.; Kumar, N.; Mäki-Arvela, P.; Tiitta, M.; Niemi, V.; Salmi, T.; Murzin, D. Y. *J. Catal.* **2004**, *222*, 65–79; c) Quintana-Solórzano, R.; Thybaut, J. W.; Marin, G. B. *Appl. Catal. A Gen.* **2006**, *314*, 184–199.

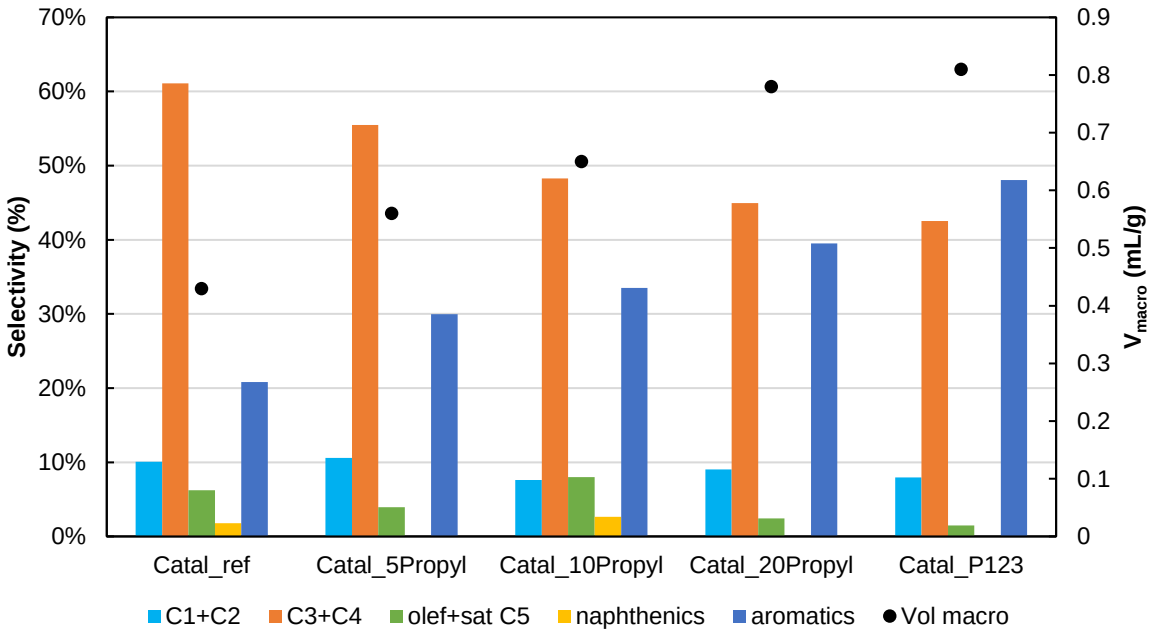

Figure 42: Products selectivity of the samples at 10% conversion: C_1 and C_2 molecules; C_3 and C_4 molecules; olefins and saturated C_5 molecules; naphthenics; and aromatics. The macroporous volume obtained by MIP in chapter 4 is also represented

In Figure 42, it can be seen that different product fractions are represented for the catalytic cracking experiment at around 10% conversion for all samples. There is a clear decrease of C_3-C_4 molecules giving rise to the presence of aromatics, while raising the macroporosity. As it was excluded in the previous sub-section that the acidity of the samples was significantly altered, it seems that the presence of macropores (and mesopores in Catal_P123) strongly influences the products selectivity. In fact, there is a clear relation between the raise in the macropore volume obtained by mercury intrusion porosimetry in Chapter 4 and the increase/decrease in aromatics/C_3-C_4 molecules.

It was observed in several publications that a higher contact time between the products and the catalyst induced secondary reactions responsible for the formation of hydrocarbons. As the zeolite structure did not suffer any changes and, in principle, maintained the same catalytic activity, the key point might be the faster arrival of the reactant to the zeolite crystals. The presence of shorter diffusional pathways in the binder may induce C_4CC_6 towards the zeolite structure faster, allowing the molecule and its products to remain longer in contact with the active sites favouring secondary reactions.

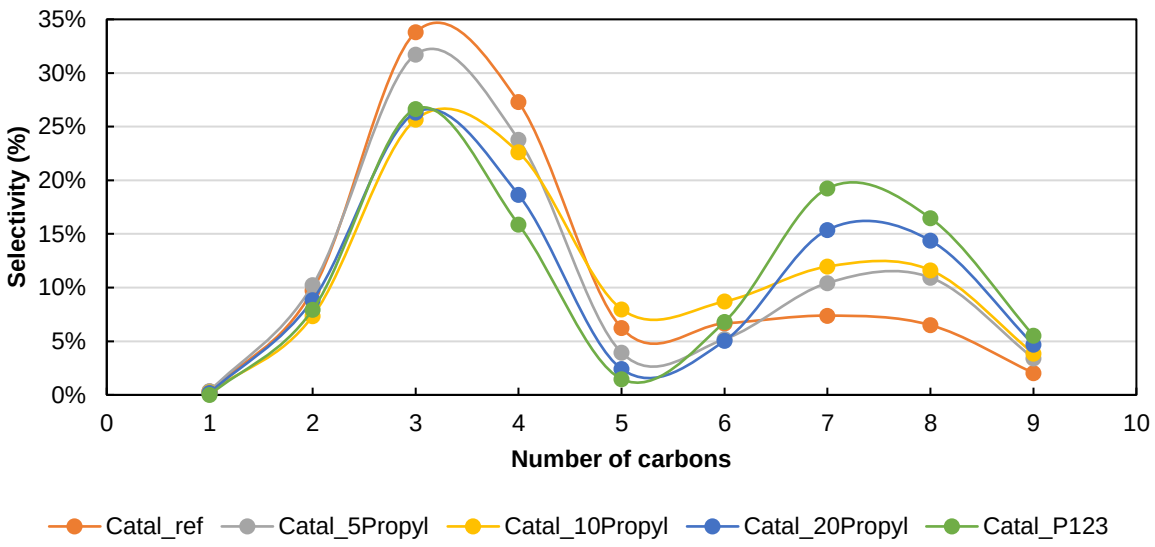

Figure 43: Selectivity of the products as a function of the number of carbons in the samples

The absence of naphthenics at the reactor outlet seems to indicate that all C_4CC_6 molecules converted suffer either ring opening or aromatization, both considered as secondary reactions of dealkylation according to the literature. Indeed, in Figure 43, a decrease in C_3-C_5 (products of the main reaction) is observed, while C_7-C_9 increases, suggesting reconversion of the first fraction into aromatics by further contact with the zeolite.

On the other side, the turnover frequency indicates a lower activity for the porous samples: (3.4, 1.7, 2.7, 2.8, and 2.8) x 10^{-3} s^{-1}, for Catal_ref, Catal_5Propyl, Catal_10Propyl, Catal_20Propyl, and Catal_P123, respectively. As seen for the cracking of n-hexane, the activity of the samples increases with the macropore volume, almost equalizing the reference sample. It seems that both shorter diffusion pathways and acidity changes can influence the performance of the catalysts.

5.3 Toluene adsorption

The adsorption of volatile organic compounds (VOCs) is of utmost interest in modernized industry, as they are released in many types of waste gases. This family of compounds, with toluene being the typical and harmful VOC, is a threat to the atmosphere and human health due to its high toxicity.[121] Therefore, many efforts have been implemented towards its removal, with the adsorption being recognized as one of the most promising technologies. This process showed to be highly efficient, easy to operate, and with an overall low-cost process.[122] Various types of adsorbents for toluene removal include carbon materials, polymeric adsorbents, and zeolites, with the later presenting important features such as large specific surface area, high adsorption capacity, good thermal stability, and good reversibility.

[121] Kamal, M. S.; Razzak, S. A.; Hossain, M. M. *Atmos. Environ.* **2016**, *140*, 117–134.
[122] Tefera, D. T.; Hashisho, Z.; Philips, J. H.; Anderson, J. E.; Nichols, M. *Environ. Sci. Technol.* **2014**, *48*, 5108–5117.

To evaluate the effects of extrusion in this process along with the procedures developed during this Thesis, some samples were tested in toluene adsorption as-prepared. At this point, only the samples that showed better catalytic results (Catal_10Propyl as representative of the Propyltex samples and Catal_P123) and the reference ones (CBV3020E, Catal_ref, BAW) were used.

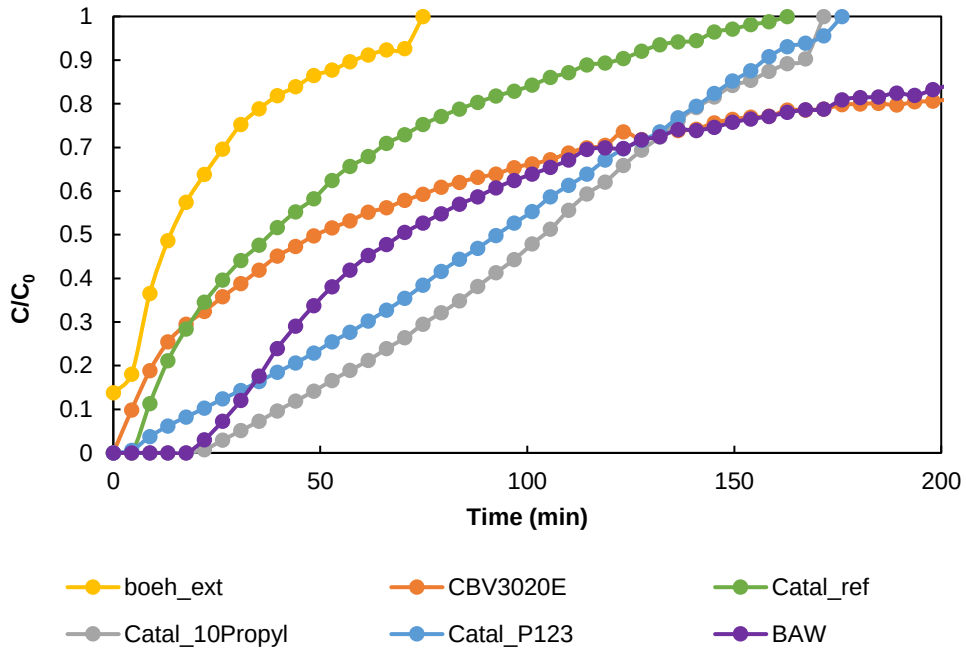

Figure 44: Breakthrough curves of toluene adsorption of selected samples

In Figure 44, the breakthrough curves of the toluene adsorption are represented by plotting the fraction of toluene present in the outlet stream (C/C_0, being C the concentration of toluene at a determined time and C_0 the initial concentration) as a function of time. This breakthrough time is defined as the duration during which the sample is able to completely adsorb toluene from the stream. Interestingly, the commercial zeolite (CBV3020E) did not exhibit any breakthrough time and, in addition, the saturation occurs with a slow pace. Upon its extrusion (Catal_ref), the concentration of toluene at the outlet remained zero for the first 4 min, rapidly increasing after that. This may be explained by the reduction of the compressibility of the zeolite crystals due to the extrusion process, allowing better access to the active sites and, consequently, quickly reaching saturation. This can be confirmed by the results of BAW, possessing hierarchical porosity, which exhibits higher volume for the adsorption of toluene and as a consequence, a higher breakthrough time. However, as it was tested in the form of powder, there was a slow saturation process caused by hindered access to the active sites. The extrudates Catal_10Propyl exhibited around 30 min of breakthrough time and a quick saturation. It seems obvious that the addition of macropores in the catalyst body caused a higher diffusion of the toluene molecules to the active sites, and plus, the higher macropore volume allowed higher efficiency, i.e., the catalyst was able to adsorb the totality of toluene concentration for a longer time. Unfortunately, this was not verified in Catal_P123, with only 8 min of breakthrough time. It seems that the mesopores

created in the binder little influenced the adsorption performance, nonetheless, the extruded form achieved faster saturation.

Table 13: Breakthrough time and capacity of toluene adsorption of the samples

	Boeh_ext	**CBV3020E**	**Catal_ref**	**Catal_10Propyl**	**Catal_P123**	**BAW**
Breakthrough time (min)	0	4	8	30	10	24
Capacity (mg/g)	15.5	68.0	60.7	70.0	62.3	65.2

In Table 13, a slight decrease in the adsorption capacity of Catal_ref in comparison with CBV3020E can be noted, which is reasonable considering that alumina adsorbs less toluene. However, extruded samples with hierarchical porosity (Catal_10Propyl and Catal_P123) led to an increase in the adsorption capacity that can be linked to the higher meso- and macropore volume, allowing multilayer adsorption. In fact, the toluene molecule has a kinetic diameter close to the pores of the zeolite, thus hampering the formation of more than a single layer, but with the creation of higher pores at the entrance of the zeolite structure, this phenomenon may occur. In the case of BAW, the alkaline treatment may have created defects in the structure, reducing its capacity. With this technique, the advantages of the method developed in this Thesis in comparison with the conventional zeolite demetalation to improve mass transport are once again proved.

5.4 Conclusion

In this chapter, the performance of as-prepared samples was evaluated in the conversion of methanol-to-hydrocarbons, the cracking of n-hexane and n-butylcyclohexane. Besides, the adsorption of toluene in VOC removal conditions was also investigated. The materials containing meso- or macropores showed an enhanced catalytic stability in the first reaction. It seems clear that an increase in the macropore volume reduces coke poisoning, keeping the active sites *clean* for longer time. This was somehow verified by the increase of the coke amount present in the catalyst after the reaction: the samples with higher macropore volume presented higher amount of coke due to longer time on stream. Nonetheless, no change in the selectivity was observed since the zeolite structure was not modified during the extrusion process.

The cracking of n-hexane and n-butylcyclohexane showed results in line with the ones obtained for MTH reaction. The samples exhibited similar selectivity and n-hexane cracking rate, due to approximately the same amount of Brønsted acid sites in all samples as this molecule does not present any diffusional constraints and the conversion remained low enough to hinder further secondary reactions that can be driven by shape selectivity. On the other side, C_4CC_6 possesses a larger diameter leading to slower diffusion that is overcome by the presence of meso- and macropores. By reaching the zeolite structure faster, it is able to remain for a longer contact with the active sites, thus promoting the reconversion of light alkenes into aromatics.

With these three types of reaction, it is given a complete study of the meso- and macropores influence on the catalytic performance of the materials. In the case of MTH reaction, our extrusion strategy greatly improves the catalyst lifetime, reducing the costs of catalyst regeneration. However, in the case of C_4CC_6 cracking, the formation of aromatics is favoured by the consumption of light olefins which is the opposite of the expected results in the cracking of naphtha fraction of oil.

Finally, there was also a positive effect of this methodology in the removal of toluene from a gas stream, with increased breakthrough time observed in the samples containing macropores.

Chapter 6 – Study of the effective diffusivity

This chapter can be considered the most important study of this manuscript. The effective diffusivity of a set of samples was obtained by three different techniques of diffusion measurements: gravimetric method, inverse gas chromatography, and pulsed-field gradient NMR. The results were carefully analysed and correlated with the catalytic and adsorption performances found in the previous chapter, giving a reliable conclusion concerning the overcome of the diffusion limitations of zeolite extrudates.

This chapter can be found in Bingre et al., *J. Phys. Chem. B* **2019**, *123*, 637-643.

6.1 Diffusion measurements

The main part of this Thesis is the study of the effective diffusivity in technical zeolite bodies. In the previous chapters, a strategy was developed to introduce hierarchical porosity in extrudates by addition of different pore former agents that enhanced the lifetime of the samples in the methanol-to-hydrocarbons reaction without significantly altering the products selectivity. Several characterization techniques assessed the presence of meso- and/or macropores and confirmed the absence of differences in the acidity, as also verified by the same catalytic activity in n-hexane cracking. The following paragraphs will be dedicated to the measurement of the diffusion of toluene or benzene, depending on the technique, in selected as-synthesised samples.

At this stage, a couple of catalysts were chosen that showed good potential to achieve an improved effective diffusivity. This was decided based on the type of pores created, additional pore volume (*meso* or *macro*), homogeneity of the pores and their sizes, and interesting catalytic performances (lifetime, reaction rate and products selectivity). Regarding the impact of mesopores, only one sample was successfully prepared (Catal_P123), while the remaining macroporous samples, Catal_10Propyl was chosen due to its regular pore size and homogeneous presence in the catalyst body and as a representative of the samples prepared with Propyltex. In addition, Catal_ref and CBV3020E were also studied to serve as a reference to the experiments.

6.1.1 Gravimetric method

Gravimetric method was one of the first techniques implemented in diffusion studies at the beginning of zeolite science. Hence, it deserves the initial position in this manuscript. Performed in the hot June of Beijing, the temperature chosen was the minimum possible (35°C) to compare with pulsed-field gradient NMR measurements performed at 25°C and described in the next sub-section. Incremental uptake was defined as the fraction of toluene adsorbed at each moment with the total toluene adsorbed at the saturation point, and it was plotted as a function of time. The uptake curves are presented in Figure 45, being q_∞ the mass of catalyst saturated, and q the mass of catalyst at a determined time.

It is noteworthy to mention that the uptake of CBV3020E extruded with the binder (Catal_ref) is slower than pristine powder commercial zeolite, thus indicating that the access of the toluene molecules to the zeolite structure is hindered by the presence of the binder. After introducing additional porosity in the catalyst body, the slope of the constant uptake becomes higher than for the reference sample, which may be explained by the presence of additional pathways in the binder. Indeed, those additional diffusion paths render easier the diffusion of the molecules throughout the catalyst body until reaching the active sites.

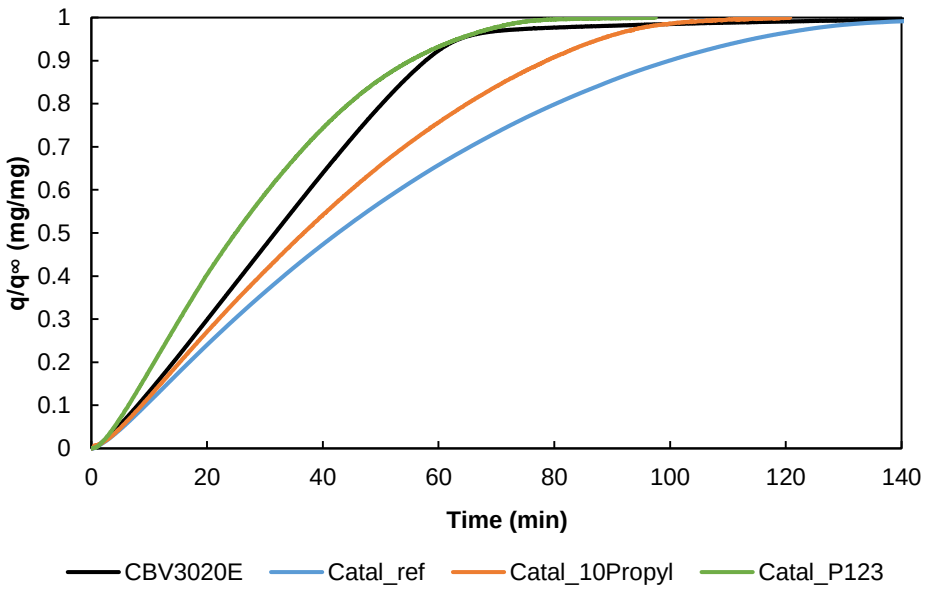

Figure 45. Toluene uptake curves of the different zeolite samples

Table 14 summarizes the effective diffusivity as well as the toluene adsorption capacity within all samples. The catalytic bodies where it was assessed the presence of meso- or macroporosity exhibit higher values of D_{eff} when compared to the reference sample, Catal_ref. Surprisingly, Catal_P123 showed faster mass transport than Catal_10Propyl, which was *'a priori'* expected considering that the macropores would contribute to an improved diffusion along with the mesopores. This was shown, by looking in-depth to the pore profile obtained by mercury intrusion of the sample Catal_P123 and related SEM images in the previous chapter, where big macropores were observed, being attributed to poor extrusion efficiency. Moreover, the catalytic results of n-butylcyclohexane cracking revealed a higher selectivity towards aromatics, which could be attributed to the presence of meso- and macropores that allowed a faster arrival of the reactant to the zeolite structure and possibly a facilitated exit of larger molecules. Hence, in this sample, both mesopores and macropores may have a playing role in the adsorption process. The toluene adsorption capacity was also increased in the porous samples, indicating that the accessibility to the active sites is enhanced by the presence of meso- and macropores, and as seen in the toluene adsorption in VOC conditions, higher pore volume may allow multilayer adsorption while pristine zeolite and its extruded parent allow only single layer adsorption.

Table 14. Effective diffusivity and capacity of the samples obtained by the gravimetric method

	CBV3020E	**Catal_ref**	**Catal_10Propyl**	**Catal_P123**
D_{eff} (m^2/s)	1.5×10^{-13}	4.8×10^{-11}	6.6×10^{-11}	9.8×10^{-11}
Capacity (mg/g)	69.7	68.5	72.5	83.0

It is important to note that transient diffusion defined in Eq. 5 depends on the particle size. Since the equivalent diameter of the extrudates was used, the two orders of magnitude difference found

between CBV3020E, with an average particle size of 87 µm, and the remaining samples can be easily explained. In this case, it is not possible to compare two different catalyst morphologies, and in further studies one must decide either to use powder or extrudate to determine the effective diffusivity.

For verification, the samples were crushed as described in the experimental section. As expected, very little difference between the samples: 1.4, 1.6, and 1.6 x 10^{-13} m^2/s for Catal_ref, Catal_10Propyl, and Catal_P123, respectively, were observed. This can be attributed to the low sensibility of the technique since it falls into a macroscopic phenomenon observation (mass change).

The diffusion behaviour in terms of temperature can be described by Arrhenius' law in Eq. 24 that correlates the diffusion coefficient with a pre-exponential factor and temperature.

$$D_{eff} = D_0 exp\left(-\frac{Q_d}{RT}\right) \tag{24}$$

being D_0 the temperature-independent pre-exponential factor, Q_d the activation energy for diffusion, R the gas constant, and T the absolute temperature given in Kelvins.

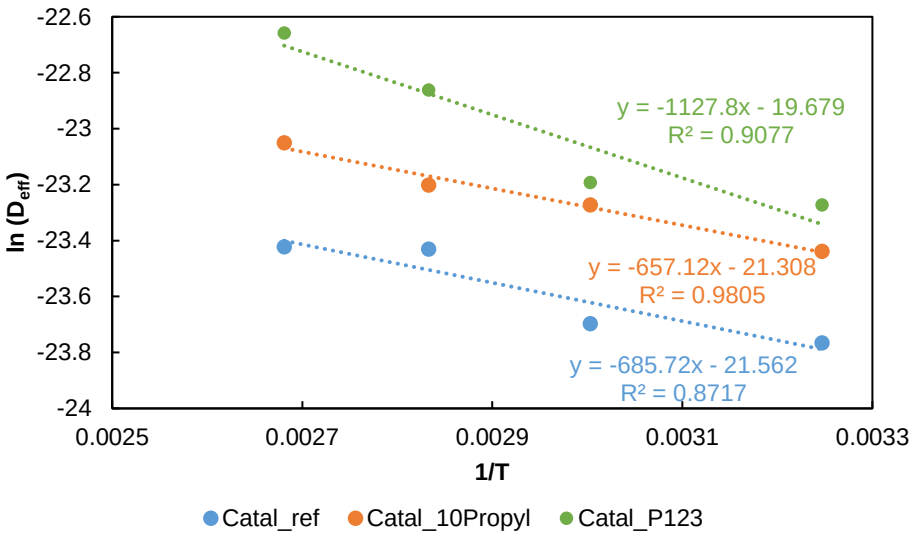

Figure 46: Arrhenius' curves of the samples

Several experiments at different temperatures were performed. By plotting the values of effective diffusivity obtained as a function of temperature (Figure 46), one may calculate the pre-exponential factor and the activation energy by linearization of Eq. 24. This allows an estimation of the effective diffusivity at temperatures different from the experimental ones as, for example, reaction temperatures.

Table 15: Parameters of the Arrhenius' law obtained for the different samples

	Catal_ref	**Catal_10Propyl**	**Catal_P123**
Slope	-685.7	-657.1	-1127.8
Q_d (J/mol)	82.5	79.0	135.7
D_0 (m^2/s)	4.32 x 10^{-10}	4.37 x 10^{-10}	2.84 x 10^{-9}

Additional effective diffusivity was obtained at 60, 80, and 100 °C in Catal_ref, Catal_10Propyl, and Catal_P123. It was observed the same tendency as the experiments at 35°C, with Catal_P123 as the sample with higher effective diffusivity, followed by Catal_10Propyl, and both higher than Catal_ref. However, surprisingly, when extrapolating the results to higher temperatures, Catal_10Propyl is only slightly improved than Catal_ref, meaning that at high reaction temperatures, it is expected both catalysts to present the same performance concerning diffusion aspects. However, one must not forget the assumptions made by the Arrhenius's law: it is considered that the pre-exponential factor is independent of the temperature, but that is not entirely true. As it is related to molecular collision, the temperature plays an important role in the phenomenon. In conclusion, the Arrhenius's law, although widely accepted and used in the science community, cannot predict with totally certainty the real effective diffusivity by extrapolation of experimental results.[123]

6.1.2 Inverse gas chromatography

Initially, during the first trials of this technique, toluene was selected as a probe molecule. Unfortunately, one of the constraints is the slowness of the process, with each injection analysis reaching up to 40 min. This induces long tailing with significant "uncertainties" in the values while treating the peaks detected by GC, particularly due to the background noise associated to infinite dilution. The probe molecule was then changed from toluene to benzene, which exhibits a faster diffusion, to minimize the errors of measurement. Figure 47 presents the van Deemter curves associated to the different samples.

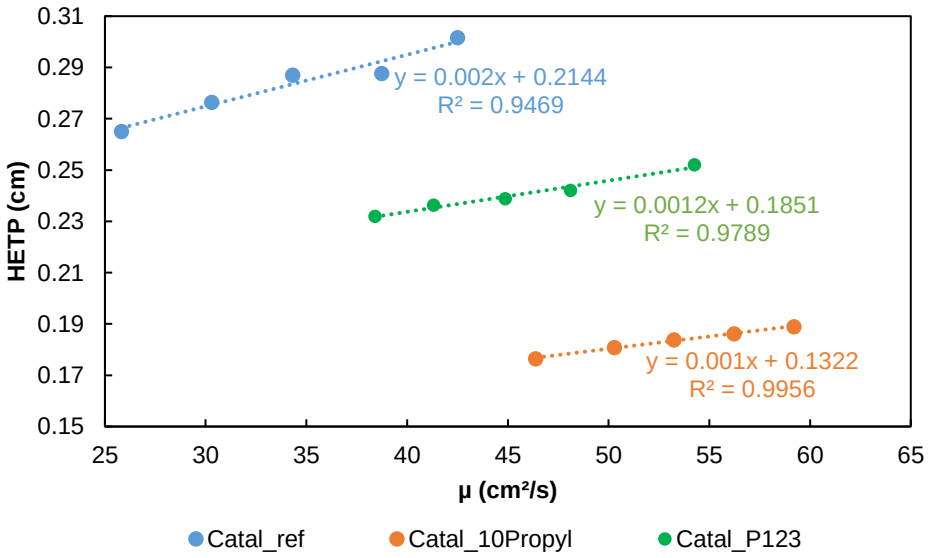

Figure 47. Comparison of van Deemter curves of benzene for different samples

The reference sample exhibited an effective diffusivity value of 1.0×10^{-4} m^2/s. Meanwhile, the samples containing hierarchical porosity exhibited higher values than Catal_ref: 1.8 and 1.5 $\times 10^{-4}$ m^2/s

[123] a) Stiller, W. *Berichte der Bunsengesellschaft für Phys. Chemie* **1992**, *96*, 450–452; b) Peleg, M.; Normand, M. D.; Corradini, M. G. *Crit. Rev. Food Sci. Nutr.* **2012**, *52*, 830–851.

for Catal_10Propyl and Catal_P123, respectively. By careful analysing the study from Wallenstein et al.[40] concerning the measurement of the effective diffusion of trimethylcyclohexane in FAU zeolites by inverse gas chromatography, the order of magnitude is in agreement with the ones obtained for our samples. The authors reported a diffusion coefficient of 10^{-6} and 10^{-7} m^2/s when injecting 0.08 molec. / u.c. In our case, the volume of each syringe was settled to 1 µL, and at least 3 dilutions were made before injecting in the GC. This led us to load around 0.2 molec. / u.c., which is similar to the one of the references and so providing a coherency between the results of both studies.

The results of this technique suggest a higher effective diffusivity for Catal_10Propyl than for Catal_P123, the inverse of what was assessed by the gravimetric method, being both higher than Catal_ref. Also, in this situation, the presence of additional porosity led to an improvement of the effective diffusivity, however Catal_P123 might have lost its macropores after crushing. In this way, only the mesopores participate in the mass transfer, being lower than the macropores verified in Catal_10Propyl.

6.1.3 Pulsed-field gradient NMR

Finally, PFG-NMR was performed, and it is analysed in detail in the following paragraphs. Firstly, pristine commercial zeolite CBV3020E was calcined to eliminate any water adsorbed, pre-mixed with toluene, and placed in the NMR tube. The spectrum obtained is presented in Figure 48.

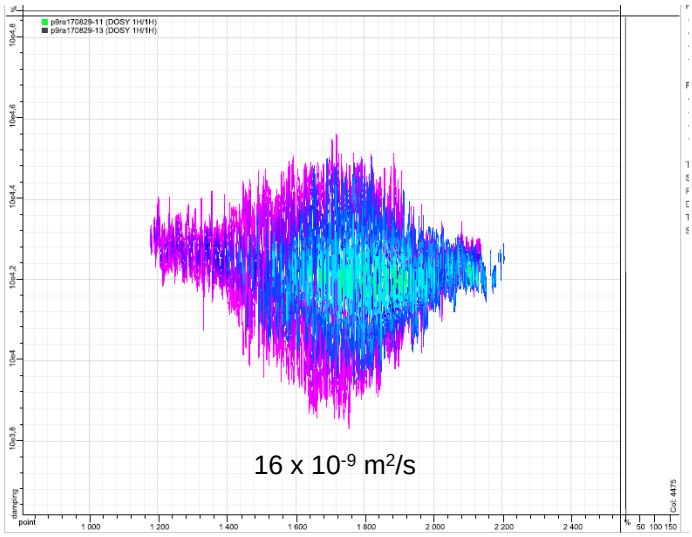

Figure 48: DOSY spectrum of CBV3020E with toluene as probe molecule

A regular diffusion profile of a toluene molecule is observed in the microporous intracrystalline structure, leading to a diffusivity of around $16x10^{-9}$ m^2/s. The measurement was performed at two different diffusion times, i.e., duration of the period where the behaviour of the molecule's diffusion is recorded. In this case, for both times – 15 and 50 ms – the diffusivity appears to be the same. This reveals a single behaviour of the molecular diffusion, which means a homogeneous microporous structure in the catalyst, without major defects. This value also shows to be in agreement with the ones obtained by adsorption-desorption measurements with infrared spectroscopy.[124] However, it is important

[124] Mukti, RR. *Sorption and transport of aromatic over MFI zeolites*, Ph.D. Dissertation, **2007**.

to note a relatively high value for the range of 10^{-9} m^2/s due to the nanometric size of the crystals and that can be associated to diffusion in intercrystalline mesoporosity. This was observed by Louis et al., where a sample exhibiting nanocrystals presented an effective diffusivity of 25 x 10^{-9} m^2/s.[35]

Next, the sample boeh_ext was tested. The pellets were crushed before being pre-mixed with the probe molecule. In this case, the sole unit cell volume of γ-Al_2O_3 was taken into account and the volume of toluene used was such that guaranteed the loading of two molecules per unit cell.

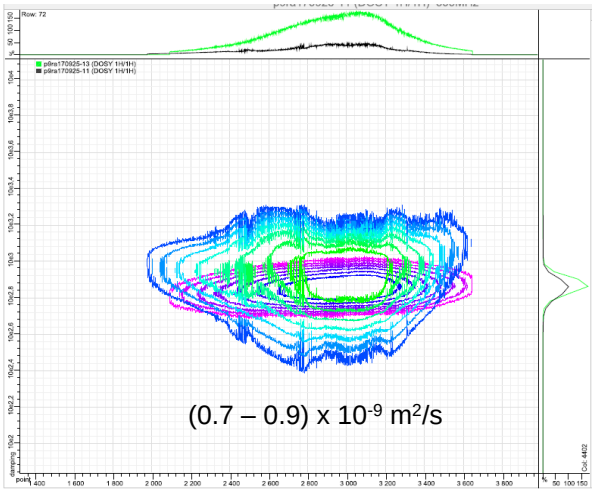

Figure 49: DOSY spectrum of boeh_ext with toluene as probe molecule

In this case, a regular diffusion of the toluene molecule in the structure of the sample can be again observed at different diffusion times, however at a much lower diffusivity: 0.7 and 0.9 x 10^{-9} m^2/s, for 100 and 50 ms, respectively (Figure 49). One can consider the difference between the two values as an error and subjectivity associated to the values reading in the NMR notebook software. However, one can assess this diffusion to be in the order of 10^{-10} m^2/s, an order of magnitude lower than CBV3020E. This is in agreement with the work of Wood and Gladden that showed an effective diffusivity of heptane of 0.8 x 10^{-9} m^2/s in CoMo/alumina.[125]

Having assessed the behaviour and determined the values of the diffusivity of the pure materials, the next step consisted in testing the mixture in terms of extrudates. For that, the sample Catal_ref, Catal_5Propyl and Catal_10Propyl were analysed, after being crushed and proceed in the same way as the previous ones.

[125] Wood, J.; Gladden, L. F. *Appl. Catal. A Gen.* **2003**, *249*, 241–253.

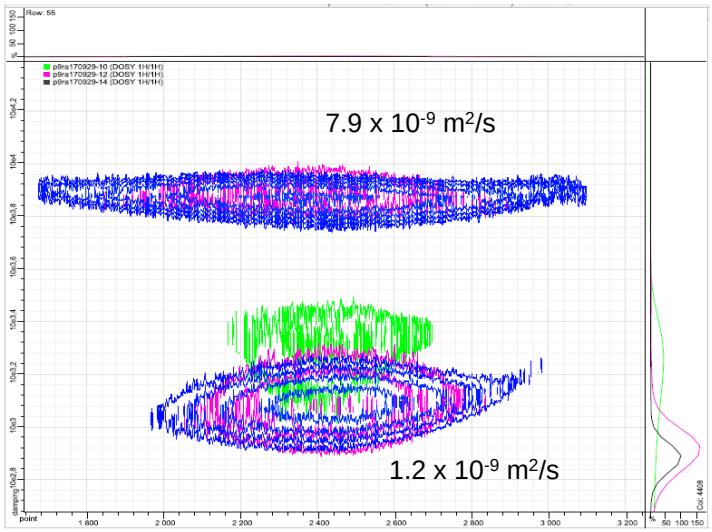

Figure 50: DOSY spectrum of Catal_ref with toluene as probe molecule

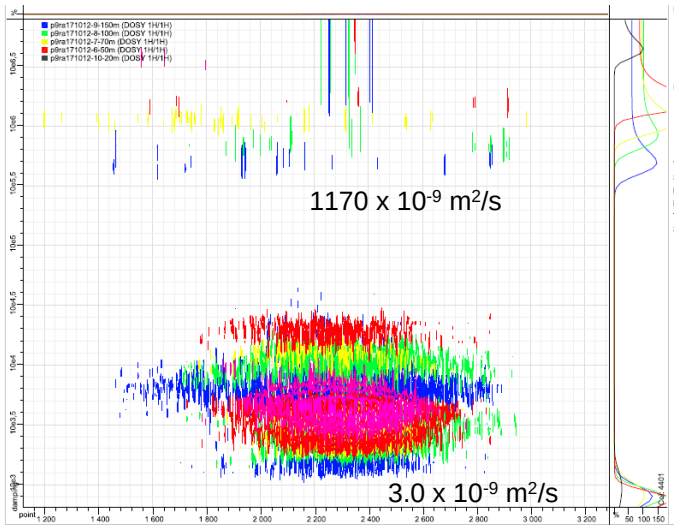

Figure 51: DOSY spectrum of Catal_5Propyl with toluene as probe molecule

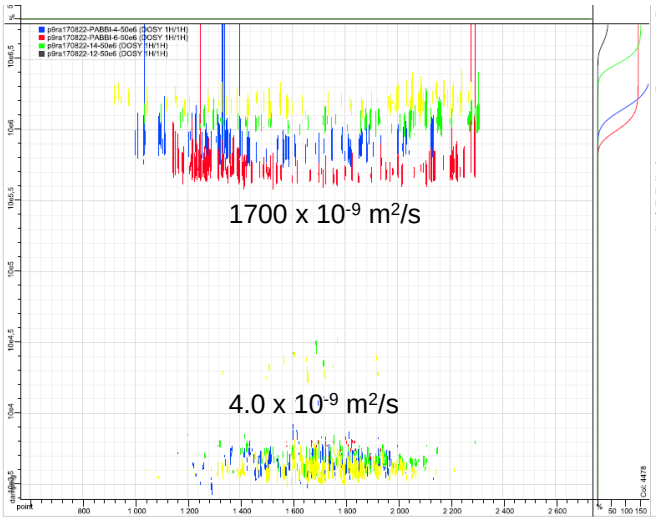

Figure 52: DOSY spectrum of Catal_10Propyl with toluene as probe molecule

Based on the spectra shown in Figure 50, Figure 51 and Figure 52, two mechanisms of diffusion are evidenced: a faster and a slower one. Concerning the reference sample, for 100 ms of diffusion time, the highest value obtained was of $7.9x10^{-9}$ m^2/s which is slower than the diffusivity of pure CBV3020E while the lowest value obtained of $1.2x10^{-9}$ m^2/s corresponds to a slightly higher value than the diffusivity in boeh_ext. Primarily, one can admit that one of the mechanisms corresponds to the diffusion in the microporous structure of the zeolite and the other to the diffusion in the structure of alumina. The first may be lower than CBV3020E as the presence of the binder might decrease the intercrystalline diffusion and, hence, the value can be assessed to toluene movement in the microporous structure.

Then, upon the introduction of additional porosity, the two mechanisms are still visible. However, at 70 ms of diffusion time, the highest values obtained for one of the behaviours was $1700x10^{-9}$ and $1170x10^{-9}$ m^2/s, for Catal_10Propyl and Catal_5Propyl, respectively, which corresponds to an effective diffusion +1000 times more than the value attributed to the diffusion in γ-alumina. It might be possible that these values correspond to the transport of toluene in the macropores formed by the addition of the pore former Propyltex. Another proof is the fact that, in Catal_5Propyl, only 5 wt% of pore former was added while in the other sample 10 wt% was used, leading to form less macropores and consequently a lower raise in the effective diffusivity, corroborated by the lower intensity of the signal of Catal_5Propyl compared with the one of Catal_10Propyl.

Besides, the second diffusion behaviour exhibited an effective diffusivity standing among (3.0 – 4.0) $x10^{-9}$ m^2/s for both samples, thus remaining slightly higher than the value obtained for the reference sample. However, due to the error and subjectivities associated to the values reading, one can consider the same toluene effective diffusivity in both samples.

Next, the effective diffusivity of the sample containing mesopores was determined by this technique. In this case, the spectrum is not presented as it was treated by different software Bruker's TopSpin 4.0. To verify the similarity of both software, it was performed a repetition of Catal_ref and the value obtained was in agreement with the one obtained by NMR Notebook: (1.2 and 8.1) x 10^{-9} m^2/s. Regarding Catal_P123, three different mechanisms were detected with values of 0.9 x 10^{-9}, 4.0 x 10^{-9}, and 19 x 10^{-9} m^2/s that can be attributed to alumina, zeolite, and mesopores present in the technical body, respectively. As seen above, the three values match the different structures mentioned, hence proving a slight increase of the effective diffusivity after the introduction of mesopores. The macropores influence is not visible, since the sample has to be crushed as specified in the technique of iGC.

Finally, with the same software, the sample BAW was investigated and a diffusivity of 24 and 64 x 10^{-9} m^2/s was obtained. The factors influencing this effective diffusivity become obvious, as it was already discussed in the previous samples: the presence of mesopores and intercrystalline mesoporosity. Moreover, remembering the study of Coasne et al.[39a)], it seems that these two types of porosity are not interconnected, as two signals were observed. The authors applied this technique in mesoporous FAU zeolite, MCM-41, and a physical mixture of FAU and MCM-41. In the latter, they observed two signals representing the diffusion in the two types of materials, while for the separate zeolites only one could be detected, suggesting that the appearance of two signals is related to different pores morphologies that are not connected between them.

6.2 Comparison of the different techniques

In all three techniques, the improvement of the effective diffusivity was assessed in Catal_5Propyl, Catal_10Propyl and Catal_P123, thus suggesting that the presence of additional porosity in the catalytic body leads to an increase in the diffusion of toluene / benzene molecules throughout the catalyst as expected (Table 16).

Table 16: Analysis conditions and effective diffusivity values obtained for the samples by the three different techniques

Parameters	**Gravimetric method**	**PFG-NMR**	**IGC**
Temperature analysis (°C)	35	25	350
Probe molecule (loading)	Toluene (11 molec/u.c./min)	Toluene (2 molec./u.c.)	Benzene (0.2 molec./u.c.)
Sample morphology	Powder or extrudate	Powder	Powder
Results	Uptake curves	3D DOSY spectrum	Retention times
Samples	**D_{eff} (m²/s)**		
	Gravimetric method	**PFG-NMR**	**IGC**
CBV3020E	1.5×10^{-13}	16×10^{-9}	-
Catal_ref	4.8×10^{-11}	1.2 et 7.9×10^{-9}	1.0×10^{-4}
Catal_10Propyl	6.6×10^{-11}	3.0 et 1700×10^{-9}	1.8×10^{-4}
Catal_P123	9.8×10^{-11}	0.9 et 4.0 et 19×10^{-9}	1.5×10^{-4}

However, Catal_P123 showed lower effective diffusivity than Catal_10Propyl according to both iGC and PFG-NMR – the opposite was assessed by the gravimetric method. So first let's remember the characteristics of each technique and sample:

- Catal_P123 exhibited the presence of mesopores and giant macropores (see Figure 24 and Figure 25), the latter attributed to cracks and fissures caused by poor extrusion efficiency. On the other side, Catal_10Propyl presented only macropores of regular size formed by the presence of the pore former agent.
- Gravimetric method was performed on the extrudate itself, which means the same shape and conditions of a catalytic reaction, while it is necessary to crush the sample in order to introduce it in the NMR tube or in the IGC column.

Analysing the two aforementioned situations, one may keep in mind that Catal_P123 has mesopores and "macropores" that can contribute to a higher effective diffusivity, explaining the tendency of effective diffusivity obtained by gravimetric method. On the other side, considering that the average particle size used for IGC and PFG-NMR was 180 µm, it seems that the macropores of Catal_P123 collapsed during the crushing step, while the macropores of Catal_10Propyl remained. This may have led to the fact that, in IGC, only the mesopores present in Catal_P123 participated in the diffusion process, while Catal_10Propyl added the contribution of macropores.

Then, one may notice the huge discrepancy in orders of magnitude between the three techniques, however, some facts have to be considered: (i) the use of benzene instead of toluene in iGC – the first, having a smaller molecular diameter, is expected to diffuse easier through the porous structure; (ii) higher analysis temperature in IGC leads to higher effective diffusivity values; (iii) the sample in the gravimetric method may suffer external mass transfer limitations, as it is present in static conditions, while in iGC this factor can be neglected due to the turbulence existence around the catalyst and in PFG-NMR self-diffusivities are measured; (iv) the three techniques use different mathematical equations to solve the problematics.

A study of Kolitcheff et al.[126] reported that the diffusion coefficient of methylcyclohexane in aluminas obtained by inverse liquid chromatography was around 10^{-9} m^2/s. Although it is a different technique from the others presented herein, it is somehow correlated by the fact that corresponds to a study in liquid phase and by inverse chromatography. This order of magnitude is in a good agreement with the results obtained by PFG-NMR in our samples.

In relation to the studies made with PFG-NMR, Dvoyashkina et al.[39b] showed a diffusion of around 10^{-9} and 10^{-10} m^2/s for alkanes in silicalite-1. In this case, the authors presented the results in a range of molecules loading per unit cell. So, they mention two other studies where this aspect was carefully taken into account: Caro et al.[127] observed an increase of the self-diffusion coefficient of propane in silicalite-1 at 300 K by a factor of 100, if the loading diminished from 13.2 to 2 molec. / u.c.; Krishna and van Baten[128] considered that in a range of 0.4 < molec. / u.c. < 4, by decreasing 2 molec. / u.c., the diffusion coefficient diminished 53%. This means, by going out of the range studied by the authors, if there is a decrease of 6.6 in the loading (the same as Caro et al.), the coefficient will increase by a factor of 90, which is in high agreement with the first study.

Saying that, by carefully analysing our results, it becomes obvious that the order of magnitude of both techniques should not be the same. In fact, the preparation of the sample for PFG-NMR consisted in the loading of 2 molec./u.c. (10 times higher than the one by iGC). If comparing the results for the sample Catal_10Propyl, the difference between the two coefficient values is nonetheless than 100. Apart from that, one needs to take into account other aspects that can influence this discrepancy: different temperatures of analysis (25°C for PFG-NMR and 350°C for IGC); the phase of the probe molecule (liquid for PFG-NMR and vapor for IGC); and the probe itself (toluene for PFG-NMR and benzene for IGC).

Moreover, the three techniques show different orders of magnitude. This is not surprising since the values of iGC are related to the analysis conditions. At higher temperatures, the effective diffusivity is higher, as proved by Arrhenius equation: $D_{eff} = D_0 \exp\left(-\frac{Ea}{RT}\right)$, being D_0 the temperature-independent pre-exponential factor, Ea the activation energy for diffusion, R=8.314 J/mol.K, and T temperature in Kelvin. Moreover, the probe molecule used in this case, benzene, suffers a faster diffusion in the zeolite structure due to its smaller diameter, leading to higher values of effective diffusivity.

[126] Kolitcheff, S.; Jolimaitre, E.; Hugon, A.; Verstraete, J.; Carrette, P. L.; Tayakout-Fayolle, M. *Microporous Mesoporous Mater.* **2017**, *248*, 91–98.
[127] Caro, J.; Bülow, M.; Schirmer, W. *J. Chem. Soc. Faraday Trans. 1* **1985**, *81*, 2541–2550.
[128] Krishna, R.; van Baten, J. M. *Chem. Eng. Technol.* **2007**, *30*, 1235–1241.

Concerning the experiments performed under similar conditions, both in temperature and with the same probe molecule (PFG-NMR and gravimetric method), the difference of two orders of magnitude has also been observed in former studies, being attributed to different experimental technologies[38b,c]. For example, uptake measurements solve Fick's law of diffusion to acquire the diffusion coefficients, while PFG-NMR uses Einstein's equation to compute the self-diffusion coefficient. Moreover, one has to keep in mind that uptake measurements detect not only the adsorption within the zeolitic pores but also the sorbate permeation through the bed of crystallites, the transport resistances at the external surface of crystallites, and the dissipation of heat adsorption. This may imply that uptake measurements are controlled by processes different from intracrystalline diffusion, leading to smaller diffusivities than PFG-NMR. Nonetheless, in both cases, Catal_10Propyl and Catal_P123 exhibited higher values than Catal_ref.

Finally, it is important to mention the effect of adsorption in the effective diffusivity measurements. Meunier et al.[129] reported that the determination of diffusion length was limited by a site-desorption controlled molecular transport, which led to a decrease of the effective diffusivity obtained by DRIFT caused by strong adsorption interactions. Although this may be applied IGC and gravimetric method, our group has shown that the density of acid sites does not affect the values of toluene's effective diffusivity obtained by PFG-NMR.[130] By maintaining the crystal size and changing the Si / Al ratio of ZSM-5 zeolite, it is assumed higher Brønsted acid sites density, which can participate in the adsorption of toluene. However, all the samples showed similar results of effective diffusivity, which implies the elimination of this issue in the PFG-NMR technique.

6.3 Conclusion

In this chapter, the effective diffusivity of the samples was measured by three different techniques. Combining pioneer ones such as the gravimetric method with the more sophisticated pulsed-field gradient NMR one may conclude that there was an improvement in the effective diffusivity thanks to the presence of meso- and macropores in the binder. Though the results of PFG-NMR suggest the absence of interconnectivity between the two pores topologies (binder and zeolite), in contrast, gravimetric method showed the opposite, with a great increase of the latter with a raise in the macropore volume.

On the other side, inverse gas chromatography mimicked realistic conditions by operating at higher temperatures and under a continuous flow. Nonetheless, the same tendency was observed: an increase in the effective diffusivity in the samples with the presence of macropores. The solely drawback of this study is the fact that it is not possible to compare the results obtained by the different techniques due to different methodologies and equations used to obtain the values.

[129] Meunier, F. C.; Verboekend, D.; Gilson, J. P.; Groen, J. C.; Pérez-Ramírez, J. *Microporous Mesoporous Mater.* **2012**, *148*, 115–121.
[130] Bingre, R.; Losch, P.; Megías-Sayago, C.; Vincent, B.; Pale, P.; Nguyen, P.; Louis, B. "PFG-NMR as a tool for determining self-diffusivities of various probe molecules through H-ZSM-5 zeolites". (submitted to ChemPhysChem)

Chapter 7 – Valorisation of biomass waste in the synthesis of zeolites

Abstract

Herein, it is presented a synthesized ZSM-5 zeolite with the lowest Si/Al ratio ever published, by introducing oxidized lignin during the synthesis as secondary sacrificial template. This material was deeply characterised by XRD, N_2-physisorption, SEM, TEM, ^{29}Si and ^{27}Al MAS NMR, and acidity measurements and the results are carefully described in the present chapter. This material was tested in the methanol-to-hydrocarbons reaction showing significant changes in comparison with the commercial zeolite used during this Thesis.

The recipe for preparing this Al-containing ZSM-5 zeolite will be patented in September 2019.

7.1 Biomass as a secondary template

The use of zeolites as catalysts has seen a great increase in the past decades due to their potential in current and emerging technologies.[116,131] In particular, ZSM-5-type being highly siliceous (Si/Al > 10) is currently explored in hydrocarbon cracking, methanol-to-olefins, isomerization, Friedel-Crafts acylation thanks to its structure of narrow pores and channels. However, many scientists have searched strategies to tune the characteristics of this zeolite for better catalytic and adsorption performances. For instance, the Rimer group has studied the impact of zeolite growth modifiers on the size and morphology of the crystals. The use of polyamines, proteins and sugars had strongly impacted the assembly of crystals allowing these to mimic biomineralization processes and giving interesting crystal features.[132] In parallel, Morris et al. have developed a smart Assembly-Disassembly-Organisation-Reassembly (ADOR) strategy to organize zeolite precursors in different ways.[133]

On another pathway, several researchers have reported the use of biomass as potential template instead of the synthetic ones as they are abundant and typically cheap. Valtchev et al. reported the use of highly reactive silica in the surface of *Equisetum Arvense* leaves facilitating zeolite nucleation and keeping the morphological features of the plant after being hydrothermally treated with a precursor solution of MFI crystals.[134] Zhang et al. infiltrated bacterial templates in an aqueous dispersion of zeolite nanoparticles for hierarchical zeolite growth.[135] Also, they used starch gels and sponges with pre-formed silicalite nanoparticles to form monoliths and thin films with a hierarchical meso- and macroporous structure.[136] Hernandez-Ramírez et al. also used carbonized coconut fibres and shells of carbon from olive seeds to synthesize zeolite Y. The typical honeycomb structure and uniform porous surfaces of biomass led to an arrayed zeolite crystal structure.[137]

Inspired by the most recent work from Louis et al.[138] that presents ZSM-5 zeolites exhibiting the lowest Si/Al = 8 reported to date, when using cheap sugarcane residues as crystal growth modifiers, it was studied in this Thesis the impact of using oxidized lignin in the synthesis of this type of MFI zeolite.

---

[131] a) Corma, A. *Chem. Rev.* **1997**, *97*, 2373–2420; b) Corma, A. and Jones S. Zeolites as catalysts for the synthesis of fine chemicals, in *Zeolites and Catalysis*, Wiley-VCH Verlag GmbH & Co. KGaA, Wienheim, **2010**; c) Jacobs, P. A.; Dusselier, M.; Sels, B. F. *Angew. Chemie - Int. Ed.* **2014**, *53*, 8621–8626; d) Dusselier, M.; Van Wouwe, P.; Dewaele, A.; Jacobs, P. A.; Sels, B. F. *Science.* **2015**, *349*, 78–80; e) Mintova, S.; Jaber, M.; Valtchev, V. *Chem. Soc. Rev.* **2015**, *44*, 7207–7233.

[132] a) Rimer, J. D.; Lobo, R. F.; Vlachos, D. G. *Langmuir* **2005**, *21*, 8960–8971; b) Lupulescu, A. I.; Rimer, J. D. *Angew. Chemie - Int. Ed.* **2012**, *51*, 3345–3349; c) Maldonado, M.; Oleksiak, M. D.; Chinta, S.; Rimer, J. D. *J. Am. Chem. Soc.* **2013**, *135*, 2641–2652; d) Lupulescu, A. I.; Kumar, M.; Rimer, J. D. *J. Am. Chem. Soc.* **2013**, *135*, 6608–6617; e) Lupulescu, A. I.; Rimer, J. D. *Science.* **2014**, *344*, 729–732.

[133] a) Eliášová, P.; Opanasenko, M.; Wheatley, P. S.; Shamzhy, M.; Mazur, M.; Nachtigall, P.; Roth, W. J.; Morris, R. E.; Čejka, J. *Chem. Soc. Rev.* **2015**, *44*, 7177–7206; b) Firth, D. S.; Morris, S. A.; Wheatley, P. S.; Russell, S. E.; Slawin, A. M. Z.; Dawson, D. M.; Mayoral, A.; Opanasenko, M.; Položij, M.; Čejka, J.; et al. *Chem. Mater.* **2017**, *29*, 5605–5611.

[134] Valtchev, V.; Smaihi, M.; Faust, A. C.; Vidal, L. *Angew. Chemie - Int. Ed.* **2003**, *42*, 2782–2785.

[135] Zhang, B.; Davis, S. a.; Mann, S.; Mendelson, N. H. *Chem. Commun.* **2000**, *2*, 781–782.

[136] Zhang, B.; Davis, S. A.; Mann, S. *Chem. Mater.* **2002**, *14*, 1369–1375.

[137] Hernandez-Ramirez, O.; Al-Nasri, S. K.; Holmes, S. M. *J. Mater. Chem.* **2011**, *21*, 16529–16534.

[138] Pereira, M. M.; Gomes, E. S.; Silva, A. V.; Pinar, A. B.; Willinger, M. G.; Shanmugam, S.; Chizallet, C.; Laugel, G.; Losch, P.; Louis, B. *Chem. Sci.* **2018**, *9*, 6532–6539.

7.2 Lowest SAR for ZSM-5

7.2.1 Oxidized lignin

Lignin is a complex biopolymer that forms key structural materials in the support of tissues of vascular plants. Lignins are abundantly found in wood and bark and their chemical structure is formed by cross-linked phenolic polymers.

The random assembly of hydrocarbons produces a hydrophobic assembly, which may influence the zeolite crystallization during the hydrothermal treatment. In this Thesis, the lignin extracted from wood waste has been treated by the group of Prof. Aleksander Vasilyev (Saint-Petersburg State University) to provide its oxidized form (Figure 53).

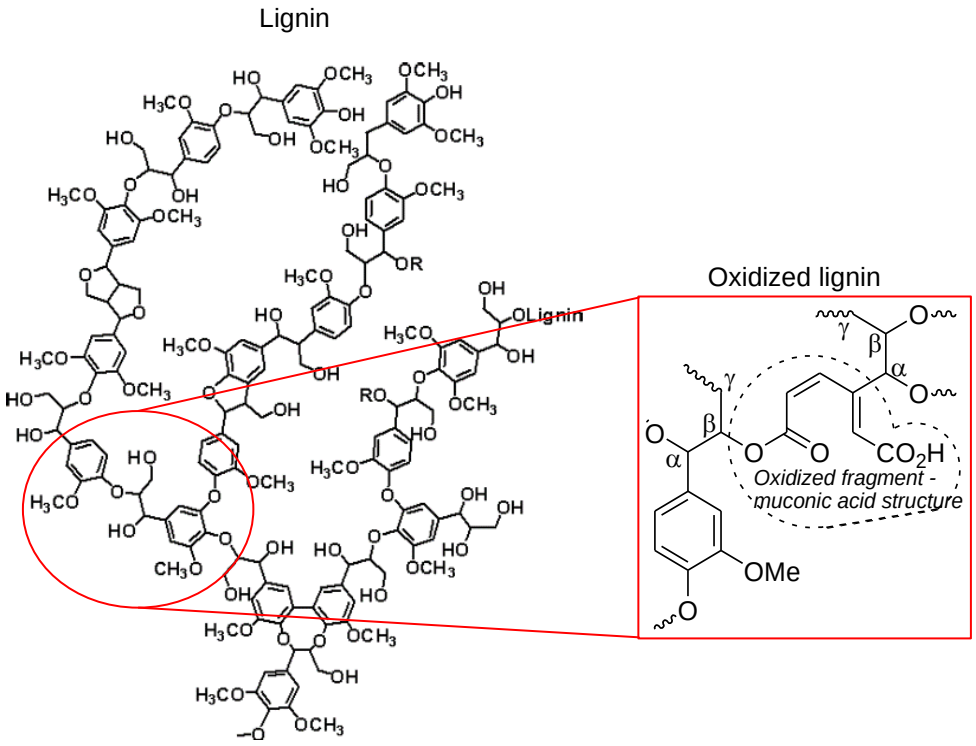

Figure 53: Structure of lignin and oxidized lignin

During the preparation of the synthesis gel, oxidized lignin was added after mixing all the other reactants. It is important to mention that even at low mass (100 mg), this compound only partially dissolved in the solution.

7.2.2 Structural properties

Figure 54 shows the diffraction patterns of as-prepared samples with different quantity of oxidized lignin after calcination step. The sole presence of MFI structure is exhibited, thus indicating the total combustion of the biomass. Moreover, the addition of oxidized lignin did neither lead to loss in crystallinity, nor contributed to the appearance of a new crystalline phase. The sample z500LO was analysed for longer time to verify the crystallinity of the structure, represented in Figure 55. Focusing on MFI main reflections between 22.5 – 25º, extra-reflections are observed at smaller 2θ angles. This was

also reported in the former lowest SAR ZSM-5 8, being attributed to the same Pnma space group but with slightly larger unit cell parameters. Although synchrotron powder diffraction and Rietveld refinement were not performed for these samples, the similarity in the diffraction patterns may indicate an extremely low SAR for zxLO.

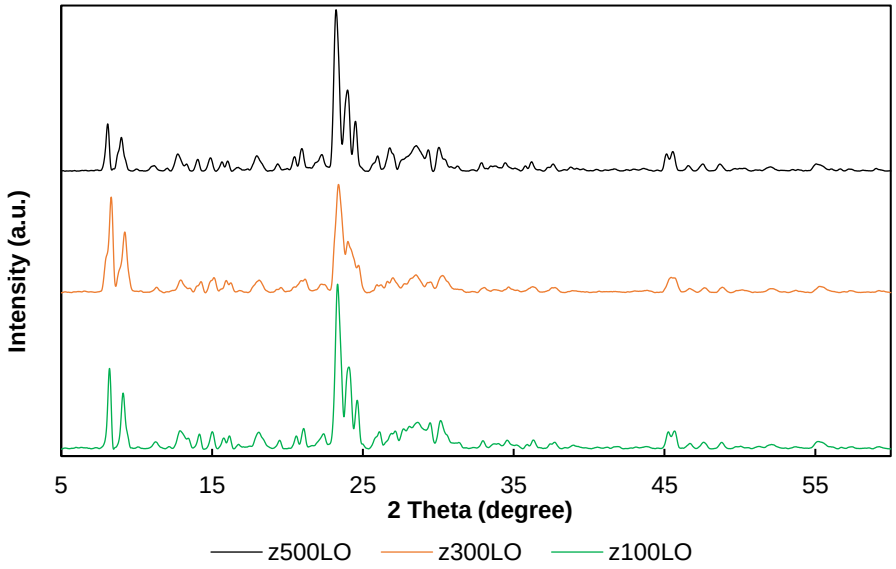

Figure 54: XRD patterns of the samples prepared with different masses of oxidized lignin

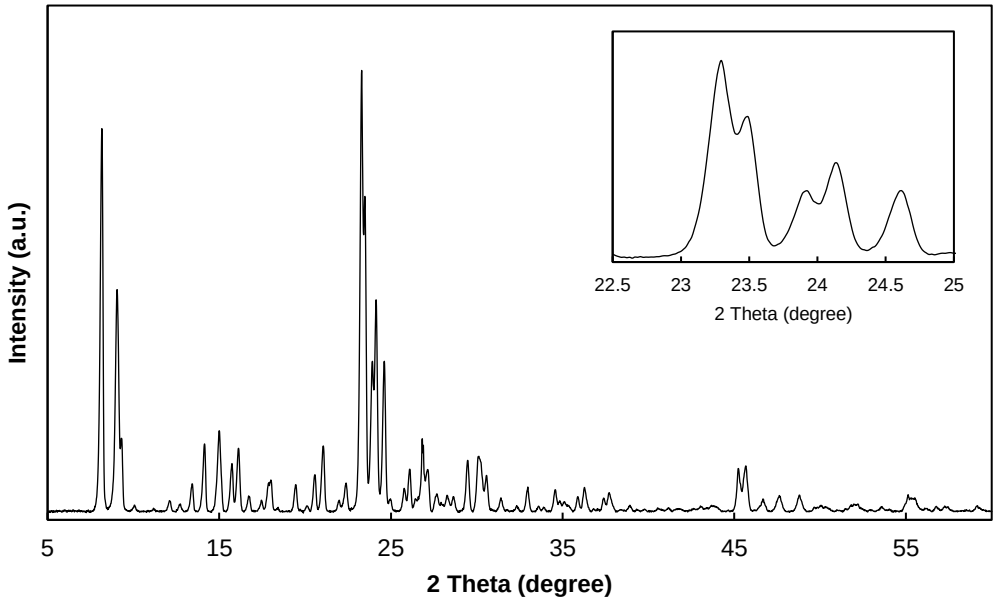

Figure 55: Closer look in the XRD pattern of z500LO

N_2 adsorption-desorption measurements reported typical type I isotherm related to microporous materials for the three samples (Figure 56). Specific surface areas (S_{BET}) of around 200 m^2/g and total pore volume of around 0.1 cm^3/g were obtained, where the microporous volume is 70% of the latter (Table 17), confirming that z_xLO possess predominantly a microporous structure. The pore profile

obtained by the BJH method also follows this observation, though some mesopores around 4 nm in size are present. This was also reported in CBV3020E in Chapter 4 and attributed to intercrystalline mesoporosity.

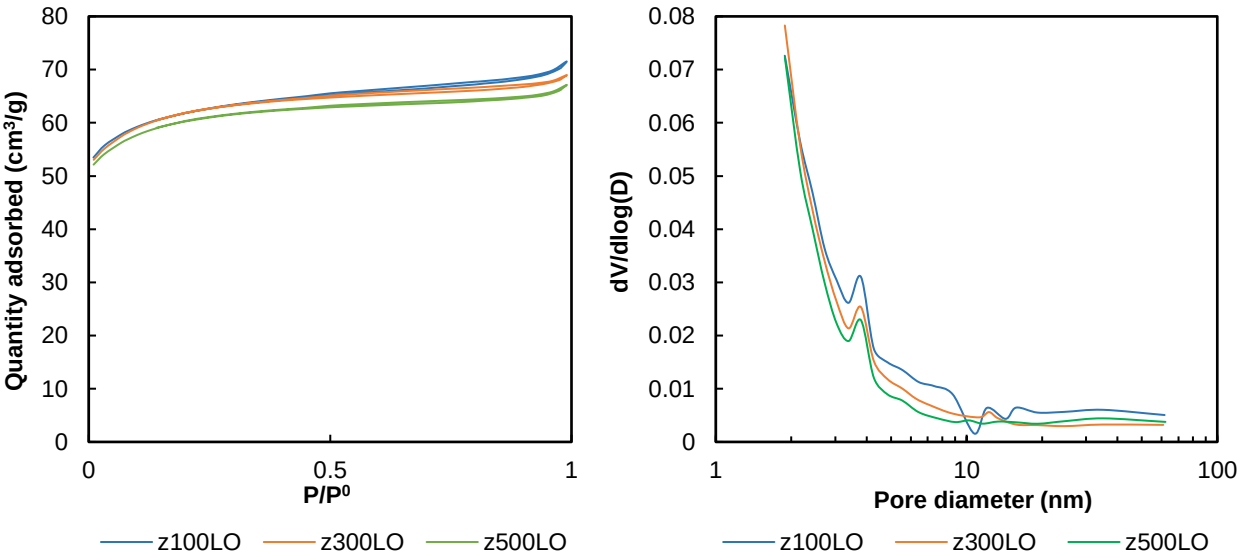

Figure 56: BET isotherms (left) and BJH pore profile (right) of the samples prepared with different quantities of oxidized lignin

Table 17: Specific surface area, S_{BET}, external surface area, S_{ext}, total pore volume, V_{pore}, and microporous volume, V_{micro}, obtained by N_2 adsorption-desorption

Sample	S_{BET} (m²/g)	S_{ext} (m²/g)	V_{pore} (cm³/g)	V_{micro} (cm³/g)
z100LO	200	55.9	0.108	0.071
z300LO	201	60.1	0.105	0.069
z500LO	195	54.7	0.102	0.069

The microstructure of the samples was analysed by SEM (Figure 57 to Figure 59). z100LO exhibits the characteristic coffin-shaped crystals associated to ZSM-5 zeolite type. Interestingly, the addition of lignin oxidized led to the formation of crystals of dimensions around 20 µm presenting the shape of a “peanut”. The increase in the biomass quantity also raises the appearance of these peculiar crystals, until higher homogeneity could be observed for z500LO. By a careful observation, these “peanuts” are nothing more than an agglomeration of elongated nanocrystals with the shape of “French fries”. It seems that these filaments grow from a nodal point of the agglomerate that can be the starting matter for those elongated needle-like shaped crystals growth. Once again, the same was observed for SAR = 8 from Louis et al., although the crystals assembly exhibited a spherical form.

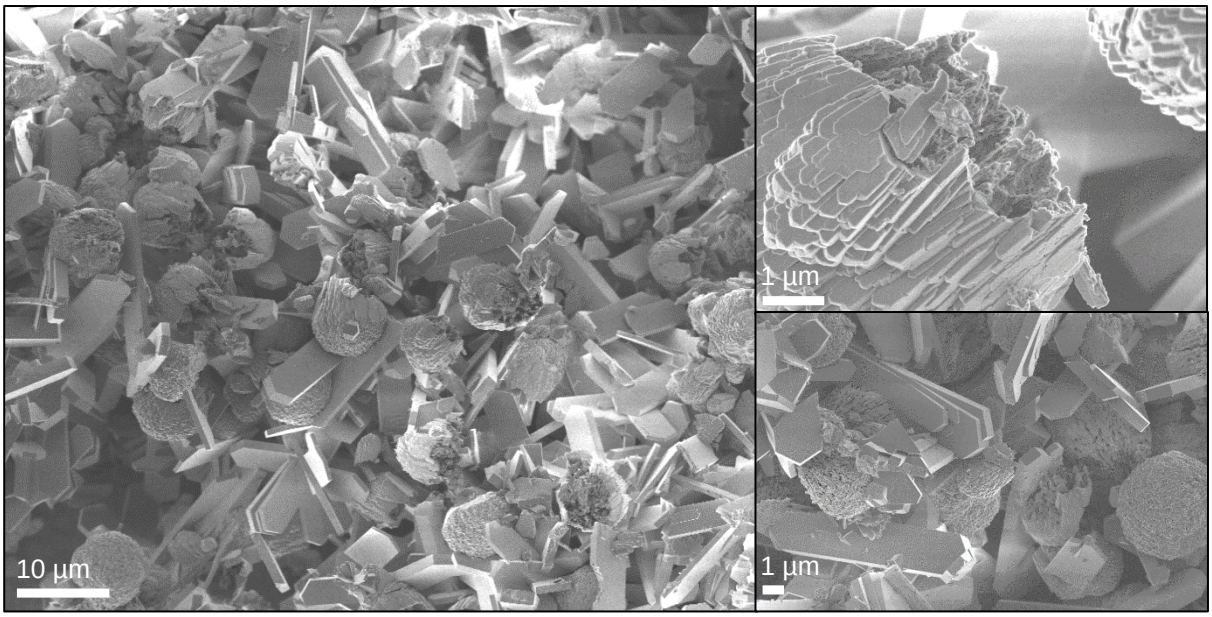

Figure 57: SEM images of z100LO

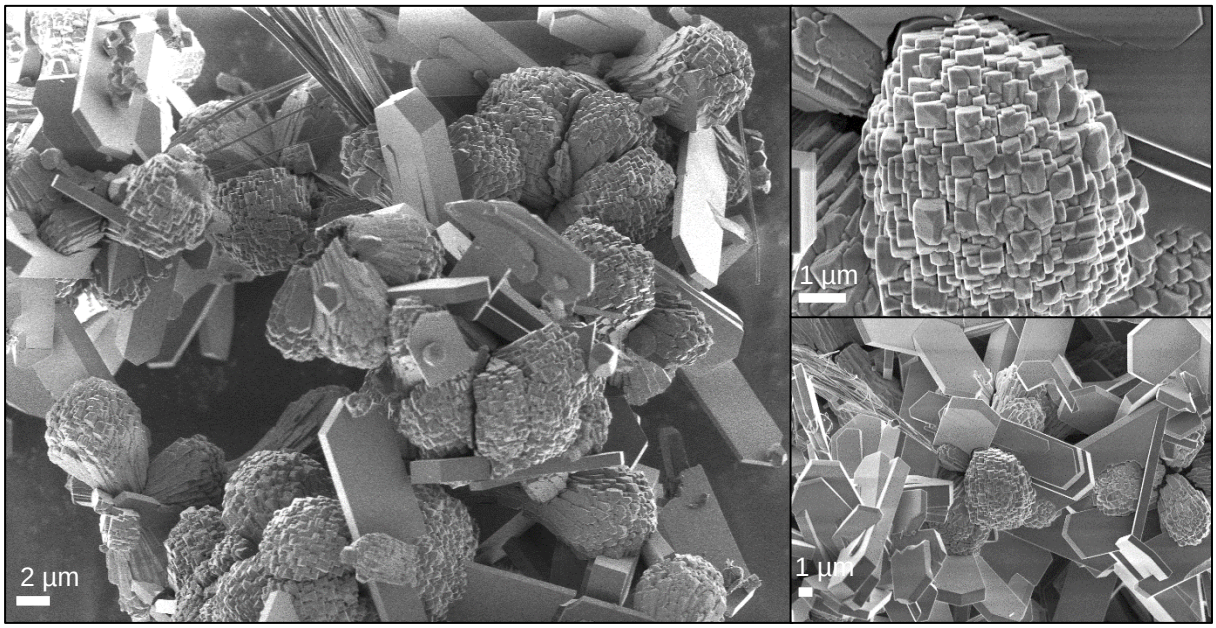

Figure 58: SEM images of z300LO

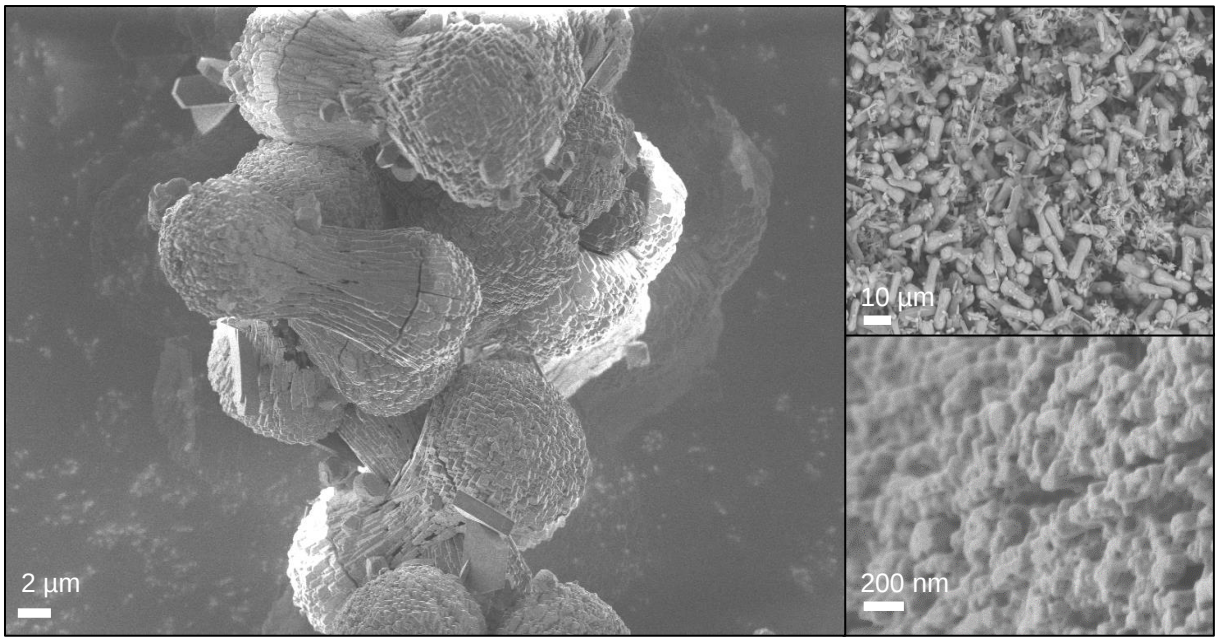

Figure 59: SEM images of z500LO

The mapping of the elements of z500LO was also performed by EDX coupled with SEM chamber (not presented), and it was detected the presence of only Si, Al, Na and O elements, confirming the previous assumption of total removal of oxidized lignin. Surprisingly, it was determined a Si/Al ratio close to 4, being the lowest ever reported for the ZSM-5 zeolite. In order to confirm those results, solid-state NMR was performed. This technique relies on the detection of relevant basic nuclei on the zeolite framework by their natural isotopes (natural abundance in parentheses): ^{29}Si (4.7%), ^{27}Al (>99.9%), and ^{17}O (0.037%)[139]. The resonance lined obtained for ^{29}Si is usually narrow and, due to their important role as framework element (besides ^{27}Al), these nuclei have been widely used in solid-state NMR studies of micro- and mesoporous (alumina)silicate materials for structural investigations. The most important application of ^{29}Si NMR is due to the relationship between the ^{29}Si chemical shift sensitivity and the degree of condensation of the SiO_4 tetrahedra, that is the number and type of tetrahedrally coordinated atoms connected to a given SiO_4 unit Si($_n$Al), with n = 0, 1, 2, 3, or 4. The chemical shift ranges from -80 to -115 ppm, with the high-field shift signal for Si($_0$Al). Here, n indicates the number of Al atoms sharing oxygens with the SiO_4 tetrahedron under consideration (Figure 60).

[139] Jochen Hoefs. *Stable Isotope Geochemistry*. Springer Verlag. **1997**

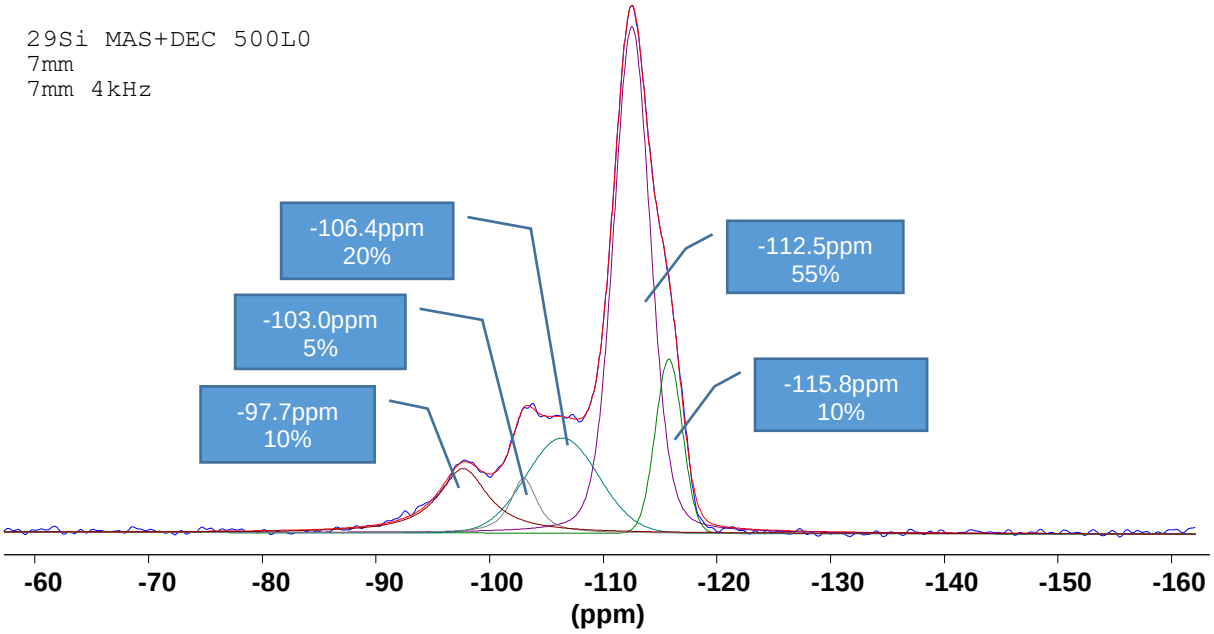

Figure 60: ^{29}Si MAS NMR of z500LO

Differences in the chemical shift between Si($_n$Al) and Si($_{n+1}$Al) are about 5 – 6 ppm. In this way, the spectra obtained can be used to calculate the framework Si/Al ratio from the NMR signal intensities (I) according to Equation 25.

$$\left(\frac{Si}{Al}\right)_{NMR} = \frac{\sum_{n=0}^{4} I_{Si(nAl)}}{\sum_{n=0}^{4} 0.25 n I_{Si(nAl)}} = \frac{0.1 + 0.05 + 0.2 + 0.55 + 0.1}{0.2 \times (4 \times 0.1 + 3 \times 0.05 + 2 \times 0.2 + 0.55)} = 2.7 \quad (25)$$

This seems to imply that the presence of oxidized lignin allows the stabilization of the aluminosilicate structure, allowing the lowest SAR ever reported. In fact, previous DFT calculations performed by Céline Chizallet, for the work of Louis et al. to access the thermodynamic stability of ZSM-5 SAR8 structure as a function of the SAR, showed a possible stabilization at SAR values 2-3 (Figure 61).

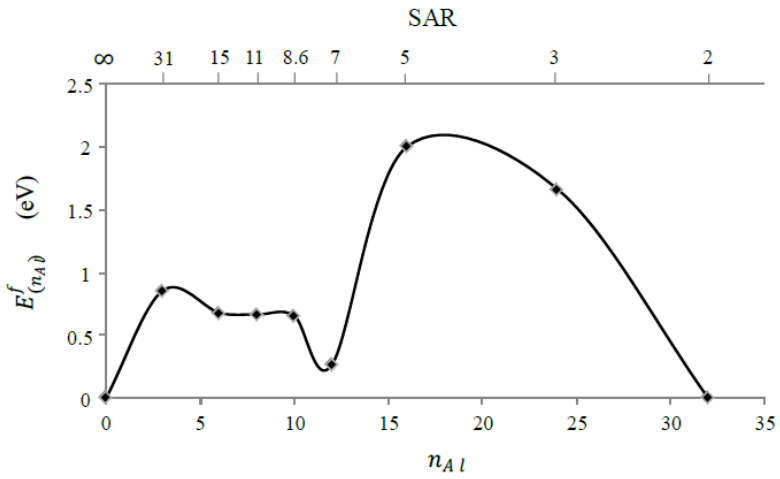

Figure 61: Evolution of the formation energy of the cells, as calculated by DFT, as a function of the SAR or the number of aluminium atoms within the cell by Louis et al.

^{27}Al NMR spectrum (Figure 62) reveals a small existence of extra-framework Al (about 0 ppm) besides the lattice aluminium (tetrahedral coordinated Al at about 40 – 65 ppm), which can be negligible and admit a real Si/Al ratio of 3 to z500LO.

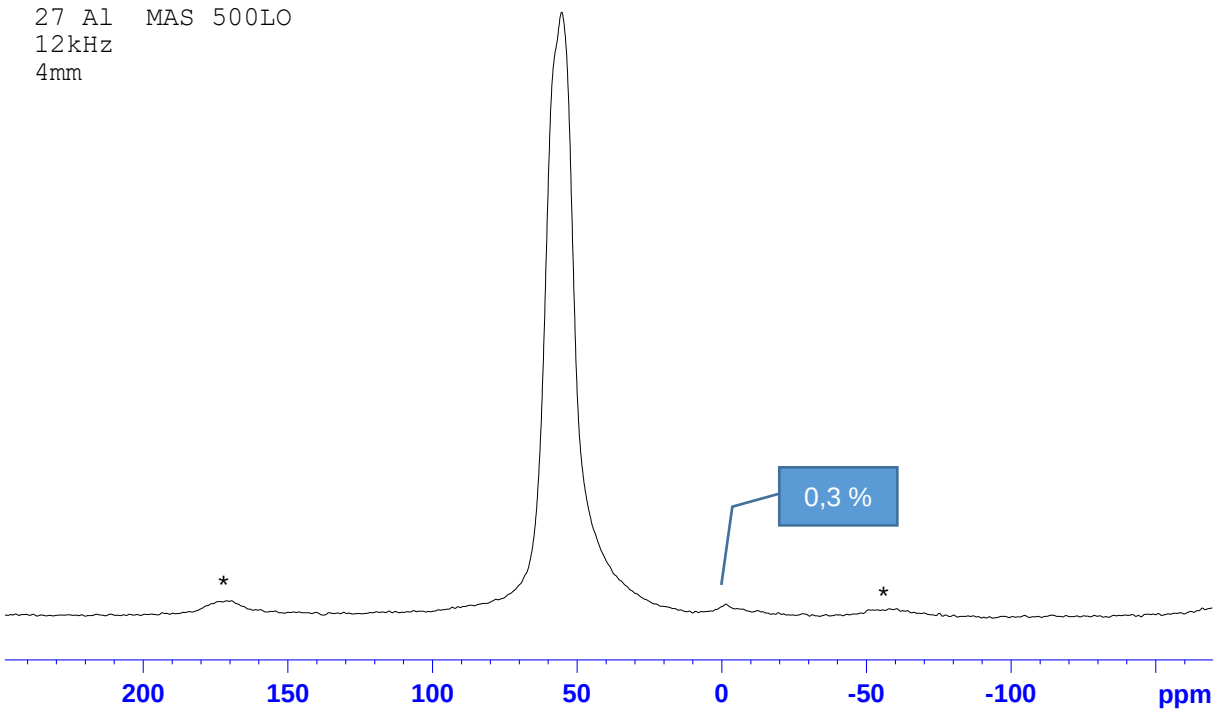

Figure 62: ^{27}Al MAS NMR of z_500LO

Brønsted and Lewis acid sites of z500LO were discriminately measured by FTIR of adsorbed pyridine and represented in Figure 63. The spectrum is similar to the one exhibited by the shaped samples with bands at the same wavenumber. By integration of the peaks at 1544 and 1455 cm^{-1} after desorption at 150°C, it was obtained 285 and 14.6 µmol/g for Brønsted and Lewis acid sites,

respectively. Moreover, the Al concentration was determined to be 1444 µmol/g. In principle, the total concentration of acid sites (Brønsted + Lewis) should be equal to the concentration of Al in the zeolite. Unfortunately, this is not the case. It might have been an error in Al quantification or a non-negligible fraction of acid sites that are not accessible to pyridine. Nonetheless, high content of Al in the aluminosilicate structure directly increases the Brønsted acidity, while Al zoning or extra-framework aluminium species (EFAl) is related to Lewis acid sites. The low value of the latter seems to confirm the nearly absence of these species, as verified by ^{27}Al MAS NMR.

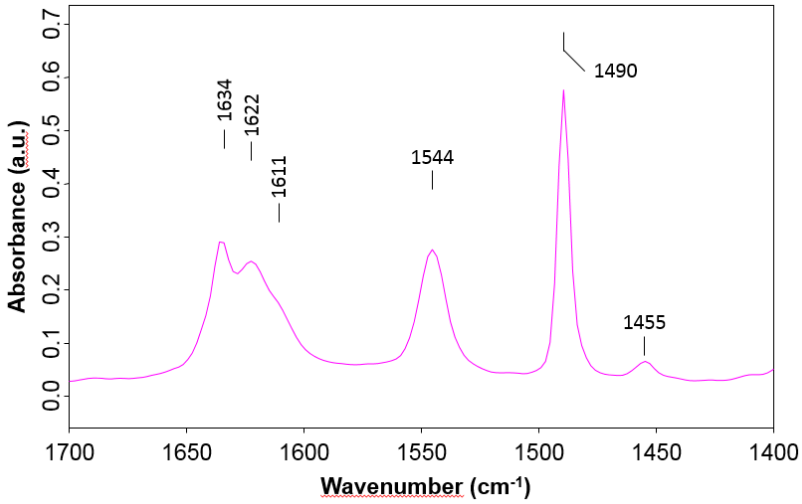

Figure 63: IR spectrum of adsorbed pyridine on z_500LO

OH DRIFT spectrum of z500LO in Figure 64 showed three bands at: (i) 3745 cm-1 characteristic of isolated Si-OH with very low intensity compared with other modified commercial zeolites; (ii) 3670 cm-1 characteristic of extra-framework aluminium Al-OH of equally low intensity; and (iii) 3620 cm-1 characteristic of zeolite framework with high intensity.[140] Once again, these results suggest the presence of (very) few EFAl species.

[140] a) Zecchina, A.; Bordiga, S.; Spoto, G.; Scarano, D.; Padovan, M.; Arean, O. *J Chem Soc Faraday Trans* **1992**, *88*, 2959–2969; b) Wakabayashi, F.; Kondo, J. N.; Domen, K. *J. Phys. Chem.* **1995**, *99*, 10573–10580.

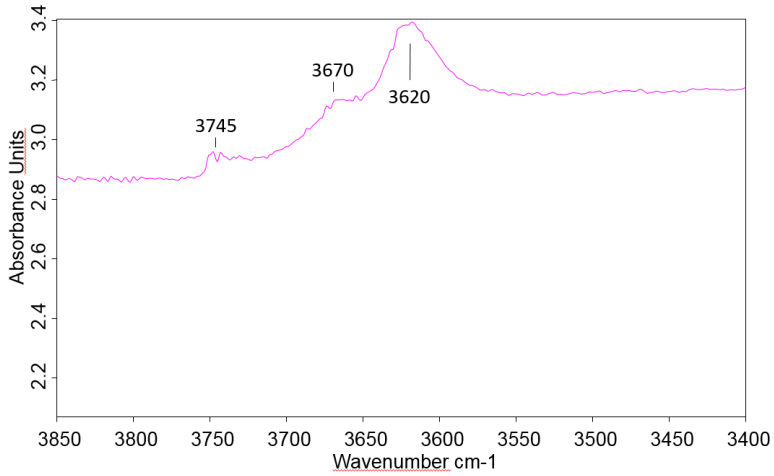

Figure 64: OH DRIFT spectrum of z_500LO

7.3 Catalytic performance in the methanol-to-hydrocarbons reaction

In the previous section, the in-depth characterization of z500LO was presented. It is expected that such low SAR may exhibit interesting catalytic performance in the MTH reaction. The catalyst lifetime in comparison with the commercial CBV3020E is presented in Figure 65 (left side) along with the coke analysis as performed in the extruded samples in Chapter 5 (Figure 65 – right side).

The sample z500LO exhibited lower capacity to maintain the full conversion of methanol and dimethyl ether than CBV3020E, however its deactivation rate showed to be slower. This may be attributed to the crystal size of the two samples. The commercial zeolite possesses nanocrystals, which means the diffusion path is shorter for the exit of the molecules being able to keep the active sites *clean* for longer time. On the other side, once the coke precursors start to poison these sites, the conversion quickly decreases. In the case of z500LO, the crystals exhibited long micrometric scales, hindering the exit of molecules that slowly deactivate the catalyst. This may be confirmed by the coke analysis that showed lower combusted coke content at 600ºC than CBV3020E. In fact, this temperature seems not sufficient enough to remove all the coke present in z500LO as there is still a decrease in the mass until the end of the experiment. This is related to the size of these molecules, which suggests that as bigger the molecules are, more energy is required to decompose them. By staying for longer time in contact with the active sites, coke precursors are able to react further. In fact, several researchers have mentioned the coke toxicity, distinguishing between soft and hard coke.[112b),141] The former is removed by combustion at relatively low temperature while the latter requires temperatures between 400 and 600ºC. These two stages of mass loss were observed in Figure 65 – right side.

[141] a) Qiao, Q.; Wang, R.; Gou, M.; Yang, X. *Microporous Mesoporous Mater.* **2014**, *195*, 250–257; b) Zhang, H.; Shao, S.; Xiao, R.; Shen, D.; Zeng, J. *Energy and Fuels* **2014**, *28*, 52–57; c) Chen, D.; Moljord, K.; Holmen, A. *Microporous Mesoporous Mater.* **2012**, *164*, 239–250.

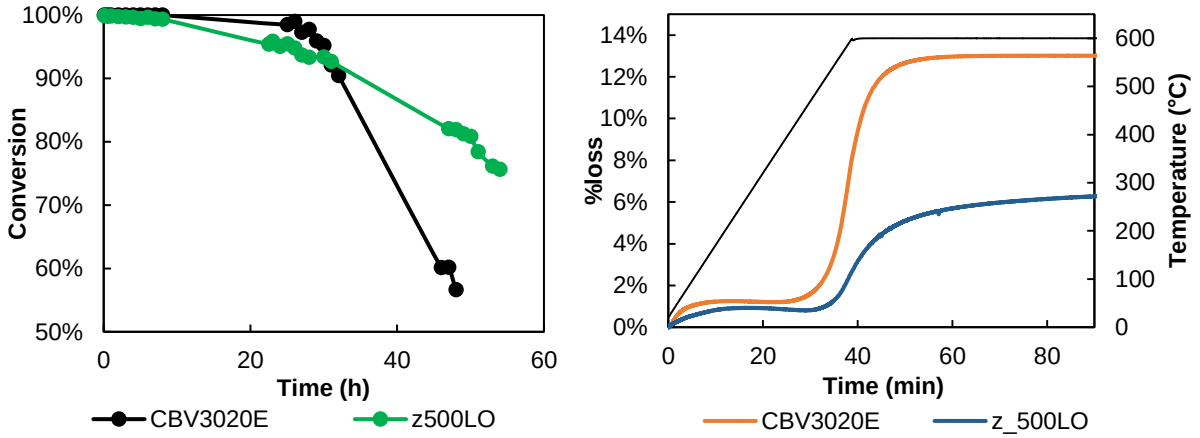

Figure 65: Catalytic performance of z_500LO in the conversion of methanol towards olefins in comparison with commercial CBV3020E (left); coke analysis of the samples (right)

Regarding the products selectivity, z500LO exhibited higher olefins selectivity than CBV3020E, particularly towards ethylene and butylene isomers. On the other side, there was a similar formation of compounds containing 5 carbons or more for both samples. This is a surprising result as the higher aluminium content is associated with higher active sites and, consequently, higher selectivity towards heavier products. It seems that the crystals morphology plays here an important role in the catalytic performance besides the acidity as suggested by Svelle et al.[142]

Table 18: Selectivity in ethylene (C_2H_4), propylene (C_3H_6), isomers of butylene (C_4H_8) and compounds with 5 carbons or more (including aromatics – C_{5+}) after 1 h reaction of the samples

Samples	$\%S_{C2H4}$	$\%S_{C3H6}$	$\%S_{C4H8}$	$\%S_{C5+}$
CBV3020E	3	26	9	30
z_500LO	15	28	13	32

7.4 Conclusion

In this chapter, the incorporation of oxidized lignin in the zeolite synthesis as an inspiration of biomass valorisation reported by previous studies was presented. In-depth characterization confirmed that one of the samples exhibited the lowest Si/Al ratio ever reported, maintaining the sole MFI microporous and crystalline structure.

The catalytic performance of this new material led to an increased olefins selectivity and longer catalyst lifetime, which may have interesting industrial applications. Nonetheless, it is necessary to optimize the synthesis strategy in order to decrease the amount of organics used, particularly TPAOH. It is also left as a perspective the study of different Si/Al ratio in the synthesis gel, hydrothermal treatment time and, eventually, other adsorption or catalytic applications.

[142] Łukaszuk, K. A.; Rojo-Gama, D.; Øien-ØDegaard, S.; Lazzarini, A.; Berlier, G.; Bordiga, S.; Lillerud, K. P.; Olsbye, U.; Beato, P.; Lundegaard, L. F.; et al. *Catal. Sci. Technol.* **2017**, *7*, 5435–5447.

General conclusion and future prospects

During this Thesis, a new method to prepare shaped zeolites was successfully developed, that can be easily implemented at large scale. By studying several types of pore former agents, we were able to select the more suitable ones to form meso- and/or macropores in the catalyst bodies with a simple preparation.

In **Chapter 1**, an insight on the zeolite history and science was reminded, particularly the ZSM-5 type, with its main applications being presented among with a very important aspect throughout this work: the effective diffusion. **Chapter 2** relied on the importance and the state-of-art of shaping technology by presenting different types of binder used industrially and the main "side" effects caused by this process. As a result, it was decided to use boehmite as a binder, which transforms into γ-alumina upon the calcination step. All the samples preparation methods and procedures were described in **Chapter 3**, along with a brief description of the techniques used to characterize the materials and the catalytic reactions where they were implemented.

Several samples presenting different types of porosity according with the type of pore former agent used were successfully prepared. This was carefully described in **Chapter 4** showing that different characterization techniques proved the existence of meso- and/or macropores in different samples without significantly altering the acidity of the catalyst. However, the mechanical strength of the extrudates was verified to strongly depend of the pore former agent used, which implies a cautious choice when selecting the extrusion method to be implemented.

The different as-prepared materials were tested in the methanol-to-hydrocarbons (MTH) reaction and it was verified a great improvement of the catalyst lifetime in the extrudates containing meso- and/or macropores, *as per* **Chapter 5**. To ensure that the results were not influenced by differences in acidity, the samples were tested in the α-test (or n-hexane cracking). By neither observing significant changes in the reaction rate nor in the selectivity, it was possible to guarantee an improvement of the catalyst lifetime in the MTH reaction solely to the presence of additional porosity. The performance in n-butylcyclohexane cracking and toluene adsorption from a gas stream was also affected by those extra-pores, and possible explanations were discussed in this chapter.

Nonetheless, the main goal of this Thesis was the study of the effective diffusivity. Three different techniques to measure the diffusion of molecules in solid catalysts were presented in **Chapter 6**. By having different operating conditions and using different mathematical approaches to reach the effective diffusivity value, the results were not quantitatively comparable among them. But most importantly, it was noted the same tendency regarding the samples having additional porosity than the pristine one. In fact, all the three techniques showed higher values of effective diffusivity for the macroporous samples in comparison with the microporous reference zeolite. This allowed the correlation between the catalytic results and the improvement of the effective diffusivity, demonstrating a paramount influence of the meso- and/or macropores presence in the binder.

With this Thesis, we hope that a step forward was brought to come closer to the comprehension and formulation of industrial catalysts with improved performances. The methods described and

analysed throughout this manuscript were of easy implementation and considerably low cost, which may allow a possible scale-up.

Finally, **Chapter 7** presented the synthesis of a new type of ZSM-5 zeolite. Although being slightly deviated from the main concept of this Thesis, it addressed a very important concept nowadays: the valorisation of bio-waste. Giving a primary look on the previous work developed by our group where ZSM-5 with Si / Al ratio of 8 (the lowest reported to date) was prepared by using cheap sugarcane bagasse. In this chapter, oxidized lignin was used as one of the synthesis reactants. Surprisingly, an in-depth characterization showed an even lower Si / Al of 3, also demonstrating interesting performance in the MTH reaction.

As final remarks, it is known that research is an endless job. This work is far from being completed and I risk saying that more questions have been raised by the end of this Thesis: What other pore former agent could be used to form mesopores? How would this technique be suitable to be implemented on other catalysts morphologies? Could the catalytic performance be further improved by using different shapes, such as trilobes? How well interconnected are the zeolite pores with the additional ones created in the binder?

The procedure developed during this Thesis may have to be optimized to be implemented at large scale, using different amounts of binder to better understand the behaviour of the pore former agents in materials with higher content of alumina. Moreover, different types of binder, such as silica that is widely used in industry, can be studied with the procedure herein described. There, the acidity will have to be studied to verify the occurrence of changes caused by the binder. Personally, I find very interesting the valorisation of bio-waste, and although the oxidized lignin was shown to be very ineffective in this case, other types of biomass may have a positive impact in the effective diffusivity of the samples. Furthermore, this may also reduce the cost of this method, as propyltex and pluronic P123 are organic materials considerable expensive.

On the other side, the study of the effective diffusivity still remains a sensitive characterization field, due to the incoherence often found between the different techniques. Besides, very few studies are devoted to the diffusion behaviour in shaped zeolites, since most techniques only use powder form. Further implementation of different techniques is required to better understand the diffusional pathways present in this type of materials. This can be correlated with the performance in different catalytic reactions or even with different zeolite / catalyst types.

Publications

Guillaume Laugel, Rogéria Bingre, Benoît Louis. "Zeolite and Silica-based CO_2 Adsorbents." in Post-combustion Carbon Dioxide Capture Materials. Royal Society of Chemistry, 25 Oct. **2018**. 76-152. DOI: 10.1039/9781788013352-00076.

Rogéria Bingre, Benoît Louis, Patrick Nguyen. "An Overview on Zeolite Shaping Technology and Solutions to Overcome Diffusion Limitations." *Catalysts* **2018**, *8*, 163. DOI: 10.3390/catal8040163.

Renna Li, Tianshan Xue, Rogéria Bingre, Yanshan Gao, Benoit Louis, Qiang Wang. "Microporous Zeolite@ Vertically Aligned Mg–Al Layered Double Hydroxide Core@Shell Structures with Improved Hydrophobicity and Toluene Adsorption Capacity under Wet Conditions." *ACS Applied Materials & Interfaces* **2018**, *10*, 34834-34839. DOI: 10.1021/acsami.8b15118.

Rogéria Bingre, Bruno Vincent, Qiang Wang, Patrick Nguyen, Benoit Louis. "Assessment of the Improvement of Effective Diffusivity over Technical Zeolite Bodies by Different Techniques." *The Journal of Physical Chemistry C* **2018**, *123*, 637-643.DOI: 10.1021/acs.jpcc.8b10914.

Rogéria Bingre, Cristina Megías-Sayago, Pit Losch, Liang Huang, Qiang Wang, Marcelo M. Pereira, Benoît Louis. "Recent progress in the biomass-mediated synthesis of porous materials." *Inorganica Chimica Acta* **2019**, *487*, 379-386. DOI: 10.1016/j.ica.2018.12.045.

Rogéria Bingre, Renna Li, Qiang Wang, Patrick Nguyen, Thomas Onfroy, Benoît Louis. “Porosity Design for Improved Catalyst Lifetime in the Methanol-to-Hydrocarbons Reaction.” *Catalysts* **2019**, *9*, 545. DOI: 10.3390/catal9060545.

Liang Huang, Cristina Megías-Sayago, Rogéria Bingre, Qianwen Zheng, Qiang Wang, Benoît Louis. “Catalytic Performance of Layered Double Hydroxides (LDHs) Derived Materials in Gas-solid and Liquid-solid Phase Reactions.” *ChemCatChem* **2019**, *11*, 3279-3286. DOI: 10.1002/cctc.201900499.

Cristina Megías-Sayago, Rogéria Bingre, Liang Huang, Qiang Wang, Benoît Louis, “CO_2 adsorption capacities in zeolites and layered double hydroxide materials.” *Frontiers in Chemistry* **2019**, *7*, 1-10. DOI: 10.3389/fchem.2019.00551.

Rogéria Bingre, Pit Losch, Cristina Megías-Sayago, Bruno Vincent, Patrick Pale, Patrick Nguyen, Benoit Louis. “PFG-NMR as a tool for determining self-diffusivities of various probe molecules through H-ZSM-5 zeolites.” *ChemPhysChem* **2019**, *20*, 1-9. DOI: 10.1002/cphc.201900672.

Communications

Rogéria Bingre, Patrick Nguyen, Benoît Louis, Groupe d'Etude en Catalyse (GECat), l'île d'Oléron, 29th May to 1st June 2017, poster.

Rogéria Bingre, Patrick Nguyen, Benoît Louis, 11th Edition of the Gay-Lussac Day (Saint-Gobain event), Domolab Aubervilliers, Paris, 6th July 2017, poster.

Rogéria Bingre, Patrick Nguyen, Benoît Louis, 1st International Edition of the Groupe Français des Zéolithes (GFZ), Village Vacances Sweet Home Cabourg, Normandy, 26th to 29th March 2018, poster.

Rogéria Bingre, Patrick Nguyen, Benoît Louis, Groupe d'Etude en Catalyse (GECat), le centre Azurera de Trégunc, 22nd to 25th May 2018, 1 poster and 1 oral.

Rogéria Bingre, Patrick Nguyen, Benoît Louis, 12th Edition of the Gay-Lussac Day (Saint-Gobain event), Domolab Aubervilliers, Paris, 5th July 2018, poster.

Rogéria Bingre, Patrick Nguyen, Benoît Louis, Groupe Français des Zéolithes (GFZ), l'Hôtel Club Igesa, l'île de Porquerolles, 2nd to 4th April 2019, poster.

Rogéria Bingre, Patrick Nguyen, Benoît Louis, 13th Edition of the Gay-Lussac Day (Saint-Gobain event), Domolab Aubervilliers, Paris, 3rd July 2019, oral.

Summer school

League of European Research Universities (LERU) Doctoral Summer School

Citizen Science – Nexus Between Research and Public Engagement

ETH Zurich, Switerland, 9-14 july 2017

Selected as one of the only two PhD candidates to represent the University of Strasbourg

Université de Strasbourg

Rogéria Paula MARTINS BINGRE DO AMARAL

EDSC École Doctorale des Sciences Chimiques

Porosity design of a shaped zeolite for improved effective diffusivity

Résumé

Les zéolithes sont des catalyseurs à base d'aluminosilicates largement utilisées dans l'industrie, particulièrement remarquables dans la catalyse. Ces matériaux sont synthétisés dans un laboratoire sous forme de poudre et doivent être mis en forme pour pouvoir être utilisés à grande échelle. Ce procédé est réalisé par l'ajout d'un liant, dans ce cas, la boehmite, pour conférer la résistance mécanique requise.

Cette Thèse décrit l'introduction d'une porosité supplémentaire dans la zéolithe mise en forme en utilisant des agents porogènes. Ces catalyseurs ont été testés dans différentes réactions catalytiques et dans l'adsorption du toluène afin d'évaluer l'effet de la présence de méso- et/ou de macropores dans le liant. Une amélioration de la performance des échantillons a été vérifiée lors de l'augmentation du volume macroporeux. Les zéolithes ont été testées en RMN à gradient de champ pulsé, en mesures d'adsorption et en chromatographie en phase gazeuse inverse pour déterminer la diffusivité effective de molécules sondes. Les résultats ont permis de corréler les performances catalytiques avec une diffusion améliorée.

Mots clés : liant, zéolithe mise en forme, méso- et macropores, diffusivité effective

Abstract

Zeolites are aluminosilicate catalysts widely used in industrial processes, with paramount importance in catalysis area. These materials are synthesized in a laboratory in a form of a powder and have to be shaped into centimeter-sized bodies to be implemented at large scale. This process is performed by the addition of a binder, in this case boehmite, to confer the mechanical strength required.

The work described in this Thesis aimed to introduce additional porosity in shaped zeolite by means of pore former agents. These catalysts were tested in different catalytic reactions and toluene adsorption to assess the effect of meso- and/or macropores presence in the binder. It was verified an improvement of the performance of the samples with a raise in the macropore volume. The samples were also tested in pulsed-field gradient NMR, uptake measurements and inverse gas chromatography to determine the effective diffusivity of probe molecules. The results allowed to establish a correlation between the catalytic performance and an improved diffusion.

Keywords: binder, shaped zeolite, meso- and macropores, effective diffusivity